

**International
Journal of
Engineering
Technologies
(IJET)**

**Printed ISSN: 2149-0104
e-ISSN: 2149-5262**

**Volume: 4
No: 1
March 2018**

© Istanbul Gelisim University Press, 2018
Certificate Number: 23696
All rights reserved.

International Journal of Engineering Technologies is an international peer-reviewed journal and published quarterly. The opinions, thoughts, postulations or proposals within the articles are but reflections of the authors and do not, in any way, represent those of the Istanbul Gelisim University.

CORRESPONDENCE and COMMUNICATION:

Istanbul Gelisim University Faculty of Engineering and Architecture
Cihangir Mah. Şehit P. Onb. Murat Şengöz Sk. No: 8
34315 Avcilar / Istanbul / TURKEY
Phone: +90 212 4227020 Ext. 221
Fax: +90 212 4227401
e-Mail: ijet@gelisim.edu.tr
Web site: <http://ijet.gelisim.edu.tr>
<http://dergipark.gov.tr/ijet>
Twitter: [@IJETJOURNAL](https://twitter.com/IJETJOURNAL)


Printing and binding:

Anka Matbaa
Certificate Number: 12328
Phone: +90 212 5659033 - 4800571
E-mail: ankamatbaa@gmail.com

International Journal of Engineering Technologies (IJET) is included in:



**International Journal of Engineering Technologies (IJET) is
harvested by the following service:**

Organization	URL	Starting Date	Feature
 The OpenAIRE2020 Project	https://www.openaire.eu	2015	Open Access



INTERNATIONAL JOURNAL OF ENGINEERING TECHNOLOGIES (IJET)
International Peer-Reviewed Journal
Volume 4, No 1, March 2018 Printed ISSN: 2149-0104, e-ISSN: 2149-5262

Owner on Behalf of Istanbul Gelisim University
Rector Prof. Dr. Burhan AYKAC

Editor-in-Chief

Prof. Dr. Mustafa BAYRAM

Associate Editors

Assoc. Prof. Dr. Baris SEVİM

Asst. Prof. Dr. Ahmet AKTAS

Asst. Prof. Dr. Yalcin CEKIC

Asst. Prof. Dr. Ali ETEMADI

Publication Board

Prof. Dr. Mustafa BAYRAM

Prof. Dr. Nuri KURUOĞLU

Asst. Prof. Dr. Ahmet AKTAS

Asst. Prof. Dr. Yalcin CEKIC

Asst. Prof. Dr. Mehmet Akif SENOL

Layout Editor

Asst. Prof. Dr. Ahmet AKTAS

Copyeditor

Res. Asst. Mehmet Ali BARISKAN

Proofreader

Asst. Prof. Dr. Ahmet AKTAS

Contributor

Ahmet Senol ARMAGAN

Cover Design

Mustafa FIDAN

Tarik Kaan YAGAN

Editorial Board

Professor Abdelghani AISSAOUI, University of Bechar, Algeria

Professor Gheorghe-Daniel ANDREESCU, Politehnica University of Timișoara, Romania

Associate Professor Juan Ignacio ARRIBAS, Universidad Valladolid, Spain

Professor Goce ARSOV, SS Cyril and Methodius University, Macedonia

Professor Mustafa BAYRAM, Istanbul Gelisim University, Turkey

Associate Professor K. Nur BEKIROGLU, Yildiz Technical University, Turkey

Professor Maria CARMEZIM, EST Setúbal/Polytechnic Institute of Setúbal, Portugal

Professor Luis COELHO, EST Setúbal/Polytechnic Institute of Setúbal, Portugal

Professor Filote CONSTANTIN, Stefan cel Mare University, Romania

Professor Mamadou Lamina DOUMBIA, University of Québec at Trois-Rivières, Canada

Professor Tsuyoshi HIGUCHI, Nagasaki University, Japan

Professor Dan IONEL, Regal Beloit Corp. and University of Wisconsin Milwaukee, United States

Professor Luis M. San JOSE-REVUELTA, Universidad de Valladolid, Spain

Professor Vladimir KATIC, University of Novi Sad, Serbia

Professor Fujio KUROKAWA, Nagasaki University, Japan

Professor Salman KURTULAN, Istanbul Technical University, Turkey

Professor João MARTINS, University/Institution: FCT/UNL, Portugal

Professor Ahmed MASMOUDI, University of Sfax, Tunisia

Professor Marija MIROSEVIC, University of Dubrovnik, Croatia

Professor Mato MISKOVIC, HEP Group, Croatia

Professor Isamu MORIGUCHI, Nagasaki University, Japan

Professor Adel NASIRI, University of Wisconsin-Milwaukee, United States

Professor Tamara NESTOROVIC, Ruhr-Universität Bochum, Germany

Professor Nilesh PATEL, Oakland University, United States

Professor Victor Fernão PIRES, ESTSetúbal/Polytechnic Institute of Setúbal, Portugal

Professor Miguel A. SANZ-BOBI, Comillas Pontifical University /Engineering School, Spain

Professor Dragan ŠEŠLIJA, University of Novi Sad, Serbia

Professor Branko SKORIC, University of Novi Sad, Serbia

Professor Tadashi SUETSUGU, Fukuoka University, Japan

Professor Takaharu TAKESHITA, Nagoya Institute of Technology, Japan

Professor Yoshito TANAKA, Nagasaki Institute of Applied Science, Japan

Professor Stanimir VALTCHEV, Universidade NOVA de Lisboa, (Portugal) + Burgas Free University, (Bulgaria)

Professor Birsen YAZICI, Rensselaer Polytechnic Institute, United States

Professor Mohammad ZAMI, King Fahd University of Petroleum and Minerals, Saudi Arabia

Associate Professor Lale T. ERGENE, Istanbul Technical University, Turkey

Associate Professor Leila PARSA, Rensselaer Polytechnic Institute, United States

Associate Professor Yuichiro SHIBATA, Nagasaki University, Japan

Associate Professor Kiruba SIVASUBRAMANIAM HARAN, University of Illinois, United States

Associate Professor Yilmaz SOZER, University of Akron, United States

Associate Professor Mohammad TAHA, Rafik Hariri University (RHU), Lebanon

Assistant Professor Kyungnam KO, Jeju National University, Republic of Korea

Assistant Professor Hidenori MARUTA, Nagasaki University, Japan

Assistant Professor Hulya OBDAN, Istanbul Yildiz Technical University, Turkey

Assistant Professor Mehmet Akif SENOL, Istanbul Gelisim University, Turkey

Dr. Jorge Guillermo CALDERÓN-GUIZAR, Instituto de Investigaciones Eléctricas, Mexico

Dr. Rafael CASTELLANOS-BUSTAMANTE, Instituto de Investigaciones Eléctricas, Mexico

Dr. Guray GUVEN, Conductive Technologies Inc., United States

Dr. Tuncay KAMAS, Eskişehir Osmangazi University, Turkey

Dr. Nobumasa MATSUI, Faculty of Engineering, Nagasaki Institute of Applied Science, Nagasaki, Japan

Dr. Cristea MIRON, Politehnica University in Bucharest, Romania

Dr. Hiroyuki OSUGA, Mitsubishi Electric Corporation, Japan

Dr. Youcef SOUFI, University of Tébessa, Algeria

Dr. Hector ZELAYA, ABB Corporate Research, Sweden

From the Editor

Dear Colleagues,

On behalf of the editorial board of International Journal of Engineering Technologies (IJET), I would like to share our happiness to publish the thirteenth issue of IJET. My special thanks are for members of Editorial Board, Publication Board, Editorial Team, Referees, Authors and other technical staff.

Please find the thirteenth issue of International Journal of Engineering Technologies at <http://ijet.gelisim.edu.tr> or <http://dergipark.gov.tr/ijet>. We invite you to review the Table of Contents by visiting our web site and review articles and items of interest. IJET will continue to publish high level scientific research papers in the field of Engineering Technologies as an international peer-reviewed scientific and academic journal of Istanbul Gelisim University.

Thanks for your continuing interest in our work,

Professor Mustafa BAYRAM
Istanbul Gelisim University
mbayram@gelisim.edu.tr

<http://ijet.gelisim.edu.tr>
<http://dergipark.gov.tr/ijet>

Printed ISSN: 2149-0104

e-ISSN: 2149-5262

International Journal of
Engineering Technologies
IJET

Table of Contents

	<u>Page</u>
<i>From the Editor</i>	<i>vii</i>
<i>Table of Contents</i>	<i>ix</i>
• Location and Multi-Compartment Capacitated Vehicle Routing Problem for Blood Banking System / Elifcan Göçmen, Rızvan Erol	1-12
• Damage Detection on Steel Plane Trusses via Harmony Search Algorithm / Musa Artar, Recep Çatar, Ayşe Daloğlu	13-20
• Optimum Design of Braced Steel Space Frames Using Teaching Learning Based Optimization / Ayşe Daloğlu, Musa Artar, Korhan Özgan, Ali İ. Karakaş	21-26
• Mucuna Pruriens as Photo-Sensitizer in Dye Sensitized Solar Cell / Charity Segun Odeyemi, Ayodeji Oladiran Awodugba	27-32
• Mechanical Properties of Steel Fiber Reinforced Self-Compacting Concrete / Anil Nis	33-40
• Mechanical Properties of Aluminum-4043/Nickel-coated Silicon Carbide Composites Produced via Stir Casting / Peter Kayode Farayibi, Basil Olufemi Akinnuli, Sylvester Ogu	41-46
• Determination of Basic Saturation Flow Rate in Istanbul / Süleyman Dündar, Kemal Selçuk Öğüt	47-52
• Gear Shift Efforts Analysis and User Interface Software Development / Emrah Arslan, Ahmet Sagirli	53-59

International Journal of Engineering Technologies, IJET

e-Mail: ijet@gelisim.edu.tr

Web site: <http://ijet.gelisim.edu.tr>
<http://dergipark.gov.tr/ijet>

Twitter: [@IJETJOURNAL](https://twitter.com/IJETJOURNAL)

Location and Multi-Compartment Capacitated Vehicle Routing Problem for Blood Banking System

Elifcan Göçmen*[‡], Rızvan Erol**

* Department of Industrial Engineering, Faculty of Engineering and Architecture, Çukurova University, 01330, Balcalı, Sarıçam, Adana/TURKEY

** Department of Industrial Engineering, Faculty of Engineering and Architecture, Çukurova University, 01330, Balcalı, Sarıçam, Adana/TURKEY

(egocmen@cu.edu.tr, rerol@cu.edu.tr)

[‡] Elifcan Göçmen; 01330, egocmen@cu.edu.tr, Tel: +90 530 244 6189,

Received: 07.09.2017 Accepted: 20.05.2018

Abstract- Blood banking is important for the healthcare system and blood products are vital needed for medical treatment, surgeries, and organ transplants. Delivery time becomes vital when a hospital needs a blood product emergently. Therefore, delivering blood products in the safest and fastest way is the main responsibility of blood banks. In this study, we aim to minimize total delivery times between depots and demand points over a time period. We propose a two-stage mathematical model to determine both location and vehicle delivery routes. This problem is defined as Location and Routing problem for blood bank operations. This study also investigates the effect of distributing blood products among multi-compartment along with routing decisions. The proposed models are tested on a real-world case data in order to demonstrate their effectiveness in producing optimal solutions. By the results the approach can minimize both delivery time and total cost. Furthermore, a computer program with a graphical user interface is developed to implement the proposed approach for different data sets.

Keywords Blood banks, location-routing problems, mathematical model.

1. Introduction

Public and private sector organizations face a continual increase in logistics costs and therefore, then need to improve the efficiency of logistics operations. The performance of these organizations depends on the location and distribution decisions based on their logistic network [4]. The location-routing problems have been critical for logistics experts [9]. These problems include both location and routing decisions.

People can die by inadequate blood needs nowadays [27]. Turkey's blood needs are provided by the Turkish Red Crescent. In 2008, Ministry of Health designated the Turkish

Red Crescent Society as an only organization to collect and distribute blood and blood products.

In Turkey, the blood banking logistics system consists of three types of centers: blood donation centers, regional blood centers and transfusion centers. The blood is collected in blood donation centers, regional blood center tests the blood, and blood transfusion centers are distributed. Blood donation centers use fixed and mobile blood donation centers. The blood is brought to blood centers; the whole blood is separated into three products: erythrocytes, platelets and plasma. The requested products are transported to hospitals with vehicles.

In the literature, location routing problems are mostly solved together. However, in this study, the problem is divided into two stages. The reasons for this are as follows:

- Modeling of location routing problem is complex and requires expertise. The type and size of the problem can receive too much computer time.
- Location is strategic decision, routing is an operational decision, so these two decisions are difficult to think together.

Although this approach minimizes the total cost of the problems, in some cases, especially at health sector, cost minimization would not be the primary aim of the problem. Therefore, we propose a two stage approach to overcome the limitations. Locations of depots are selected according to minimizing direct service time of depots to each customer. Number and location of the depots are decided with regard to keep installation and general expenses cost relatively low. In the second model routing cost which is not the primary aim of the problem is minimized according to located depots.

The main contributions of this study are two-folds: (i) proposed two-stage mathematical programming model considers distributing blood products to multi-compartments along with location of distribution centers and delivery routing, (ii) this study provides the proposed model is applied for a regional blood banking using a computer program.

We give literature work in Section 2. We present the problem description in Section 3. We provide the mathematical formulations in Section 4. In Section 5, an interface is proposed. We give a case study to illustrate the benefit of the models in Section 6. Discussion is presented in Section 7. A summary of the study and future directions are provided in Section 8.

2. Literature Review

2.1. Literature Review on Location and Routing Problem (LRP)

Many studies about location routing problem are conducted by many researchers. They use exact formulations or/and heuristic algorithms.

Some papers propose exact solutions for the problem. The problem is considered with capacity constraints, solved this problem with a branch and price algorithm [2]. A model for locating and routing dangerous waste with two objectives is presented. They present a mixed integer approach and apply this model with 92 nodes [3]. A branch-and-cut algorithm for at most 50 customers is developed [5]. A location routing industrial hazardous waste with two objectives including total cost minimization and transportation risk minimization is developed. In the study, a mathematical model is developed and application is tested in Markazi province in Iran [6].

A mathematical model for designing an internet access is proposed [15]. A branch-and-price-and-cut algorithm including prices, strengthening cuts, a heuristic for a generalized location and distribution problem is presented [7]. A locating routing problem with risks is considered. A mixed-integer programming formulation is formulated and a three-phase heuristic is designed to solve the problem [1]. Branch and cut algorithms are used to solve the problem [8].

A comprehensive framework for the LRP is proposed. Exact algorithms are intended to solve medium-scale instances. Therefore, some of the studies are focused on heuristic approaches [17]. A two-phase Tabu search for the LRP with capacitated routes and incapacitated depots for up to 200 customers is proposed [25]. Multi depot location routing problem with a clustering based heuristic is dealt [14]. A hybrid metaheuristic algorithm including Tabu search and neighborhood search heuristics for LRP is studied [16]. A two phase heuristic based on a Tabu search and ant colony algorithm for the location routing problem is developed [26]. A framework for depot location, fleet assignment and routing decisions using a Greedy Randomized Adaptive Search Procedure combined with an Evolutionary Local Search is proposed [11]. A mixed integer programming formulation for a multi depot location problem and also proposed a new algorithm and a heuristic within a simulated annealing method is developed [10]. A metaheuristic

algorithm for location and routing is developed [24]. A heuristic for a combined maximal covering location problem is formulated [20]. The problem of locating and routing of unmanned aerial vehicles to maximize of the total score collected at points by flight routes of those vehicles is addressed. He formulates this problem as an integer linear program and develops a metaheuristic [28]. A metaheuristic approach for location and routing for the cross docks is provided [12].

2.2. Literature Review on LRP for the Blood Banking System

Location - routing on blood centers have been interested by some of the authors. The optimal number and locations of blood centers in Chicago is studied and thus system is intended to ensure adequacy to meet hospital demand Due to general structure of the problem is a complex, the problem is required to divide into two sub-problems [18]. Blood banking to minimize the biggest blood problems is studied. A linear programming model is developed about transfusion of blood units from the center to hospitals taking into account the characteristics of hospitals in order to ensure delivery [22]. Blood donation location problems in Quebec are examined [19]. Virginia blood products' collection, testing and distribution system is studied and established two models in order to improve. In the first model, the distance between collecting place of blood products and blood bank is tried to minimize. In the second model, the distance between hospital and the blood bank was tried to minimize. A p-median model is used to find a solution to the problem [13]. A blood bank system is introduced. They approach the problem in three stages. A median problem, set covering models are given in the problems [23]. Central Anatolia Region's problems by establishing distribution centers at various points are solved. In this system distribution centers are closer to the hospital, the time to reach the demand and the rate of elimination reduces. Hospitals that are assigned to distribution centers receive blood products once every day with their own vehicles in an emergency case to meet the needs [21]. Blood supply chain is designed for a disaster relief. The model is formulated by a fuzzy-stochastic mixed integer programming model. Total costs are tried to minimize for a real case [29]. A

solution is proposed for a robust and flexible approach for red blood cells to prevent the shortage. Supply and demand of blood are considered as uncertain. Sensitivity analysis is conducted on four scenarios [30]. An other recent study is about fresh food location routing problem. The study considers environmental conditions such as carbon emissions. A heuristic algorithm is developed for this model. Carbon tax conditions are added to this model and this situation could reduce the carbon emissions for a clean environment [31]. A blood supply chain is investigated based on location, inventory, routing problems and uncertain data is considered. A meta-heuristic algorithm called Simulated Annealing and Harmony is proposed for larger cases [32].

The recent blood chain works generally uses metaheuristic approaches for larger problems and consider uncertain conditions, environmental policies.

3. Problem Definition

In this study, a new system is proposed to solve problems caused by the central structure. Some hospitals in the region are assigned as Distribution Center (DC) as an additional layer between Regional Blood Center (RBC) and hospitals to distribute blood products. The proposed model solves the optimum number and location of distribution centers, and routes from RBC to DC and from DC to hospitals. Delivery time of blood products at emergency cases is markedly decreased by new DCs. The system is shown on Figure 1.

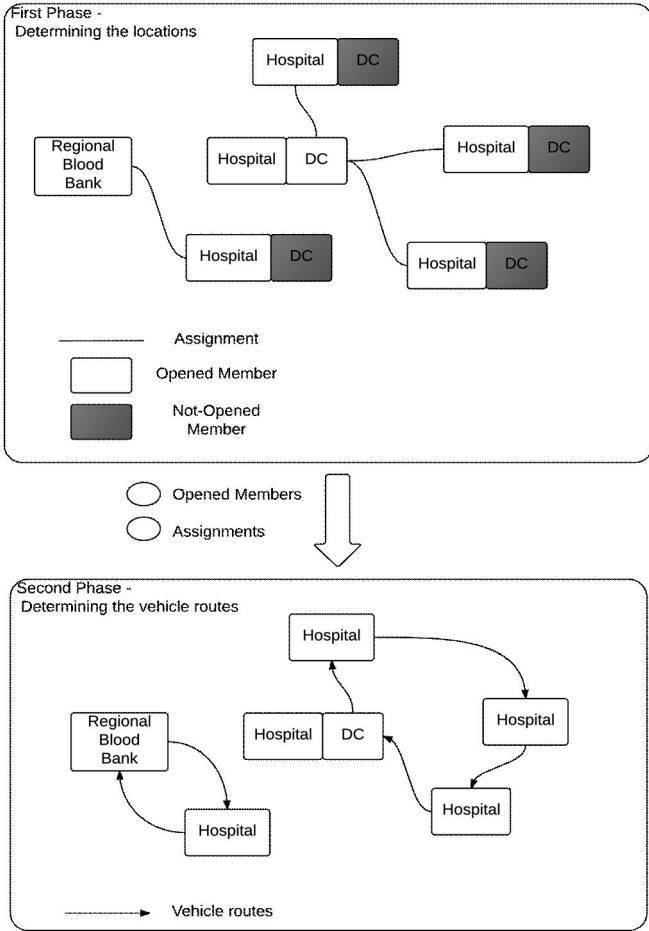


Fig. 1. Framework of the proposed system

In the problem, we have only one RCB which has no opening cost since the center is already available in the current system. All hospitals and the RCB can be authorized as DC. We assume that the system's costs are assumed for 10 years and net present value of the costs is found. The system is assumed to be installed at the start of the year. In the first model, the problem is considered as a two level problem: RBC to DC and DC to hospitals. The second model is considered as one level problem: DC to the hospitals. Blood demands of the hospitals are deterministic. Furthermore, we assume that there is no restriction on the number of DCs to be installed. The distribution vehicles have limited compartment capacities for each type of blood product, which are 180 unit products for erythrocytes, 30 unit products for platelets and 90 unit products for plasma. The total demand for each blood product type is partitioned between hospitals according to their patient capacities. Each DC is served one time in a week

from RBC. Each hospital is served three times in a week from DC.

4. Mathematical Models

The model is a complex structure, thus problem is converted into two problems. The first problem is minimization of average distances between the regional blood bank - the distribution centers, the distribution centers - the hospitals, distribution center setup and general expenses. The second sub-problem aims to minimize periodic transportation costs between hospitals and distribution centers.

The notation used for mathematical modeling of the problem is as follows;

I,J,T represent the set of hospitals, candidate distribution centers and the time periods, respectively. d_{ij} is the distance between the distribution centers and the hospitals. $\hat{\delta}$ is the percentage of emergency cases required by the hospitals. M is the maximum travelled distance of the vehicles. C is the transportation cost per km. B is the maximum budget to open distribution center. k is the interest rate. K_j is the setup cost at distribution center j and f is the yearly general expenses of the distribution centers. The decision variable is y_j 1 if a distribution center is at point j, 0 otherwise. The decision variable x_{ij} will be 1 if the i. hospital at is assigned to the distribution center at point j.

The objective function (1) minimizes the total costs including the initial investment cost of building a distribution center, annual operating costs for ten years and the delivery cost based on demand-weighted distances between the regional blood bank- the distribution centers and the distribution centers-the hospitals. The constraint (2) ensures that each hospital is assigned to only one distribution center.

Minimize:

$$\sum_{j=1}^J y_j K_j + \sum_{j=1}^J \sum_{t=1}^T f y_j (1+k)^{-t} + \sum_{j=1}^J C d_{0j} y_j + \sum_{i=1}^I \sum_{j=1}^J \hat{\delta} C d_{ij} x_{ij} \quad (1)$$

$$\sum_{j \in J} x_{ij} = 1 \quad i \in I \quad (2)$$

$$x_{ij} \leq y_j \quad i \in I, j \in J \quad (3)$$

$$\sum_i x_{ii} * f \leq B \quad (4)$$

$$x_{ij} * d_{ij} \leq M \quad i \in I, j \in J \quad (5)$$

$$y_j = (0,1) \quad j \in J \quad (6)$$

$$x_{ij} = (0,1) \quad i \in I, j \in J \quad (7)$$

The constraint (3) ensures that each hospital is assigned to itself if the hospital is opened as a distribution center. The constraint (4) allows to open the distribution center within the scope of a given budget criteria. The constraint (5) ensures the distance between distribution centers and hospitals, should be within the scope of a given maximum distance constraints. Constraints (6) and (7) are binary. (D_{0j}) is taken as the distances between the regional blood center and the distribution centers, (D_{ij}) is taken as the distances between the distribution centers and hospitals, and (M) is taken as the maximum distance that limits the distance between opened distribution center and hospital. The second sub-problem is formulated as a classical vehicle routing problem. I, J, K, P represent the set of hospitals, distribution centers, vehicles and blood products, respectively. d_{ij} is the distance between the distribution centers and the hospitals. \hat{d} is the number of weekly referrals. Q_{pk} is compartment capacity of blood product p by vehicle k . C is the transportation cost per km. D_{ip} is the demand of the blood product p by hospital i . F is the annual operating cost of the vehicles. H is the number of hospitals. The decision variable Z_{ijk} will be 1 if the vehicle k travels from point i to point j directly, 0 otherwise. The decision variable v_k will be 1 if the vehicle k is used. The decision variable T_{ipk} will be 1 if the hospital at point i is

distributed the blood product p by the vehicle k , 0 otherwise. W_{mk} is the auxiliary variable for the sub-tour elimination constraint. Min:

$$\sum_{k \in K} F * v(k) + \sum_{i \in U} \sum_{j \in U} \sum_{k \in K} (C * d_{ij} * Z_{ijk} * \alpha) \quad (8)$$

Constraints:

$$\sum_{i \in I} D_{ip} * T_{ipk} \leq Q_{pk} * 1 \quad \forall k \in K \quad \forall p \in P \quad (9)$$

$$\sum_{i \in U} Z_{ijk} - \sum_{i \in U} Z_{jik} = 0 \quad \forall j \in U \quad \forall k \in K \quad (10)$$

$$\sum_{i \in U} Z_{i0k} \leq v_k \quad \forall j \in U \quad \forall k \in K \quad (11)$$

$$\sum_{i \in U} Z_{0ik} \leq v_k \quad \forall j \in U \quad \forall k \in K \quad (12)$$

$$T_{ipk} \leq \sum_{i \in U} Z_{ijk} \quad \forall p \in P \quad \forall i \in I \quad \forall k \in K \quad (13)$$

$$\sum_{k \in K} T_{ipk} = 1 \quad \forall i \in I \quad \forall p \in P \quad (14)$$

$$\sum_{i \in U} \sum_{k \in K} Z_{ijk} = 1 \quad \forall j \in U, \quad (15)$$

$$W_{mk} - W_{ik} + H * Z_{jik} \leq H - 1 \quad \forall c, i \in I, \forall k \in K \quad (16)$$

$$T_{ipk} = (0,1) \quad \forall p \in P \quad \forall k \in K \quad (17)$$

$$Z_{ijk} = (0,1),$$

$$v_k = (0,1)$$

$$W_{ik} \geq 0$$

The objective function (8) minimizes the annual operating cost of the vehicle and the cost of demand-weighted distances between the distribution centers and the hospitals. The constraint (9) ensures total product demand of hospitals in the route of the vehicle, must not be more than the capacity of the vehicle compartment. The constraint (10) ensures that the vehicle returns to start point. The constraints (11) and (12) show the start and end of the route. The constraint (13) ensures p product is delivered to the hospital by the vehicle if the hospital is on the route from the distribution center to the hospital. The constraint (14) allows that a product is carried by only one vehicle and to only one hospital. The constraint (15) shows that each blood product ordered by a hospital is delivered by one vehicle. The constraint (16) is sub tour elimination constraint. The last constraint (17) is binary constraint.

5. Blood Location Allocation and Routing Planner GUI

The location routing problem discussed as a two stage should be solved again according to the problem structure. This structure should be able to run again for the next planning period by the end of the planning period. In order to respond quickly to the end user and ensure the ease of provision in practice, an interface called Blood Location Allocation and Routing has been proposed.

In Figure 2, a login screen of Blood Location and Routing planner is shown. In this screen, the number of blood centers, the number of distribution centers and hospitals and periods are determined and receiving the data from the Excel file is available.

In Figure 3, location assignment model which is the first stage of the location routing problem is solved. By the output of this model, hospitals (red circle) are assigned to the blood centers (black square) and the distribution centers (red square). According to the distribution center data obtained, the routing problem is solved.

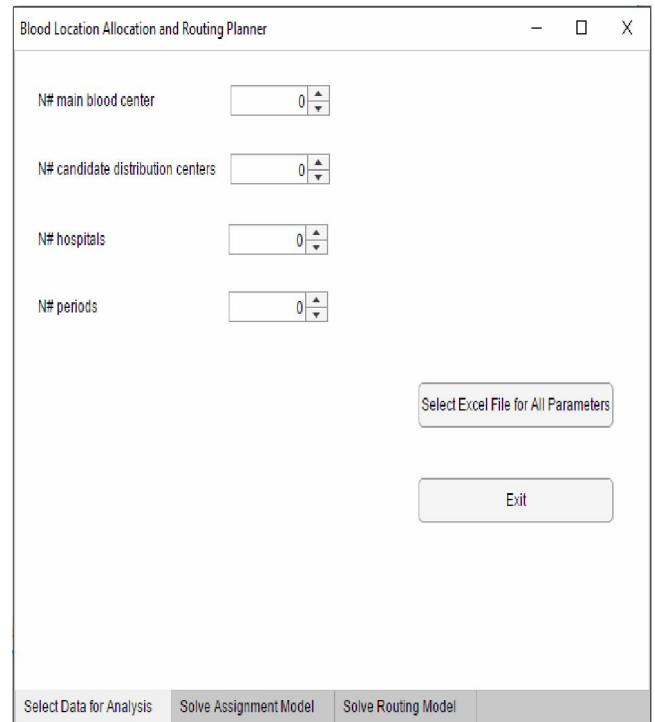


Fig. 2. Login screen of Blood Location and Routing planner

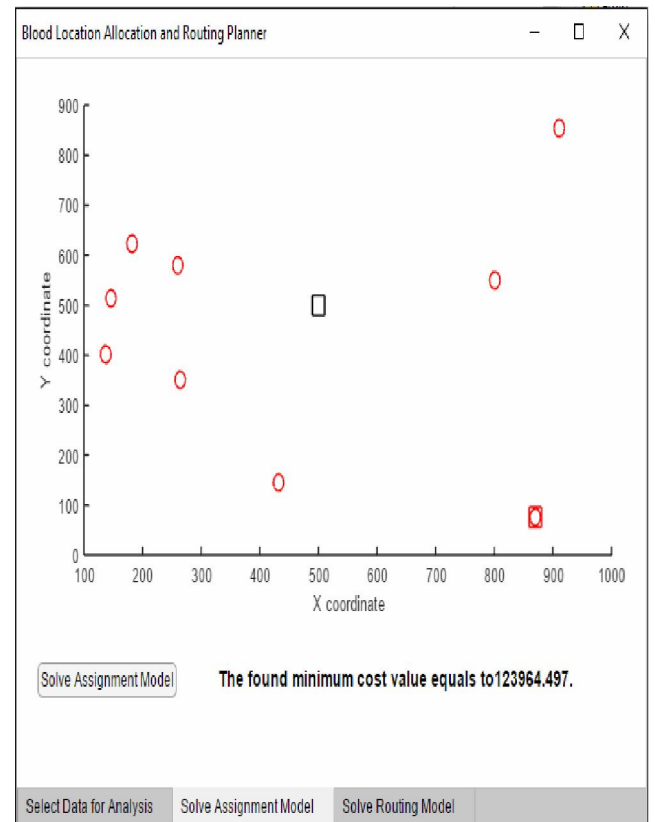


Fig. 3. Location assignment model

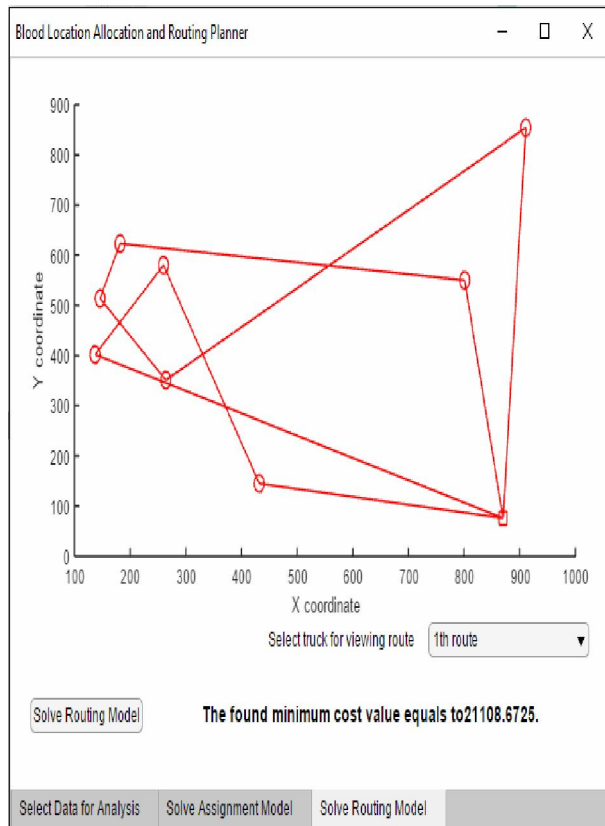


Fig. 4. Routing model

In Figure 4, routing model which is the second stage of the location routing problem is solved. By this model, the routes for carrying the products from the distribution centers to the demand points (hospitals) are determined. Each route is showed graphically.

6. Case study and numerical analysis

In this part the results for the models are revealed. Central Mediterranean Regional Blood Center (CMRBC) established in Adana in 2010 has fed the hospitals from a single center. Hospitals which are located in Adana, Mersin, Hatay and Osmaniye cities (Figure 5) demand blood products (erythrocytes, platelets and plasma) from this center. There are 77 hospitals and 8 vehicles in the system.

6.1. Output of the first model

As a result of the first model, distance constraint shows that at 25- 50- 75 km restrictions, total cost are significantly increased due to the initial investment of DCs. At 100- 125-

150 km restrictions, the total cost shows little differences, the results are presented in table 1.



Fig. 5. Locations of Adana, Mersin, Hatay and Osmaniye

In Osmaniye and Hatay, only one DC is enough to cover all hospitals within 100 km since the area is not large and opening the second DC is costly. As Mersin has large area, two hospitals are assigned as DC. Adana has a different situation than other ones. The reason of that is, CMRBC already exists within the city, so it needs any installation cost. This causes the CMRBC is selected as one of the DCs in Adana. A hospital, which is too far from all other hospitals, is also opened as a DC and assigned only to itself.

6.2. Output of the second model

Second model answers the vehicle routes and vehicle numbers by the outputs of the first model.

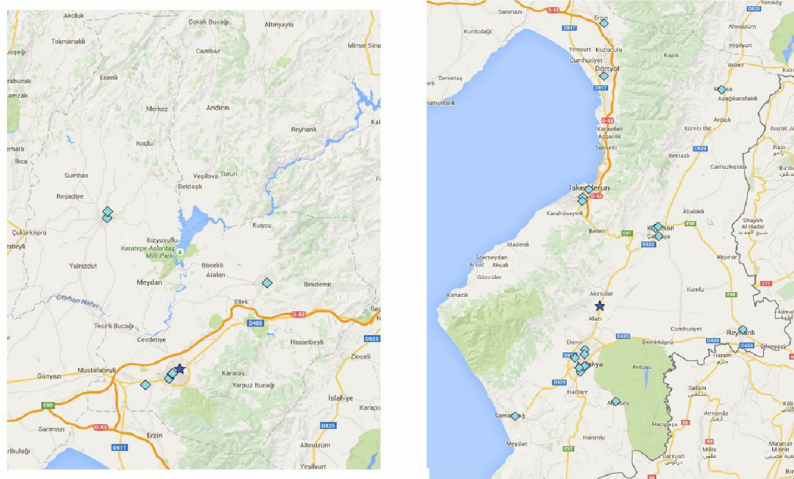
Osmaniye and Hatay have small geographic areas, thus, only one route is able to give optimum results (Figure 6). In Mersin, there are two routes starts from each DC (Figure 7(a)). As it can be seen in Figure 7(a), two vehicles should be used for meeting the total blood products, which are demanded from CMRBC. On the other hand, other DC in Adana (Figure 7(b)) is not assigned to any hospital, thus there is no route starting from the hospital. But a vehicle is assigned to the DC in case of emergent blood product demand.

Furthermore, in the proposed model, 7 vehicles are enough for delivery of blood products, whereas the number is 8 in the current system. Except CMRBC, only one vehicle is assigned to each DC. Total demands of hospitals that are assigned to CMRBC are more than the capacity of a distribution vehicle so; two vehicles have to be assigned to the center.

7. Discussion

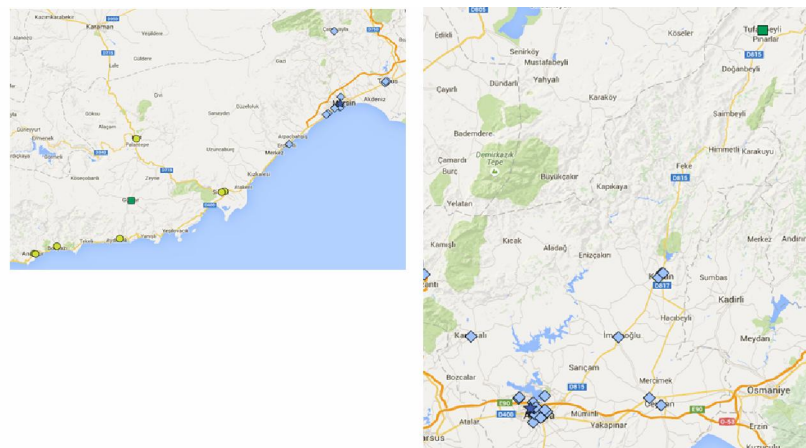
A comparison of the current system and the proposed system may be summarized as follows.

With newly opened DCs, the service time is significantly decreased for periodic distribution and emergent blood products demand. The results show that the proposed model compensates the initial investment in 10 years. The routing and emergency service times of current and propose models' results are shown in Table 2. And cost comparison of the current and proposed systems for 10 years are presented in Table 3.



^α “★” indicates the location of DC, “◆” indicates the location of hospitals

Fig. 6. The result of the routing (a) for Osmaniye (b) for Hatay ^α



^α “★” indicates the location of DC at first route , “◆” indicates the location of hospitals at first route

^β “■” indicates the location of DC at second route , “●” indicates the location of hospitals at second route

Fig. 7. The result of the routing for Mersin (a) for Adana (b) ^{α,β}

Table 1. The number of opened distribution center, number of vehicle and total cost of the system versus distance

Name of the city	Distance Constraint	Number of opened distribution center	Number of vehicle	Costs (TL)
Osmaniye	25	3	3	4.736.456,7
	50	1	1	1.663.285,3
	75	1	1	1.663.285,3
	100	1	1	1.663.285,3
	125	1	1	1.663.285,3
	150	1	1	1.663.285,3
Hatay	25	5	5	8.108.274,3
	50	2	2	3.361.227,9
	75	2	2	3.361.227,9
	100	1	1	1.839.690,4
	125	1	1	1.839.690,4
	150	1	1	1.839.690,4
Mersin	25	9	9	14.397.446,6
	50	5	5	8.133.824,6
	75	3	3	5.150.581,8
	100	2	2	3.566.485,9
	125	2	2	3.566.485,9
	150	2	2	3.559.108,2
Adana	25	6	6	7.982.666
	50	4	4	4.956.703
	75	4	4	4.949.876
	100	2	2	2.025.530
	125	2	2	2.005.964
	150	2	2	1.997.884

As noted in Table 1, number of opened distribution center and number of vehicles decreases by increasing the distance constraint and also the total costs. Number of tours decreases by increasing the distance constraint. The significant cost differences are in Hatay by 77 % , in Mersin 75%, in Adana 74% and in Osmaniye 65%, consecutively. In the context of the costs, for the all provinces, the significant cost reduction occurs by increasing the distance constraint from twenty five to fifty. As a result, the distance constraints affect the results directly.

Table 2. Results for the routing and emergency service times of all cities

	Total Routing Times		Total Emergency Service Time	
	Current System (min)	Proposed System (min)	Current System (min)	Proposed System (min)
Osmaniye	253	128	695	119
Hatay	432	296	2933	545
Mersin	573	518	2614	617
Adana	572	364	728	558

Delivery time becomes vital when a hospital requires a blood product. As seen in Figure 8 and Table 2, total routing times and total emergency service times decrease comparing to the previous system, but especially total emergency service times are reduced as required for the demands in the proposed system.

As it can be compared from table 3, at the proposed system, there is not a significant difference about the total costs; the difference is at routing costs. The current system has a route that starts at Regional Blood Center and finishes the tour after visiting all hospitals in need. The

proposed system’s advantage is that the route starts at every distribution centers, visits the near hospitals and finishes the tour at the same distribution center.

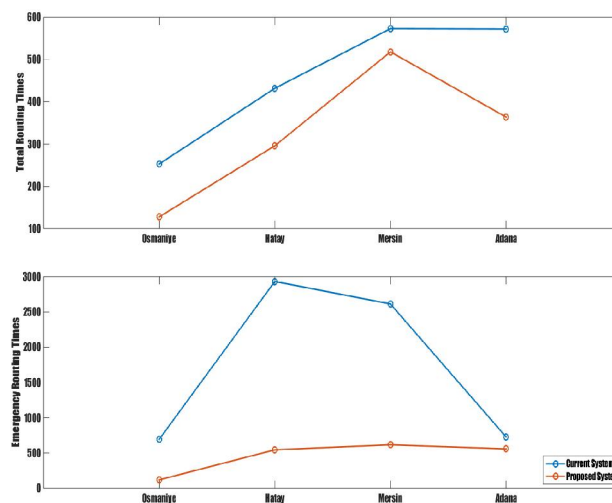


Fig. 8. Comparisons of delivery times between the current system and the proposed system

Table 3. Comparison of the current and proposed systems

	Current System	Proposed System
Routing	1.862.091 TL	1.278.987,1 TL
Vehicle cost	480.000 TL	420.000 TL
Fixed costs	31.840.974,4 TL	32.003.111,7 TL
Installation	0	480.000 TL
Total costs for ten years	34.183.065,4 TL	34.182.098,8 TL

However, to meet the needs in time improvements are observed in Osmaniye, Hatay and Mersin. This case shows effectiveness of the new system. Regional Blood Center continues to serve as the distribution center for hospitals in Adana, and so the times to meet the urgent for blood products remains unchanged.

8. Conclusion

Blood products management is one of the important problems with the complex structure in the field of health logistics. Blood products are vital for surgery, accidents, and chronic diseases. Therefore, the desired products must be available at the demand point. The problem is approached in two steps. We give a p-median type model that the locations of the distribution centers, the allocation of the hospitals to the distribution centers are determined in step I. According to the first model's outputs, in stage II a classical vehicle routing problem model is formulated with adding new constraints including vehicle compartment capacities. These location-allocation-routing models are formulated not only to find a solution to the current structure of the RBC, but also to use these models at different systems.

Case study shows that, by opening new DCs, total routing and emergency service time are significantly decreased with compensating initial investment of the proposed system.

There may be limitations in this study. The proposed model can be used different systems (private, government, clinics, etc.).

8.1. Recommendations and future direction

There are some future suggestions that may be considered as follows. Larger case study such as whole country's blood management can be conducted for investigating the effects of the proposed methods. Heuristic methods can be applied for large case problems.

References

- [1] A. Ahmadi-Javid, and AH. Seddighi, "A location-routing problem with disruption risk", *Transportation Research Part E. Logist. Trans. Rev.*, vol. 2, pp. 63–82, 2013.
- [2] Z. Akca, R.T. Berger, and T.K. Ralphs, "Modeling and Solving Location Routing and Scheduling Problems". Working paper, COR@L Lab, Lehigh University 2008.
- [3] S. Alumur, and B.Y. Kara, "A new model for the hazardous waste location-routing problem", *Computers and Operations Research*, vol. 34, pp. 1406–1423, 2007.
- [4] J.M. Belenguer, E. Benavent, C. Prins, and RW. Calvo, "A Branch and Cut Method for the Capacitated Location-Routing Problem", *Service Systems and Service Management*, vol 2, 2006.
- [5] J.M. Belenguer, E. Benavent, C. Prins, C. Prodhon, and R. Wolfler Calvo, "A branch-and-cut method for the capacitated location-routing problem", *Computers & Operations Research*, vol. 38, pp.931–941, 2011.
- [6] O. Boyer, T.S. Hong, A. Pedram, R. Yusuff, B.M., and N. Zulkifli, "A mathematical model for the industrial hazardous waste location-routing problem". *Journal of Applied Mathematics*, pp. 1–10, 2013.
- [7] A. Ceselli, G. Righini, and E. Tresoldi, "Combined location and routing problems for drug distribution", *Discrete Applied Mathematics*, vol. 165, pp. 130–145, 2014.
- [8] C. Contardo, V. Hemmelmayr, and T.G. Crainic, "Lower and upper bounds for the two-echelon capacitated location-routing problem". *Computers & Operations Research*, vol. 39, pp.3185–3199, 2012.
- [9] V.M. Dalfard, M. Kaveh, and N.E. Nosrati, "Two meta-heuristic algorithms for two-echelon location-routing problem with vehicle fleet capacity and maximum route length constraints". *Neural Computing and Applications*, vol. 23, pp. 2341–2349, 2013.
- [10] S.H. Doulabi, and A. Seifi, "Lower and upper bounds for location-arc routing problems with vehicle capacity constraints". *European Journal of Operational Research*, vol. 224, pp. 189-208, 2013.
- [11] C. Duhamel, P. Lacomme, C. Prins, and C. Prodhon, "A memetic approach for the capacitated location routing problem". In *Proceedings of the EU/meeting 2008 workshop on metaheuristics for logistics and vehicle routing*. University of Technology of Troyes, France, 2008.
- [12] A.H. Goodarzi, and S.H. Zegordi, "A location-routing problem for cross-docking networks: A biogeography-based optimization algorithm". *Computers & Industrial Engineering*, pp. 132-146, 2016.
- [13] D.A. Jacobs, M.N. Silan, and B.A. Clemson, "An analysis of alternative locations and service areas of american red cross blood facilities", *Interfaces* vol.26, pp.40-50, 1996.
- [14] M. Lam, J. Mittenthal, and B. Gray, "The impact of stopping rules on hierarchical capacitated clustering

- in location routing problems”, *Academy of Information and Management Sciences Journal*, vol. 12, pp. 13-28, 2009.
- [15] Y. Lee, S.I. Kim, S. Lee, and K. Kang, “A location-routing problem in designing optical internet access with WDM systems”, *Photonic Network Communications*, vol. 6, pp.151–160, 2003.
- [16] J. Melechovsky, C. Prins, and R. Wolfler Calvo, “A metaheuristic to solve a location-routing problem with non-linear costs”. *Journal of Heuristics*. Vol. 11, pp. 375-391, 2005.
- [17] G. Nagy, and S. Salhi, “Location- routing: Issues, models and methods”. *Eur. J. Oper. Res.* 176, 649–672, 2007.
- [18] I. Or, and W.P. Pierskalla, “A transportation location-allocation model for regional blood banking”, *AIIE Transactions* vol. 11, pp.86-95, 1979.
- [19] W.L. Price, and M. Turcotte, “Locating a blood bank”, *Interfaces*, vol. 16, pp.17-26, 1986.
- [20] F. Rahim, and C. Sepil, “A location-routing problem in glass recycling”, *Annals of Operations Research*, vol. 223, pp.329-353, 2014.
- [21] A.C. Randa, A. Cömert, B. Adigüzel, C. Balıkçioğlu, C. Örnekol, P. Bayındır, and I.S. Bakal, “Türk kızılaiy Orta anadolu bölgesi kan ürünleri tedarik zinciri yönetimi projesi”, *Endüstri Mühendisliđi Dergisi* vol. 22, pp. 22-70.
- [22] C. Sapountzis, “Allocating blood to hospitals from a central blood bank”, *European Journal Of Operational Research* vol. 16, pp. 157-162, 1984.
- [23] G. Şahin, H. Sural, and S. Meral, “Locational analysis for regionalization of turkish red crescent blood service”, *Computer & Operations Research*, vol.34, pp. 692-704, 2007.
- [24] C.J. Ting, and C.H. Chen, “A multiple ant colony optimization algorithm for the capacitated location routing problem”, *International Journal of Production Economics*, vol.141, pp. 34–44, 2013.
- [25] D. Tuzun and L.I. Burke, “A two-phase tabu search approach to the location routing problem”. *Eur J Oper Res*, vol. 116, pp.87–99, 1999.
- [26] X. Wang, X. Sun, and Y. Fang, “A two-phase hybrid heuristic search approach to the location-routing problem”, *IEEE International Conference on Systems, Man and Cybernetics*, vol. 4, pp. 3338–3343, 2005.
- [27] World Health Organization. <http://www.who.int>, (10.03.2018).
- [28] E. Yakıcı, “Solving location and routing problem for UAVs”. *Computers & Industrial Engineering*, pp.294-301, 2016.
- [29] S. Cheraghi, and S.M. Hosseini-Motlagh, “Optimal blood transportation in disaster relief considering facility disruption and route reliability under uncertainty”, *International Journal of Transportation Engineering* vol. 4, pp. 225-254, 2016.
- [30] F. Jafarkhan, and S. Yaghoubi, “An efficient solution method for the flexible and robust inventory-routing of red blood cells”, *Computers & Industrial Engineering*, vol. 117, pp. 191-206, 2018.
- [31] S. Wang, F. Tao, and Y. Shi, “Optimization of location–routing problem for cold chain logistics considering carbon footprint”. *International Journal Environmental Research Public Health*, vol. 15, pp. 86, 2018.
- [32] M. Eskandari-Khanghahia, R. Tavakkoli-Moghaddam, A.A. Taleizadeh and S.H. Amin, “Designing and optimizing a sustainable supply chain network for a blood platelet bank under uncertainty”, *Engineering Applications of Artificial Intelligence*, vol. 71, pp. 236-250, 2018.

Damage Detection on Steel Plane Trusses via Harmony Search Algorithm

Musa Artar*[‡], Recep Çatar**, Ayşe T. Daloğlu***

*Department of Civil Engineering, Engineering Faculty, Bayburt University, 69000, Bayburt, Turkey

** Department of Mechanical Engineering, Engineering Faculty, Bayburt University, 69000, Bayburt, Turkey

***Department of Civil Engineering, Engineering Faculty, Karadeniz Technical University, 61000, Trabzon, Turkey

(martar@bayburt.edu.tr, rcatar@bayburt.edu.tr, aysed@ktu.edu.tr)

[‡]Corresponding Author; First Author, 69000 Bayburt Turkey, Tel: +90 458 211 11 77,

Fax: +90 458 211 11 78, martar@bayburt.edu.tr

Received: 08.09.2017 Accepted: 08.11.2017

Abstract- A damage detection study is presented on steel plane truss structures via harmony search algorithm which is one of the basic metaheuristic methods. This algorithm method mimics better musical harmony procedures. Optimum solutions are carried out by a harmony memory matrix consisting of a predetermined number of solution vectors. Scenario damages are considered on truss models. The locations of the damages are tried to determine by using the dynamic parameters. To obtain damage locations, a program based on the finite element method is coded in MATLAB programming. The dynamic parameters of damaged models are obtained by SAP2000 software. By using MATLAB programming, the scenario damage locations considered in SAP2000 programs are tried to determine by approaching the dynamic values of the damaged model as a result of a series of iterations. The results are presented by tables and figures. The results show that scenario damages on truss models are successfully detected by using dynamic parameters in MATLAB programming.

Keywords Optimum design, harmony search algorithm, damage detection, steel truss.

1. Introduction

Metaheuristic algorithm methods are commonly selected for solutions of various optimization problems. Some of them are listed as genetic algorithm method, particle swarm optimization method, ant colony algorithm method, artificial bee algorithm method, harmony search method, bat inspired algorithm method, and teaching learning based optimization method and the other methods.

Harmony search (HS) algorithm method is selected in this study to obtain optimum solutions. HS mimics musical harmony procedures, and has been used for various structural problems in last years by many researchers. Lee and Geem [1] developed harmony search algorithm on structural optimization in 2004. Saka [2] researched optimum design of steel sway frames to BS5950 using harmony search algorithm in 2009. Değertekin et al. [3] used harmony search algorithm method for optimum design of geometrically non-linear steel frames with semi-rigid connections in 2009.

Değertekin and Hayalioglu [4] studied harmony search algorithm for minimum cost design of steel frames with semi-rigid connections and column bases in 2010. Değertekin et al. [5] focused on optimum design of geometrically nonlinear steel frames with semi-rigid connections using improved harmony search method in 2011. Toğan et al. [6] studied optimization of trusses under uncertainties with harmony search in 2011. Artar [7] used harmony search algorithm method for comparative study on optimum design of multi-element truss structures in 2016. Daloğlu et al. [8] studied optimum design of steel space frames including soil-structure interaction using harmony search algorithm method in 2016. Artar and Daloğlu [9] researched optimum weight design of steel space frames with semi-rigid connections using harmony search and genetic algorithms in 2016. Artar [10] applied harmony search algorithm on optimum design of steel space frames under earthquake effect in 2016.

In this study, scenario damages on steel plane truss structures are investigated by using Harmony Search Algorithm method. To detect damages, a program based on finite element method was coded in MATLAB programming. Harmony search algorithm method applied the procedures for better musical harmony. The locations of the damages are tried to determine by using the dynamic parameters. The presence of damages in structural elements is identified by stiffness reduction as a reduction in modulus of elasticity. In this study, two different examples having various damage scenarios are modeled in SAP2000 software to obtain the experimental dynamic parameters. The scenario damage locations considered in SAP2000 programs are tried to detect by approaching the dynamic values of the damaged model as a result of a series of iterations by using the program developed in MATLAB programming. Thus, the locations of simulated damages are determined by updated numerical model. The results obtained from solutions prove that scenario damages on plane truss structures are successfully determined by using dynamic parameters. Moreover, solutions show that robustness and acceptability of harmony search algorithm method.

2. Harmony Search Algorithm

Harmony Search (HS) Algorithm, a basic metaheuristic algorithm method, is developed in 2004 by Lee and Geem [1]. This algorithm method includes some procedures which mimics better musical harmony processes. Analyses in HS are conducted by harmony memory matrix (HM). Each row in the matrix represents a structural model. Harmony memory matrix is determined as

$$H = \begin{bmatrix} x_1^1 & x_2^1 & \dots & x_{n-1}^1 & x_n^1 \\ x_1^2 & x_2^2 & \dots & x_{n-1}^2 & x_n^2 \\ \dots & \dots & \dots & \dots & \dots \\ x_1^{HMS-1} & x_2^{HMS-1} & \dots & x_{n-1}^{HMS-1} & x_n^{HMS-1} \\ x_1^{HMS} & x_2^{HMS} & \dots & x_{n-1}^{HMS} & x_n^{HMS} \end{bmatrix} \quad (1)$$

Harmony Memory Size (HMS) shows a specified number of solution vectors. Values in harmony matrix are updated by harmony memory consideration rate (HMCR) and pitch adjustment ratio (PAR). The operators (HMCR and PAR) provides a stronger harmony memory matrix for better optimum solution vectors. HMCR and PAR are calculated as below,

$$\begin{cases} x_i^{nh} \in \{x_i^1, x_i^2, \dots, x_i^{HMS}\} \text{ with probability of HMCR} \\ x_i^{nh} \in X_{st} \text{ with probability of } (1 - HMCR) \end{cases} \quad (2)$$

$$\begin{cases} \text{Yes, with probability of PAR} \\ \text{No, with probability of } 1 - PAR \end{cases} \quad (3)$$

3. Theoretical Background

Detection of scenario damages is researched by using reduction factor for modulus of elasticity of each member in structural model. In this study, four different reduction factors such as 1.00, 0.75, 0.50 and 0.25 are applied in the analyses. While the reduction factors equal to 1.00, the

element has not damaged. On the other hand, if the reduction factor of member is 0.75, the member in the structure model has 25% of damage. Natural frequencies of simulated damaged model are predefined by using SAP2000 and entered as input data. The program developed in MATLAB programming tries to determine the locations of damages using Harmony search algorithm. Local stiffness (k), mass (m) and transformation (T) matrices of each element are calculated. Thus, global stiffness (K) and mass (M) of structural system are calculated and natural frequencies of numerical model are determined as below,

$$(K - \lambda_i M) \phi_i = 0 \quad i=1 \dots \dots \dots n \quad (4)$$

$$\sqrt{\lambda_i} = w_i \quad f_i = \frac{w_i}{2\pi} \quad (5)$$

where K and M are the global stiffness and mass matrices, respectively. w_i is angular vibration frequency of structure (rad/s), ϕ_i is eigenvector (mode shape), λ_i is eigenvalue and n is total number of mode shapes. f_i is vibration per second (Hz). Then, the objective function value of each row in HS for each mode is determined as below [11],

$$F_{frequencies,i} = \left| \frac{f_i^E - f_i^N}{f_i^E} \right| \quad i=1 \dots \dots \dots m \quad (6)$$

$$F_{t,i} = \sum F_{frequencies,i} \quad (7)$$

f_i^E and f_i^N stand for experimental and numerical natural frequencies, respectively. $F_{frequencies,i}$ and $F_{t,i}$ show objective function value for i^{th} mode and total objective function value of all modes, respectively. When the total objective function value is equal to zero, the difference between updated numerical model and simulated damaged model is same.

A flowchart of Harmony Search Algorithms is shown in Fig.1.

4. Numerical Examples

4.1. 20-Element steel plane truss model

A 20-element steel plane truss example is presented in Fig. 2. All members are pipe section of 10x1 as seen Fig.2. The modulus of elasticity is $E=2.00 \times 10^8$ kN /m² and material density is $\rho = 7.85$ ton/m³. The same example is studied for two different damage scenarios. In case 1, member no. 15 has 50% of damage and in case 2, member no. 11 has 75% of damage. Table 1 presents the values of the first three natural frequencies obtained from MATLAB and SAP2000 software for undamaged and damaged cases. While Fig 3 presents results for case 1, Fig 4 shows results of case 2. Fig. 5 shows first three mode shape of undamaged model.

As presented in Table 1, the results of natural frequencies in MATLAB and SAP2000 programs are very close for first three modes in undamaged and damaged cases. In case 1, member no.15 has 50 % damage and the program using MATLAB is carried out around the 30th iterations as

seen in Fig.3a. Fig. 3b proves that member 15 has 50% reduction in modulus of elasticity. Similarly, in case 2, member no.11 has 75% damage and the program coded in

MATLAB is carried out at about the 30th iterations as shown in Fig.4b. Also, Fig. 4b presents that the member no.11 has 75% reduction in modulus of elasticity.

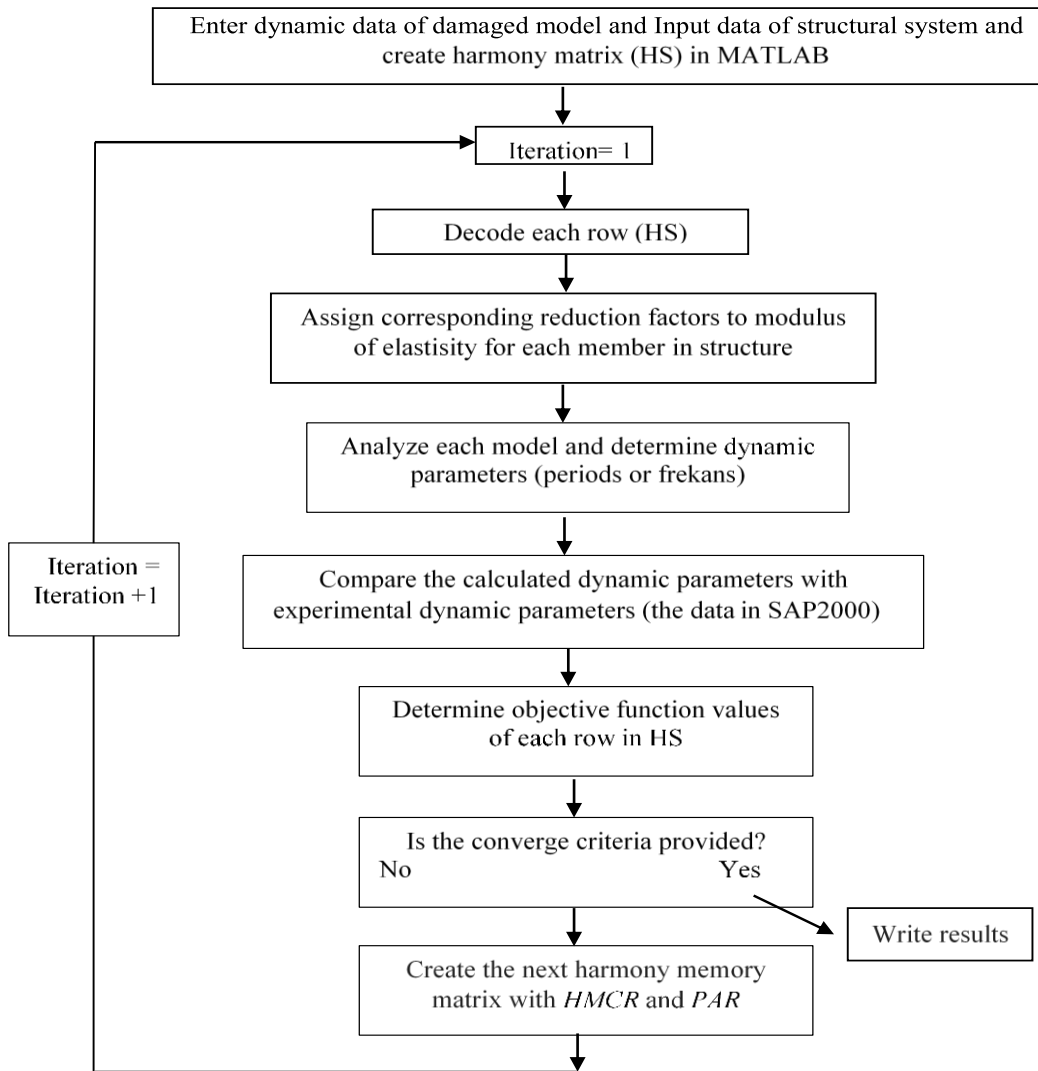


Fig. 1. Flowchart for the optimum solution procedures for damage detection in HS algorithm.

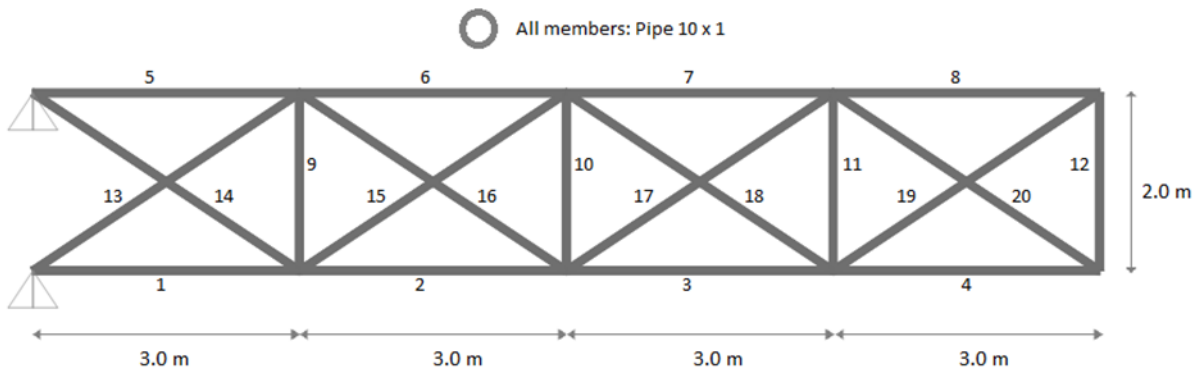


Fig. 2. 20-element steel plane truss.

Table 1. Natural frequencies (Hz)

Mode	Undamaged Case (Hz)		Case 1 member no.15: 50% damaged		Case 2 member no.11: 75% damaged	
	SAP2000	MATLAB	SAP2000	MATLAB	SAP2000	MATLAB
1	10.96797	10.9679	10.89275	10.8927	10.96797	10.9679
2	50.95267	50.9525	50.13671	50.1365	50.95267	50.9525
3	77.89691	77.8966	76.73378	76.7335	77.18673	77.1864

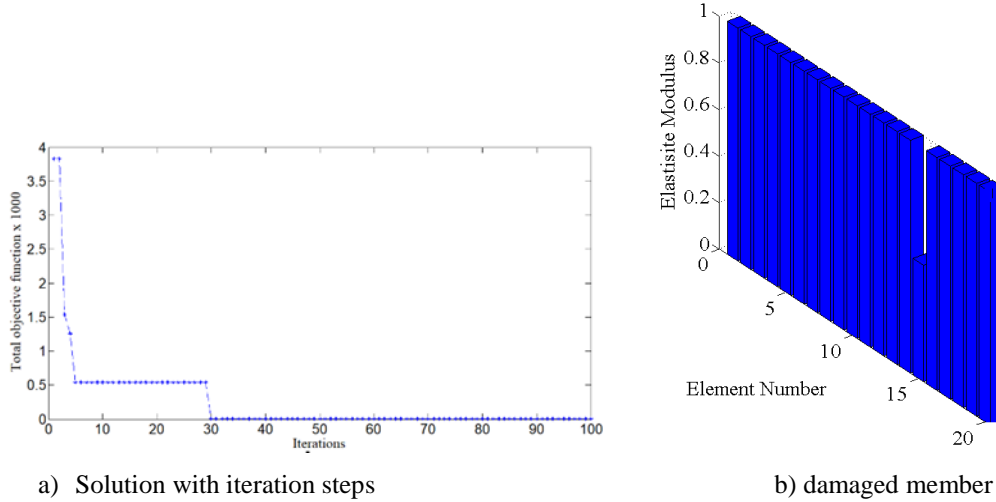


Fig. 3. Results for case 1

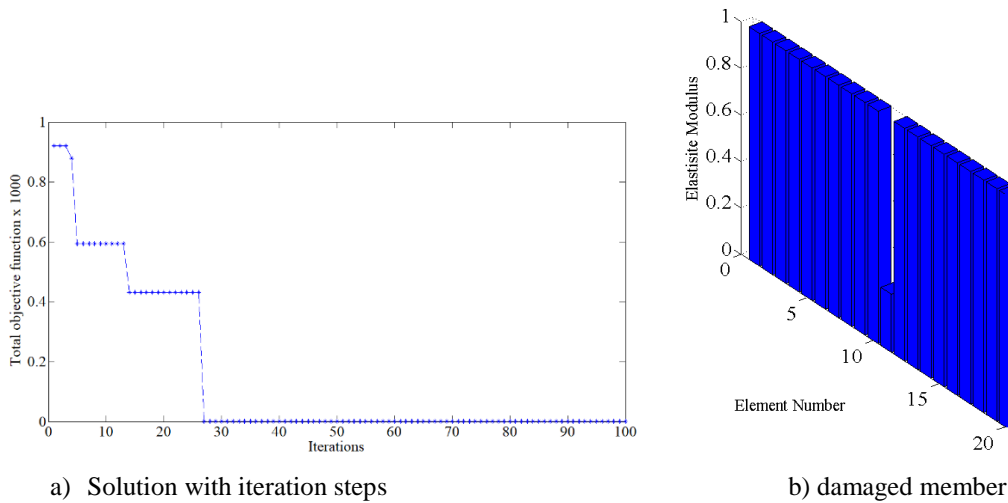


Fig. 4. Results for case 2

As presented in Table 1, the results of natural frequencies in MATLAB and SAP2000 programs are very close for first three modes in undamaged and damaged cases. In case 1, member no.15 has 50 % damage and the program using MATLAB is carried out around the 30th iterations as seen in Fig.3a. Fig. 3b proves that member 15 has 50% reduction in modulus of elasticity. Similarly, in case 2, member no.11 has 75% damage and the program coded in MATLAB is carried out at about the 30th iterations as shown in Fig.4b. Also, Fig. 4b presents that the member no.11 has 75% reduction in modulus of elasticity.

4.2. 33-Element steel plane truss bridge

Fig. 6 presents a 33-element steel plane truss bridge along with all the distances and sizes. The modulus of elasticity $E=2.00 \times 10^8$ kN/m² and material density $\rho = 7.85$ ton/m³. Two different damage scenarios with one and two damages are carried out. In case 1, member no.3 has 50% damage. In case 2, member no.3 has 50% and member no.14 has 25% damages. Table 2 presents the values of the first three natural frequencies obtained from MATLAB and SAP2000 software for undamaged and damaged cases. Fig 7 and 8 show solution figures for case 1 and case 2, respectively. Fig. 9 presents first three mode shape of undamaged model.

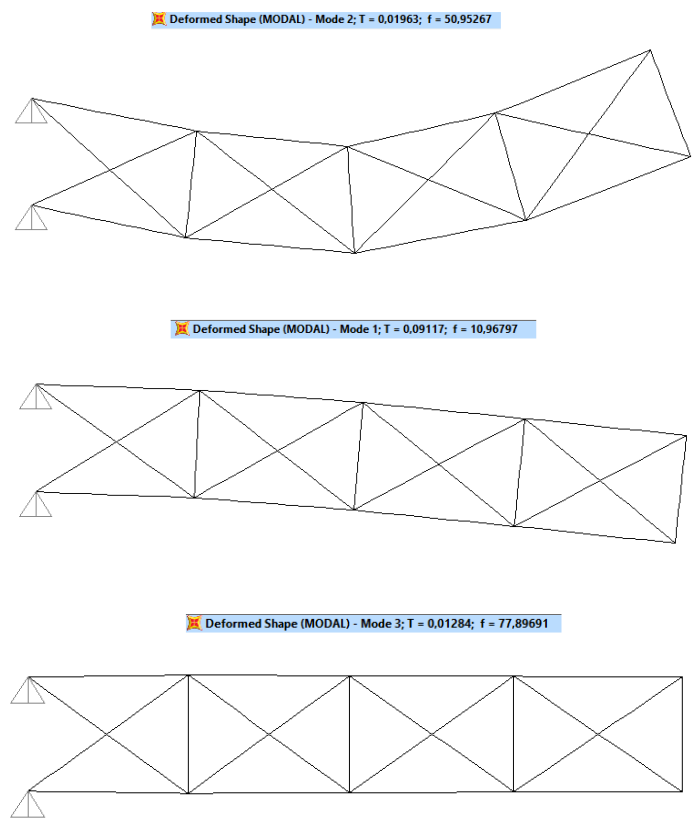


Fig. 5. First three mode shape of undamaged model

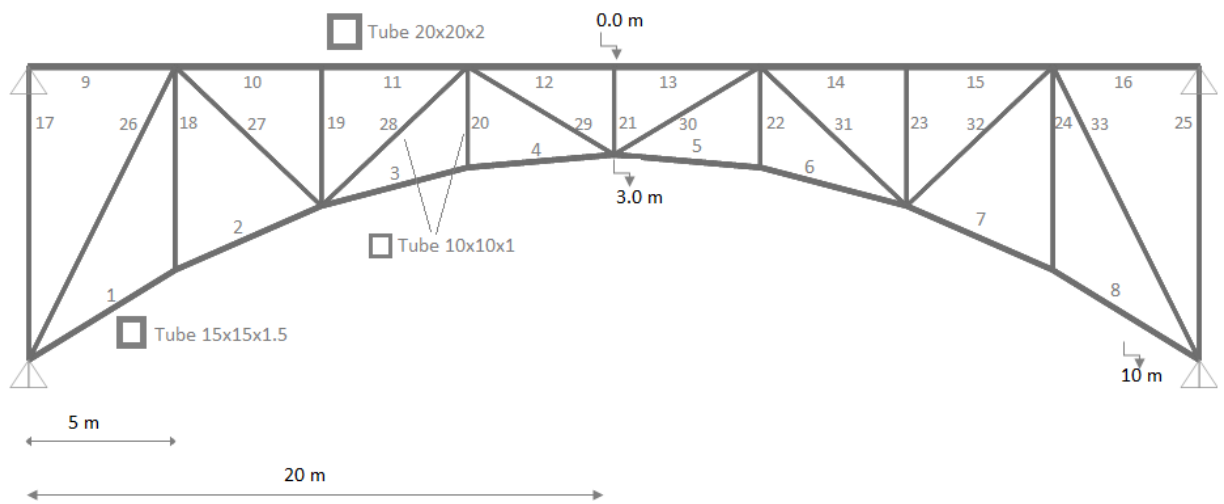
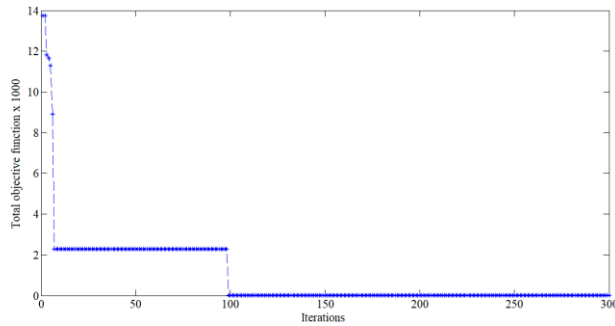


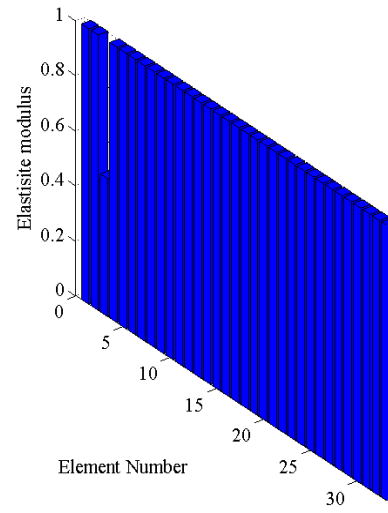
Fig. 6. 33-element steel plane truss bridge

Table 12. Natural frequencies (Hz)

Mode	Undamaged Case (Hz)		Case 1: One damaged member no.3 : 50% damaged		Case 2: Two damaged Case element no.3 : 50% and element no.14: 25% damaged	
	SAP2000	MATLAB	SAP2000	MATLAB	SAP2000	MATLAB
1	16.14925	16.1492	16.12883	16.1288	16.12673	16.1267
2	20.75732	20.7572	20.68065	20.6806	20.67982	20.6797
3	25.76528	25.7652	25.54086	25.5408	25.52803	25.5279

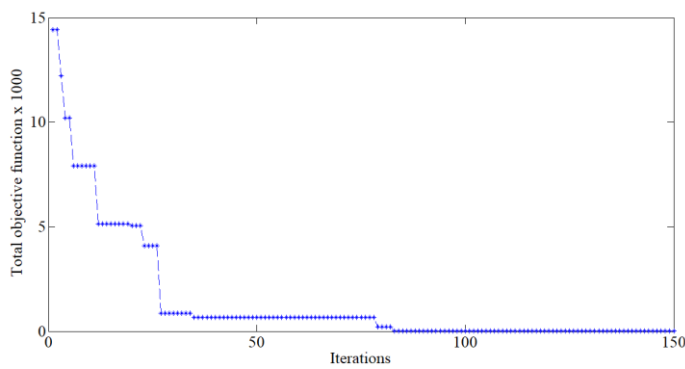


a) Solution with iteration steps

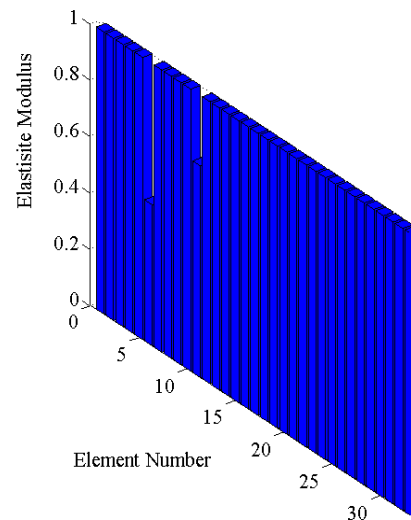


b) damaged member

Fig. 7. Results for case 1

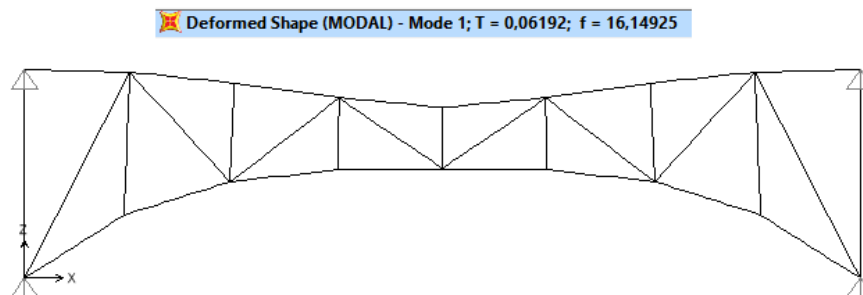


a) Solution with iteration steps



b) damaged member

Fig. 8. Results for case 2



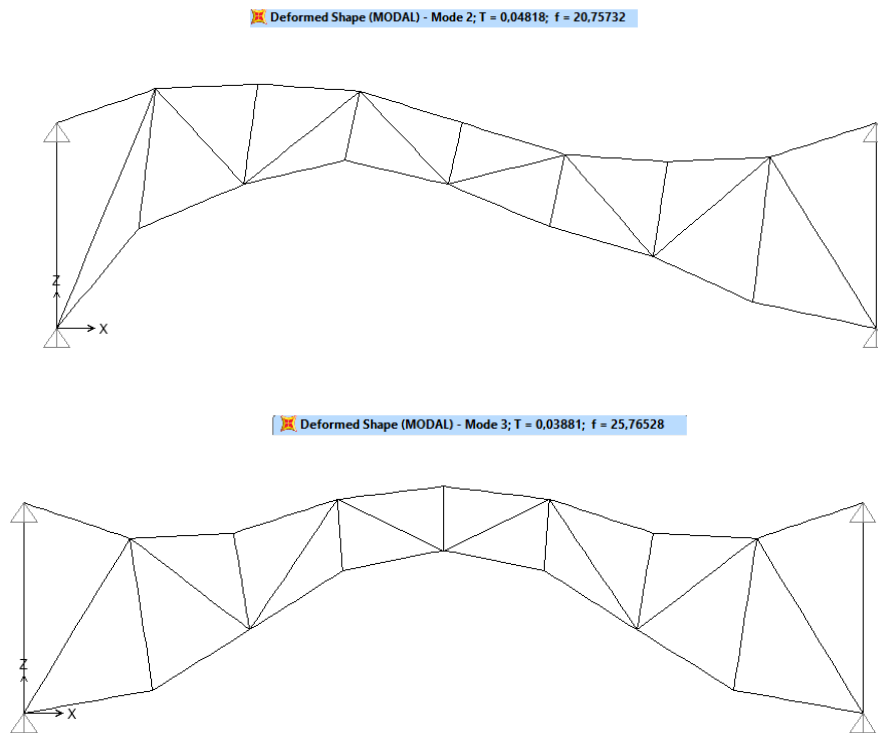


Fig. 9. First three mode shape of undamaged model

As it is observed from Table 2, the results of natural frequencies in MATLAB and SAP2000 programs are very similar for first three modes in undamaged and damaged cases. In case1, only member no 3 has 50% damage. Fig. 7a presents that solution of case 1 is carried out after 100 iterations and Fig. 7b proves that member no 3 has 50% reduction in modulus of elasticity in case 1. On the other hand, in case 2, member no.3 has 50% damage and member no.14 has 25% damage. Fig. 8a shows that solution of case 1 is obtained at about 85th Iterations. Also, Fig. 8b presents that member no.3 and member no. 14 has 50% and 25% reduction in their modulus of elasticity.

5. Conclusions

This paper presents a damage detection study on steel plane truss structures using harmony search algorithm. Two different examples having various damage scenarios are studied in SAP2000 software to obtain the experimental dynamic parameters. To determine the location and severity of damages, a program based on finite element method was coded in MATLAB programming. The scenario damages are tried to determine by approaching the dynamic values of the damaged model as a result of a series of iterations by using the program developed in MATLAB programming. Thus, the locations of simulated damages are determined by updated numerical model. In this study, a 20-element steel plane truss and a 33-element steel plane truss bridge are investigated for different damage cases. The results obtained from solutions prove that scenario damages on simulated plane truss structures are successfully

determined by using dynamic parameters. Also, the solutions indicate the robustness and applicability of harmony search algorithm method.

References

- [1] Lee, K.S. and Geem, Z.W. (2004), "A new structural optimization method based on the harmony search algorithm", *Comput. Struct.*, 82(9-10), 781-798.
- [2] Saka, M.P. (2009), "Optimum design of steel sway frames to BS5950 using harmony search algorithm", *J.Constr. Steel Res.*, 65(1), 36-43.
- [3] Değertekin, S.O., Hayalioglu, M.S. and Gorgun, H. (2009), "Optimum design of geometrically non-linear steel frames with semi-rigid connections using a harmony search algorithm", *Steel Compos. Struct., Int. J.*, 9(6), 535-555.
- [4] Değertekin, S.O. and Hayalioglu, M.S. (2010), "Harmony search algorithm for minimum cost design of steel frames with semi-rigid connections and column bases", *Struct. Multidisc. Optim.*, 42(5), 755-768.
- [5] Değertekin, S.O., Hayalioglu, M.S. and Görgün, H. (2011), "Optimum design of geometrically nonlinear steel frames with semi-rigid connections using improved harmony search method", *Mühendislik Dergisi, Dicle University, Department of Engineering*, 2(1), 45-56.
- [6] Toğan, V., Daloğlu, A.T. and Karadeniz, H. (2011), "Optimization of trusses under uncertainties with

- harmony search”, *Struct. Eng. Mech., Int. J.*, 37(5), 543-560.
- [7] Artar, M., (2016), A comparative study on optimum design of multi-element truss structures, *Steel and Composite Structures*, 22(3), 521-535.
- [8] Daloglu, A. T., Artar, M., Özgan, K. and Karakas, A. İ., (2016), Optimum design of steel space frames including soil-structure interaction, *Struct. Multidisc. Optim.* 54,117–131.
- [9] Artar, M., Daloglu, A. T. Optimum weight design of steel space frames with semi-rigid connections using harmony search and genetic algorithms, *Neural Comput & Applic*, DOI 10.1007/s00521-016-2634-8.in press.
- [10] Artar, M., (2016), Optimum design of steel space frames under earthquake effect using harmony search, *Structural Engineering and Mechanics*, 58(3),597-612.
- [11] B.A. Zarate, J.M. Caicedo, (2008), Finite element model updating: Multiple alternatives, *Eng. Struct.* 30, 3724-3730.

Optimum Design of Braced Steel Space Frames Using Teaching Learning Based Optimization

Ayşe T. Daloğlu*, Musa Artar**[‡], Korhan Özgan* and Ali İ. Karakaş*

*Department of Civil Engineering, Engineering Faculty, Karadeniz Technical University, 61000, Trabzon, Turkey

**Department of Civil Engineering, Engineering Faculty, Bayburt University, 69000, Bayburt, Turkey

(aysed@ktu.edu.tr, martar@bayburt.edu.tr, kozgan@ktu.edu.tr and alihsan.karakas@ktu.edu.tr)

[‡] Corresponding Author; Musa Artar, 69000 Bayburt Turkey, Tel: +90 458 211 11 77,

Fax: +90 458 211 11 78, martar@bayburt.edu.tr

Received: 08.09.2017 Accepted: 05.12.2017

Abstract- In this study, optimum design of braced steel space frames is obtained via a novel metaheuristic method, teaching learning based optimization. This algorithm method consists of the two basic phases. The first phase is called as teaching; In this phase, the knowledge interaction occurs between students and teacher. In the second phase, learning phase, the knowledge interaction occurs among students in the class. Optimum profiles are selected among 128 W taken from American Institute of Steel Construction (AISC). The constraints imposed on the frame example are stress constraints as stated in AISC-ASD specifications, geometric constraints and displacement constraints. To obtain optimum solutions, a program is coded in MATLAB programming to incorporate with SAP2000 - Open Application Programming Interface (OAPI). The results are compared through tables and figures. The results indicate that teaching learning based optimization method and MATLAB SAP2000 OAPI technique are applicable even for complex problems and present practical solutions.

Keywords Optimum design, teaching learning based optimization, braced steel space

1. Introduction

In this study, optimum design of a five story braced steel space frame is carried out. The cross sections for the structural members are selected from a list of 128 W profiles taken from AISC (American Institute of Steel Construction). A novel metaheuristic algorithm method, teaching learning based optimization method, is applied on analyses. A program was developed in MATLAB programming to interact with SAP2000-OAPI (Open Application Programming Interface) to get optimum solutions for X braced and unbraced cases of space frames. The stress constraints according to AISC-ASD specifications (American Institute of Steel Construction- Allowable stress design), geometric size (column-column and column-beam) constraints, top displacement and inter story drift constraints are applied to both solutions. The results are compared through tables and figures. The results obtained from the analysis show that teaching learning based optimization method and MATLAB SAP2000 OAPI technique are very applicable and robust for structural optimization of complex structures. Moreover, X braces provide a decrease in the minimum steel weight of space frames.

Teaching learning based optimum design is applied for the optimum design of structural systems as can be found in the literature. Rao et al. [1] studied teaching-learning-based optimization for constrained mechanical design optimization problems. Toğan [2] focused on optimum design of planar steel frames via this novel method. Rao and Patel [3] used this algorithm method for solving unconstrained optimization problems. Dede and Ayvaz [4] studied structural optimization by using teaching-learning-based optimization algorithm. Artar [5] studied optimum design of braced steel frames by using this algorithm method.

In this study, teaching learning based optimization is used for the optimum design of braced steel space frame. A program is developed in MATLAB [6] programming to interacted with SAP2000 [7] OAPI. The results evaluated are presented with the help of tables and figures. The results show that teaching learning based optimization method and MATLAB - SAP2000 OAPI technique is applicable and robust for even very complex structural optimization problems.

2. The Formulation of Optimum Design

The discrete optimum design for minimum weight of plane steel frames is calculated as below,

$$\min W = \sum_{k=1}^{ng} A_k \sum_{i=1}^{nk} \rho_i L_i \quad (1)$$

where W is the weight of the frame, A_k is cross-sectional area of group k , ρ_i and L_i are density and length of member i , ng is total number of groups, nk is the total number of members in group k .

$$\varphi(x) = W(x) \left(1 + P \sum_{i=1}^m c_i \right) \quad (2)$$

where P is a penalty constant, $\varphi(x)$ is objective function, c_i is constraint violations. The constraint violations are calculated as follows;

$$g_i(x) > 0 \rightarrow c_i = g_i(x) \quad (3)$$

$$g_i(x) \leq 0 \rightarrow c_i = 0 \quad (4)$$

The stress constraints according to AISC-ASD [8] specifications (American Institute of Steel Construction-Allowable stress design) are applied.

Geometric size (column-column and column-beam) constraints, are determined as below,

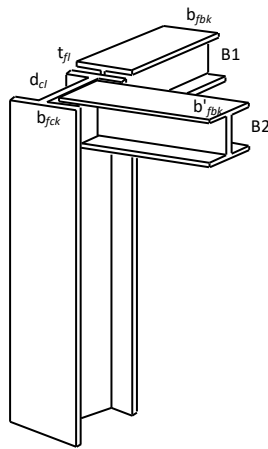


Fig. 1. Beam to column connection geometric constraints

Column-to-column geometric constraints are calculated as below,

$$g_n(x) = \frac{D_{um}}{D_{ln}} - 1 \leq 0 \quad n = 2, \dots, ns \quad (5)$$

where D_{um} is the depth of upper floor column, D_{ln} is the depth of lower floor column.

The beam-to-column geometric constraints are calculated as below,

$$g_{bb,i}(x) = \frac{b_{fbk,i}}{b_{fck,i}} - 1 \leq 0 \quad i = 1, \dots, n_{bf} \quad (6)$$

where n_{bf} is number of joints where beams are connected to the flange of column and are flange widths of the beam and column, respectively.

Displacement constraints are calculated as below,

$$g_{jl}(x) = \frac{\delta_{jl}}{\delta_{ju}} - 1 \leq 0 \quad \begin{matrix} j = 1, \dots, m \\ l = 1, \dots, nl \end{matrix} \quad (9)$$

where δ_{jl} is the displacement of j th degree of freedom under load case l , δ_{ju} is the upper bound, m is the number of restricted displacements, nl is the total number of loading cases.

Inter-storey drift constraints are calculated as below,

$$g_{jil}(x) = \frac{\Delta_{jil}}{\Delta_{ju}} - 1 \leq 0 \quad \begin{matrix} j = 1, \dots, ns \\ i = 1, \dots, nsc \\ l = 1, \dots, nl \end{matrix} \quad (10)$$

where Δ_{jil} is the inter-storey drift of i th column in the j th storey under load case l , Δ_{ju} is the limit value, ns is the number of storey, nsc is the number of columns in a storey.

3. Teaching Learning Based Optimization

Teaching learning based optimization is a novel metaheuristic algorithm method which is developed by Rao et al. in 2011. This algorithm method has two basic phases. In the first phase which is called teaching, the knowledge interaction occurs between students and teacher. In the second phase, learning phase, the knowledge interaction occurs among students in the class. The sharing of information provides a better solution. The first class as solution vectors is randomly prepared in matrix form as below,

$$\text{class}(\text{population}) = \begin{bmatrix} x_1^1 & x_2^1 & \dots & x_{n-1}^1 & x_n^1 \\ x_1^2 & x_2^2 & \dots & x_{n-1}^2 & x_n^2 \\ \dots & \dots & \dots & \dots & \dots \\ x_1^{S-1} & x_2^{S-1} & \dots & x_{n-1}^{S-1} & x_n^{S-1} \\ x_1^S & x_2^S & \dots & x_{n-1}^S & x_n^S \end{bmatrix} \rightarrow \begin{matrix} f(x^1) \\ f(x^2) \\ \dots \\ f(x^{S-1}) \\ f(x^S) \end{matrix} \quad (11)$$

In here, each row in matrix indicates a student and it gives a solution vector. S is the number of students in class, n shows the number of design variables, $f(x^1), f(x^2), \dots, f(x^S)$ are objective function value of each row in matrix form. In the class, the minimum objective function value represents the best information level. Thus, the student having the best objective value is assigned as the teacher of the class. The teacher shares his or her information with the other students as below,

$$x^{new,i} = x^i + r(x_{teacher} - T_F x_{mean}) \quad (12)$$

In here $x^{new,i}$ is the updated (new) student, x^i is the current (old) student, r is a random number in the range $[0,1]$, T_F , a teaching factor, is either 1 or 2. x_{mean} is the mean of the class is defined as $x_{mean} = (\text{mean}(x_1), \dots, \text{mean}(x_n))$. If the

new student has better information ($f(x^{new,i})$), the new student is replaced with the old student.

In the second step, learning step, the sharing of information occurs among students. Mentioned as below, if the new student has better information, it is replaced with the old student.

$$\text{if } f(x^i) < f(x^j) \Rightarrow x^{new,i} = x^i + r(x^j - x^i)$$

$$\text{if } f(x^i) > f(x^j) \Rightarrow x^{new,i} = x^i + r(x^j - x^i) \quad (13)$$

The flowchart of processes in MATLAB-SAP2000 OAPI developed to get optimum solutions are shown as below,

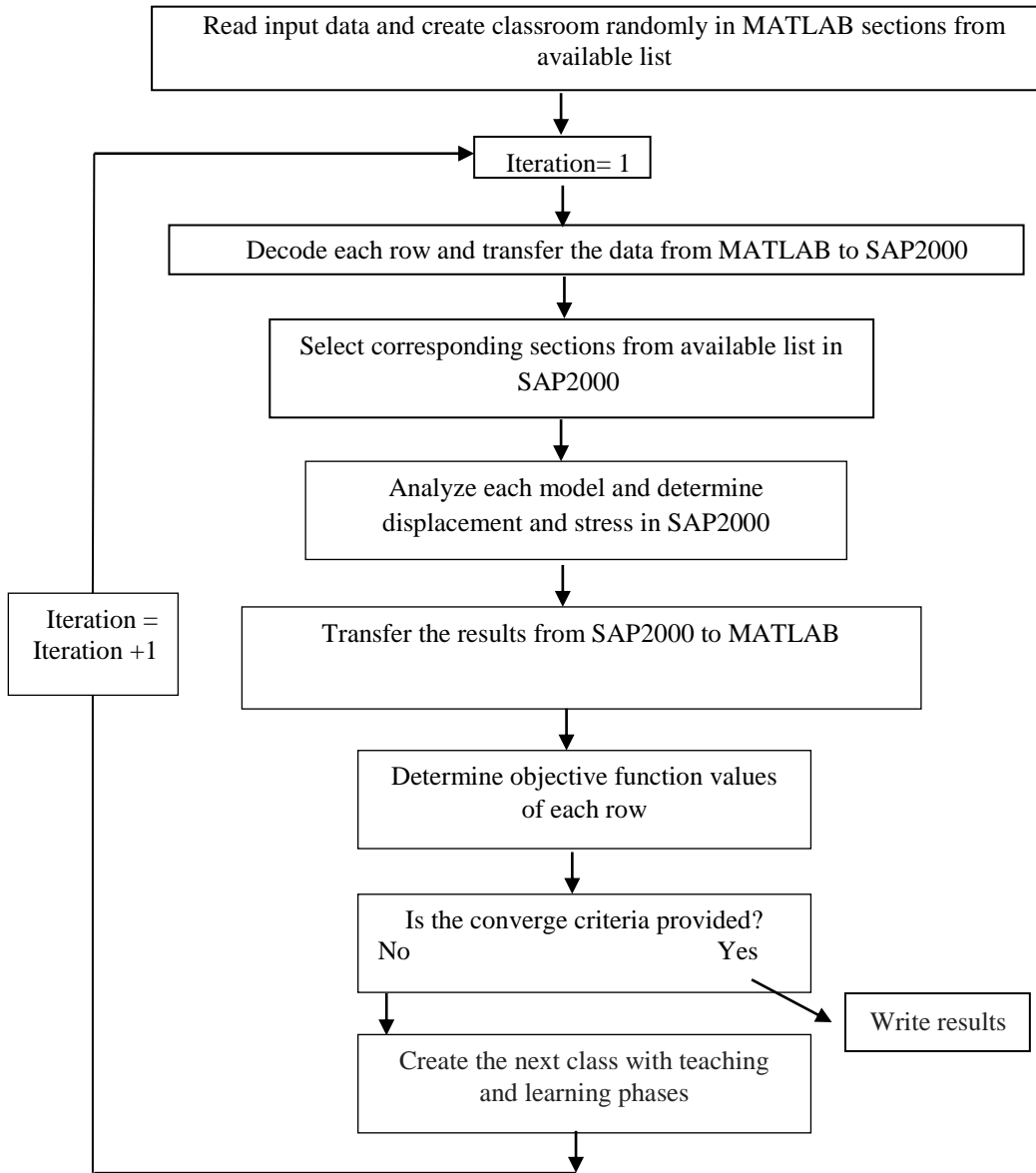


Fig. 2. Flowchart for the optimum design procedure of steel space frames

4. Design Example

A 5-storey braced and unbraced steel space frame is shown Fig.3. Moreover, in this figure the plan view, braced space frame and unbraced frame views are presented.

All members are collected in 19 groups as given in Table 1. According to ASCE7-05 [9], dead load (2.80 kN/m²) and live load (2.39 kN/m²) are applied. Wind load is exposed in X direction according to TS498 [10] as wind speed 30m/s. The top displacement and inter story drifts are restricted to

4.75 cm (H/400) and 0.95 cm (h/400), respectively. Optimum cross sections are selected from a specified list including 128 W taken from AISC. The material properties are E=200 GPa, fy=250 MPa and ρ=7.85 ton/m³. Optimum solutions for both cases are also given Table 2. Fig 4 presents the both optimum solutions with iteration steps.

As it is observed from Table 2 that the minimum weight of unbraced steel space frame is 504.79 kN. On the other hand, the minimum weight of X braced steel space frame is 377.18 kN. It is nearly %25 lighter. Also, significant

reduction is observed in cross sections. Moreover, in the solution of unbraced frame, the maximum lateral (top) displacement and inter storey drift values are 2.03 cm and

0.62 cm, respectively. These values are more than the values in X braced steel frame.

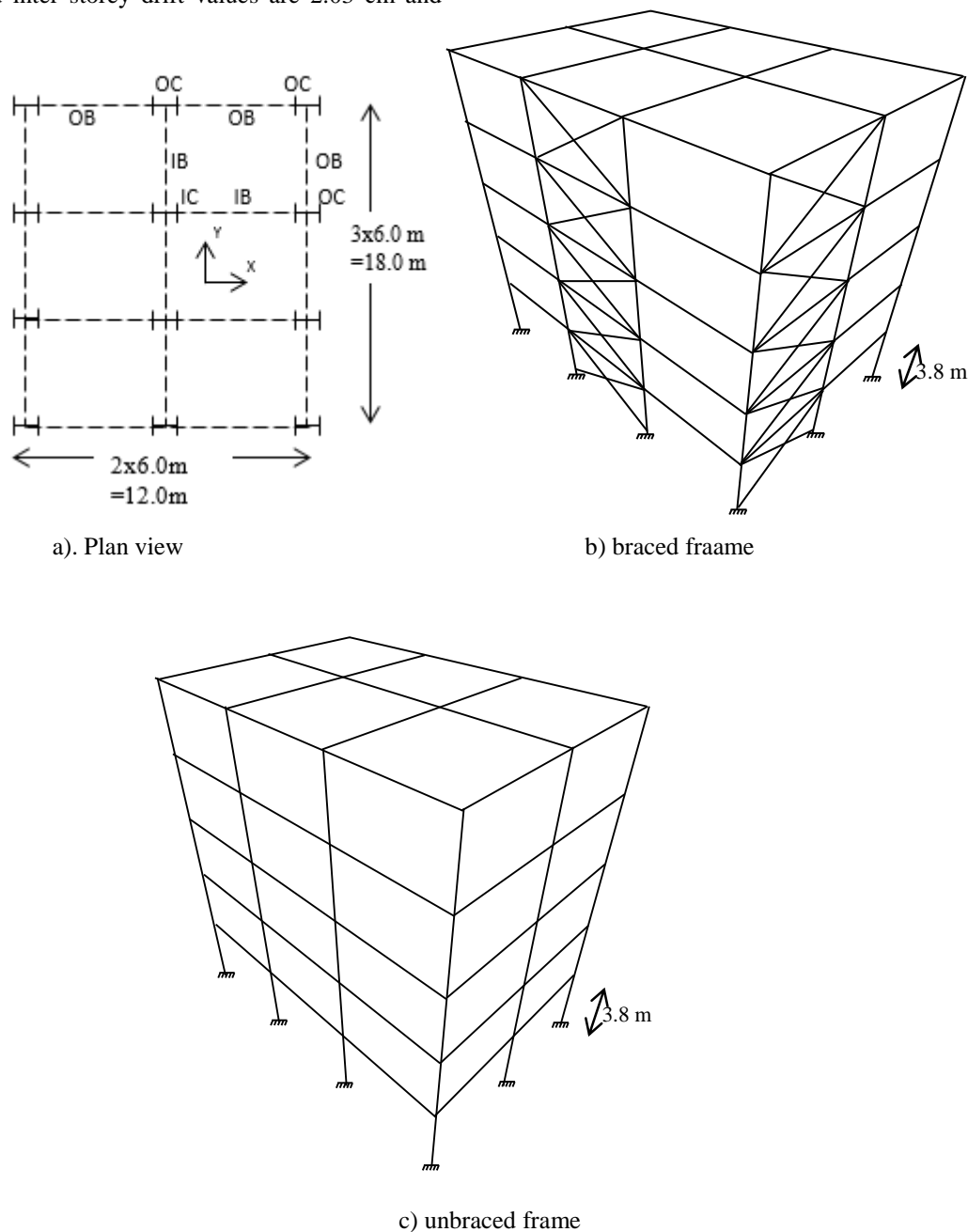


Fig. 3. A 5-storey braced and unbraced steel space frame

Table 1. Group member numbers

Floors	Outer column	Inner column	Outer beam		Inner beam		X Braced
			X direction	Y direction	X direction	Y direction	
1	1	2	7	8	9	10	19
2,3	3	4	11	12	13	14	19
4,5	5	6	15	16	17	18	19

Table 2. Optimum solutions of both cases

Group no	X braced	unbraced
1	W8X35	W30X148
2	W18X55	W44X285
3	W8X31	W18X65
4	W12X40	W18X55
5	W8X24	W12X65
6	W8X24	W16X45
7	W3X26	W8X24
8	W3X26	W6X20
9	W12X35	W8X31
10	W14X34	W8X31
11	W8X24	W12X30
12	W8X24	W8X24
13	W10X33	W16X45
14	W14X34	W14X34
15	W8X24	W12X26
16	W12X26	W6X20
17	W18X40	W21X50
18	W14X34	W8X31
19	W12X14	-
Weight (kN)	377.18	504.79
Max.lateral disp. cm	1.63	2.03
Max.inter storey drift cm	0.38	0.62

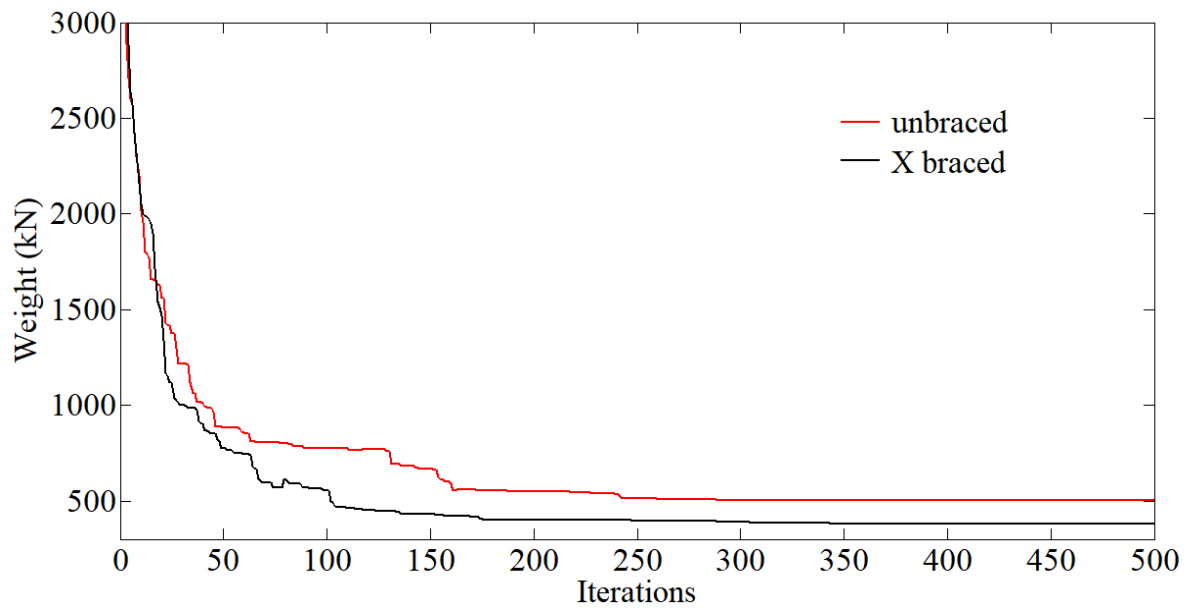


Fig. 4. Optimum solutions with iteration steps

5. Conclusions

This study presents optimum structural design of a five story steel space frame for X-braced and unbraced cases. The cross sections of structural members are selected from 128 W profiles taken from AISC (American Institute of Steel Construction). A new metaheuristic algorithm method, teaching learning based optimization method is used in the analyses. To obtain optimum solution, a program was coded in MATLAB programming to incorporate with SAP2000 OAPI (Open Application Programming Interface) simultaneously. The stress constraints according to AISC-ASD (American Institute of Steel Construction- Allowable stress design), geometric size (column-column and column-beam) constraints, top displacement and inter story drift constraints are applied to both solutions. According to optimum solutions, the minimum weight of X-braced steel frame is nearly %25 lighter than the minimum weight of unbraced frame. The results also show that teaching learning based optimization method and MATLAB SAP2000 OAPI technique are applicable and robust on structural optimization.

References

- [1] Rao, R.V., Savsani, V.J. and Vakharia, D.P. (2011), "Teaching-learning-based optimization: A novel method for constrained mechanical design optimization problems", *Computer-Aided Design*, 43(3), 303-315.
- [2] Togan, V. (2012), "Design of planar steel frames using teaching-learning based optimization", *Eng. Struct.*, 34, 225-232.
- [3] Rao, R.V. and Patel, V. (2013), "An improved teaching-learning-based optimization algorithm for solving unconstrained optimization problems", *Sci. Iran*. 20 (3), 710-720
- [4] Dede, T. and Ayvaz, Y. (2013), "Structural optimization with teaching-learning-based optimization algorithm", *Struct. Eng. Mech., Int. J.*, 47(4), 495-511.
- [5] Artar, M. (2016), "Optimum design of braced steel frames via teaching learning based optimization", *Steel Compos. Struct., Int. J.*, 22(4), 733-744.
- [6] [MATLAB (2009), *The Language of Technical Computing*; The Mathworks, Natick, MA, USA.
- [7] SAP2000 (2008), *Integrated Finite Elements Analysis and Design of Structures*; Computers and Structures, Inc., Berkeley, CA, USA
- [8] AISC-ASD (1989), *Manual of Steel Construction: Allowable Stress Design*, American Institute of Steel Construction, Chicago, IL, USA.
- [9] ASCE (2005), *Minimum design loads for building and other structures*, ASCE7-05, New York, NY, USA.
- [10] TS 498 (1997), *Turkish Standard: Design loads for buildings*, Ankara, Turkey.

Mucuna Pruriens as Photo-Sensitizer in Dye Sensitized Solar Cell

Charity Segun Odeyemi*[‡], Ayodeji Oladiran Awodugba**

*Department of Electrical Electronics Engineering, School of Engineering and Engineering Technology, Federal University of Technology P. M. B 704 Akure Nigeria

**Department of pure and Applied Physics, Faculty of Pure and Applied Sciences, Ladoke Akintola University of Technology P. M. B. 4000 Ogbomoso Nigeria

[‡]Corresponding Author; Odeyemi Charity Segun, Department of Electrical Electronics Engineering, Federal University of Technology P. M. B 704 Akure Nigeria. +234 806 643 9866, charityodeyemi@gmail.com

Received: 27.09.2017 Accepted: 05.12.2017

Abstract- In a dye sensitized solar cell (DSSC), the dye sensitizer plays important role in absorbing sunlight and transporting electrons into the conduction band of the semiconductor thus converting the solar energy into electric energy by photovoltaic effect. This study focus on the investigation made on the leaves and stem of *Mucuna Pruriens* extract as photosensitizers for dye sensitizer solar cell (DSSC). The DSSC was based on titanium dioxide nanopowder as the photoanode semiconductor material and potassium iodide solution as electrolyte. The pigment was extracted from dry leaves and stem of *Mucuna Pruriens* in water, ethanol and acetone. The photo absorption spectral of *Mucuna Pruriens* was investigated in cold and hot extraction media. Dye sensitized solar cell was fabricated using Michael Gratzel method. The cell was connected to a variable external load and exposed to illumination at 100mW/m². As the load is varied, the short circuit current I_{sc} and the corresponding open circuit voltage V_{oc} were observed. An *IV* characteristics was plotted and the fill factor and efficiency were computed as 0.8 and 0.37% for *Mucuna pruriens* extracted in water, 0.88 and 1.16% for *Mucuna pruriens* extracted in ethanol, 0.93 and 2.08% for *Mucuna pruriens* extracted in acetone respectively. The pigment extracted in cold acetone has the best light absorption and efficiency. This study shows that *Mucuna Pruriens* has prospect as sensitizer in DSSC.

Keywords Photosensitizer, Photoanode, Nanopowder, Mucuna Pruriens, Titanium dioxide.

1. Introduction

A Dye sensitized solar cell (DSSC) is a low cost solar cell which belongs to the thin film solar cell group [1]. It is a photo-electrochemical system which is based on a semiconductor formed between a photo sensitized anode and an electrolyte. The low cost material components, simple method of fabrication and availability of major materials have made DSSC receive much attention from researchers in recent time. DSSC also has the unique feature of having photon absorption and electrons transport carried out by different components of the cell [2]. This feature also allows each components of DSSC to be improved upon and possibly substituted for better performance of the cell without necessarily affecting the system structure. The main components of DSSCs are; the working electrode which is made of semiconductor oxide (TiO₂) on transparent conductive surface), the organic dye sensitizer, the electrolyte and the counter electrolyte.

A very good feature of dye sensitized solar cell is the fact that every stage and process is carried out by different component. On exposure to sunlight, the incident photons travel the transparent glass substrate (which is conductive on one side) of the working electrode to the dye. Depending on the colour of the pigment, light photons of certain wavelengths are absorbed. That is, not all incident photons are absorbed. The photo absorption capacity of a particular colourant is its light harvesting efficiency (LHE) [3]. The dye molecules therefore gain energy resulting in the liberation of electrons and the dye becomes oxidized. The liberated electrons travels through the TiO₂ to the conducting surface of the glass substrate of the working electrode. There is an external load connected across the working electrode and the counter electrode. These mobile electrons travel through the external load to the counter electrode and back to the system. The dye regains its lost electrons through the electrolyte and the electrolyte from the graphite coated surface of the counter electrode and the cycle continues.

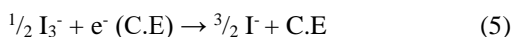
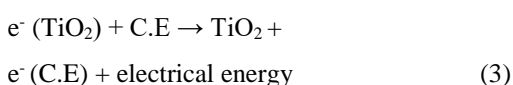
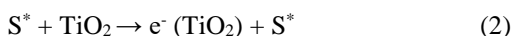
Although, the supply of the raw material which is sunlight is unlimited, the dye plays two major roles of photon absorption and release of electrons which are transported through the electrode to the conductor to produce electricity[4] & [5]. This process is represented in the equations (1) to (5):

If C.E = Counter Electrode

TiO₂ = Electrode

S = Dye

S* = Excited Dye



In producing a DSSC, the choice of the organic dye sensitizer is very crucial to obtain good light harvesting efficiency (LHE) which is a determinant of photo conversion efficiency[6]. Because of the importance of the role of dye in DSSC, efforts have been directed towards developing different organic dyes and metal complexes. Although most of these complexes have good absorbance, yet they suffer from the disadvantages of high cost and sophisticated method of preparation [6]. Hence, studies have been carried out on alternative organic pigments that will foster a good DSSC performance with cheap and easier method of preparation. The main features of a good sensitizer is good photo absorption, low cost, availability and environmental friendliness [7]. In this study, the photo absorption spectral of *Mucuna Pruriens* extract was observed and the extract also used to sensitize a titanium dioxide based DSSC.

Mucuna Pruriens (Velvet beans) is a tropical legume of West Africa origin. It is found in abundance in the Southern Nigeria. It belong plant family of *Fabaceae*. This climbing plant is notorious for the extreme itchiness it causes on contact especially with its young foliage and seed pods. Its seeds are used as soup thickeners while the leaves and stem of *Mucuna pruriens* are used for various medicinal purposes such as curing diseases like diabetes, arthritis, dysentery, and cardiovascular diseases[8]. Its extract is a very strong pigment which is used in the local African dye but has never been considered for any photovoltaic purpose. As shown in Table 1, previous research findings revealed that phytochemical compositions of Velvet beans (*Mucuna pruriens*) extracts possesses *Saponins* (a compound responsible for bitter taste), likewise *Terpenoids* (a phenolic compound that gives flavor and yellowish red dye). The

Table 1: Phytochemical composition of water and ethanol extracts of *Mucuna pruriens*.

Phytochemical	WMP	EMP
<i>Alkaloids</i>	-	-
<i>Saponins</i>	*	*
<i>Phlobatanins</i>	***	***
<i>Terpenoids</i>	*	*
<i>Tannins</i>	***	***
<i>Anthraquinones</i>	***	***
<i>Flavonoids</i>	**	**
<i>Cardiac glycosides</i>	*	*

*** Detected in abundant concentration

** Detected in moderate concentration

* Detected in slight concentration

- Not detected

extract is very rich in *Tannins* (a deep brown dye, also gives flavor), *Anthraquinones* (a strong dye with colours ranging from yellow to gray-green), *Flavonoids* (a plant dye with red, purple and blue colouration. It is also a phenolic compound), and *Phlobatanins* (a greenish black dye) [8].

2. Method

2.1. Extraction and Characterization of Dyes

The plant, *Mucuna Prurien* was collected Akure, a city in the south western Nigeria. The extraction of dye was done by Soxhlet extraction method. The plant part – leaves and stem were washed with distil water and dried at room temperature for about two weeks. After drying, the collections were crushed in a wooden mortal to smaller pieces which were further grounded in a ceramic mortal to almost powdery form. After grinding, about 25g of the sample was weighed into the chamber of the Soxhlet extractor. Before the extraction was carried out, the plant sample was defatted with N-Hexane in the extractor for about two hours to remove the plant fat and oil [9]. After these, the sample was dried and loaded into the extractor with 250ml of ethanol as the extracting solvent.

During extraction the solvent is heated to reflux and the solvent vapour travels up a distillation arm and floods into the chamber housing the thimble of solid. The condenser ensures that any solvent vapour cools, and drips back down into the thimble housing the solid material. The chamber containing the solid material slowly fills with warm solvent. Some of the desired compound dissolves in the hot solvent. When the Soxhlet chamber is almost full, the chamber is emptied by the siphon. The solvent is returned to the distillation flask. The thimble ensures that the rapid motion

of the solvent does not transport any solid material to the still pot. This cycle was repeated many times for six hours. The Soxhlet extraction method was also modified for cold extraction. The cold extraction was carried out by weighing 25g of the semi-powder sample and soaked in 250ml of n-Hexane for about 6 hours at room temperature. After that the mixture was stirred vigorously then separated by sheaving. Clean n-Hexane was further added and stirred and then sheaved out to remove the fat. The sample was allowed to dry at room temperature for about 3 hours. The defatted sample was soaked in 250ml of ethanol for 24 hours. After 24 hours, the mixture was stirred vigorously and the solid sheaved out. The remaining solution was filtered and dried at a room temperature in a dark room. Three extracting solvents namely; water, ethanol and acetone were used in this study. The pH of the extracted sample was analyzed using pH meter manufactured by Jenway Instrument Inc. Japan, model 3510. The spectrophotometric study was also carried out by scanning the pigment across visible and ultra violet region using computerized UV-Vis-Nir Spectrophotometer double beam model Shimadzu UV 1800 manufactured by Shimadzu.

2.2. Fabrication of Dye Sensitized Solar Cell

A self-assembled dye sensitized solar cell (DSSC) was fabricated using titanium dioxide as the semiconductor deposited on a transparent conductive glass substrate and the *Mucuna Pruriens* extract under study as the sensitizer. About 2g of nanoparticle Titanium dioxide was mixed with 8ml of Acetic Acid in a mortar while grinding with pestle to break the aggregates and to produce a uniform and lump-free suspension. A drop of surfactant, like colourless detergents in 1ml of distill water was then added. The conductive side of the electrode substrate tested with a continuity tester then cleansed with ethanol and two third coated with the Titanium dioxide paste using Doctor Blade technique [10]. This technique consists of a flat sharp object like a razor blade or a round thin object like a glass stirrer, which is used to lay a layer of slurry with a thickness determined by the spacer. The spacer is an adhesive tape normally with a thickness of 8-10 nm. It is placed opposite sides of the area where the film is to be laid and the doctor blade dragged across. After deposition, it was sintered at 450°C for 30 minutes. The electrode was then placed faced down in a filtered dye solution and allowed to soak the Titanium dioxide surface for about five minutes and then allowed to dry in a dark at room temperature. The conductive side of the counter-electrode was tested with continuity tester. The conductive surface was cleansed with ethanol, coated with graphite and gently placed face down on the Titanium IV Oxide coated part of the electrode so as to offset leaving one third uncoated conductive surface exposed on both the electrode and the counter electrode. They were then held firmly together with two alligator clips. Two drops of the electrolyte were introduced at one edge of the slides and allowed to spread by

capillary action. The assemblage was then tested with the electrode faced up for light photons collection as the positive terminal while the counter electrode will be the negative terminal connected to a digital multimeter. A highly sensitive and versatile digital multimeter from Fluke Instruments England was utilized to measure the open-circuit voltage (V_{oc}) and short-circuit photocurrent (I_{sc}) of the DSSC. A light intensity of 100 mW/m² was used to illuminate the solar cell. The conversion efficiency of the solar cell was computed by equation (6)

$$\eta = \frac{V_{oc} \times I_{sc} \times ff}{P_{in}} \times 100\% \quad (6)$$

3. Results and Discussion

At equal concentration, the UV-visible absorption spectral of *Mucuna pruriens* extracted in cold ethanol shows a stronger light absorption than the one extracted in a hot ethanol. The photo absorption occurred at wavelength range of 595 – 600 nm which is in the visible region of the electromagnetic spectrum ems [11] & [12]. The wavelength of maximum absorption (λ_{max}) is 535 nm. Cold extraction of *Mucuna pruriens* gave a stronger photo absorption than hot extraction as shown in Figures 1 and 2.

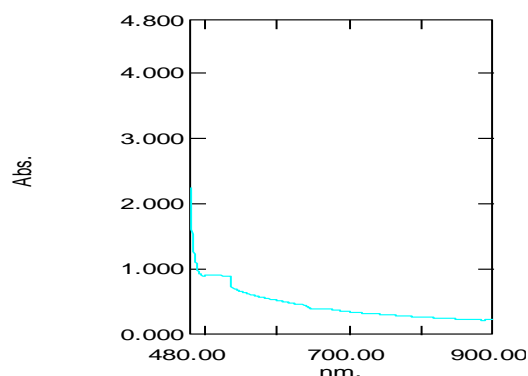


Fig 1. UV-vis absorption spectra of *Mucuna Pruriens* extracted in hot ethanol

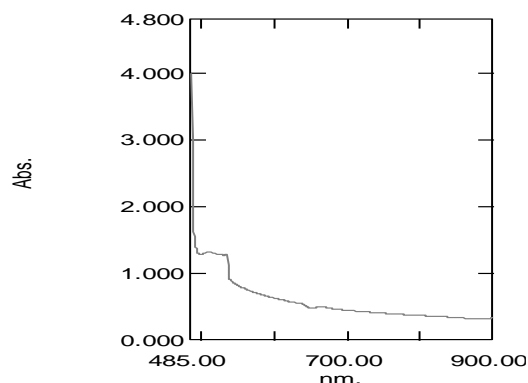


Fig 2. UV-vis absorption spectra of *Mucuna Pruriens* extracted in cold ethanol.

The results of the extracts obtained in three cold media – cold water, cold ethanol and cold acetone (Figures 2, 3 and 4). The absorption in water was very weak with no recognised peak. The UV-visible absorption spectral of *Mucuna pruriens* extracted in cold ethanol show a fairly strong peak of absorption at a wavelength range of 595 – 600 nm as shown in Figure 2. In Figure 4, the sample extracted in cold acetone shows very strong light absorption with three distinct absorption peaks. The photo-absorption covers a wavelength range of 590 – 690 nm which is in the visible region of the electromagnetic spectrum ems.

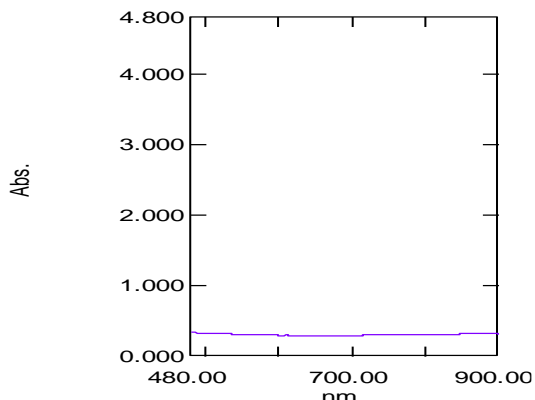


Fig 3. UV-vis absorption spectra of *Mucuna Pruriens* extracted in cold water.

The wavelengths of maximum absorption (λ_{max}) are 505, 535, and 640 nm. The light absorption fell in the green end of the electromagnetic spectrum while magenta is transmitted. The implication of this that *Mucuna pruriens* extracted in cold acetone was able to absorb light in a wider range of wavelength in the electromagnetic spectrum than

those of ethanol and water. Stronger absorption in cold acetone also shows that the *Mucuna pruriens* are highly non polar substances that dissolve better in strong non polar solvent like acetone. That is, *Mucuna pruriens* has a high photon harvesting efficiency which is a major determinant of the conversion efficiency of dye sensitised solar cell when it is extracted in cold acetone[7].

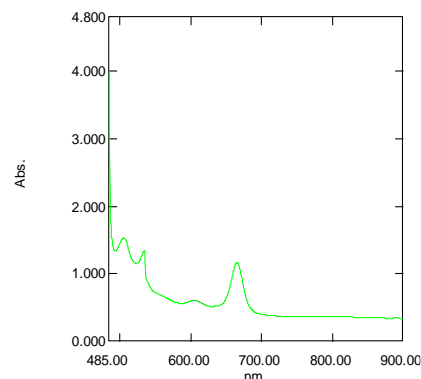


Fig 4. UV-vis absorption spectra of *Mucuna Pruriens* extracted in cold Acetone.

Mucuna Pruriens whose physico-chemical parameters were shown in Table 2, recorded better performance in term photon harvesting when extracted in acetone. The electrical measurement recorded from the solar cells fabricated using *Mucuna Pruriens* pigment extracted in cold water, cold ethanol and cold acetone are as shown in Table 3. An efficiency of 0.8% was recorded from the DSSC sensitized with cold water extracted *Mucuna Pruriens*, 1.16% from the DSSC sensitized with cold ethanol extracted *Mucuna Pruriens* and 2.08% efficiency from the DSSC sensitized with cold acetone extracted *Mucuna Pruriens*.

Table 2: The Physico-chemical properties of *Mucuna pruriens*.

Botani-cal Name	Engli-sh Name	Local Name (Yoruba)	Plant Part Utilized	Place of collect-ion (Nigeria)	Pigment's colour	Extraction medium	pH	Wavele-ngth of maxim-um absorption (λ_{max}) nm
<i>Mucuna Pruriens</i>	Velvet beans	Ijokun	Leaves & stem	Akure	Blueish-black	Water/ Ethanol/ Acetone	6.5	663

Table 2: The Physico-chemical properties of *Mucuna pruriens*.

Botanical Name	English Name	Local Name (Yoruba)	Plant Part Utilized	Place of collection (Nigeria)	Pigment's colour	Extraction medium	pH	Wave-length of maximum absorption (λ_{max}) nm
<i>Mucuna Pruriens</i>	Velvet beans	Ijokun	Leaves & stem	Akure	Blueish-black	Water/ Ethanol/ Acetone	6.5	663

Table 3: Electrical measurement from the DSSCs sensitized by the three extracts

Dye	$V_{oc(max)}$ (mV)	$I_{sc(max)}$ (mA)	FF	Efficiency (η)
<i>Mucuna Pruriens</i> extracted in Water	361.00	0.30	0.86	0.80
<i>Mucuna Pruriens</i> extracted in ethanol	385.00	0.30	0.88	1.16
<i>Mucuna Pruriens</i> extracted in Acetone	546.00	0.38	0.93	2.08

4. Conclusion

The conclusion The UV-visible absorption spectra of *Mucuna Pruriens* pigment extracted in different media consistently show its prospect as sensitizer in dye sensitized solar cell. However, cold extraction yielded stronger light absorption than hot extraction. The UV-visible absorption spectral and the efficiencies measured from the fabricated solar cells have consistently shown the potential of *Mucuna Pruriens* as dye sensitizer in dye sensitized solar cell. They also reveal that *Mucuna Pruriens* extracted in acetone is stronger in term of light absorption and consequently photon harvesting.

References

- [1] O. Adedokun, K. Titilope and O. A. Awodugba (2016): Review of natural dye sensitized solar cells (DSSC). International journal of engineering technologies. 2 (2), 34-41. (Article)
- [2] B. O'Regan, M. Gratzel (2012): Solar energy in dye sensitized solar cell. Journal of photochem. Photobiol. 3, 126-133. (Article)
- [3] U. Mehmood, S. Rahman, K. Harrabi, I. A. Hussein, and B. V. S Reddy (2014). Advances in Dye Sensitized Solar Cells. Advances in Materials Science and Engineering, (3) 7, 204. (Article)
- [4] C. Lung-Chien, H. Chih-Hung, C. Po-Shun, Z. Xiuyu and H. Cing-Jhih (2014). Improving the performance of dye-sensitized solar cells with TiO₂/graphene/TiO₂ sandwich structure. Nanoscale Research Letters (1) 9,380. (Article)
- [5] Institute for Chemical Education ICE (2012): Nanocrystalline Solar Cell Manual. Department of Chemistry, University of Wisconsin-Madison. 1101 University Avenue Madison, WI 53706 USA. 43 (Standards and Reports)
- [6] E. J. Khalil (2011): Dye Sensitized Solar Cells - Working Principles, Challenges and Opportunities. (1) 84. (Book)
- [7] J. Kawakita (2010): Trends of Research and Development of Dye-Sensitized Solar Cells. Science and Technology Trend, (2) 35, 46. (Article)
- [8] K. N. Agbafor, and N. Nwachukwu, (2011): Phytochemical Analysis and Antioxidant Property of Leaf Extracts of Vitex doniana and Mucuna pruriens. Biochemistry Research International, (2011), 4. (Article)

- [9] N. Biodun (1995): Dyes from plants, Jide publishing house Lagos, 88-89, 113-119. (Book)
- [10] A. O. Awodugba and A. O Ilayas (2013): Fabrication of Dye Sensitized Solar Cell (DSSC) using ZnO Nanoparticles Synthesized from Zinc Nitrate Hexahydrate. Canadian Journal of Pure and Applied Sciences, Academic Publishers, British Columbia (7) 3 2635-2638. (Article)
- [11] V. A. Popoola (2015): The chemistry of colours in dyes and pigments. Wits Publishing Ltd. 48-51. (Book)
- [12] R. M. Christies (2001): Colour chemistry, Royal society of chemistry, UK 172-177. (Book)

Mechanical Properties of Steel Fiber Reinforced Self-Compacting Concrete

Anıl Niş* ‡

* Department of Civil Engineering, Faculty of Engineering and Architecture, Istanbul Gelisim University, Istanbul, Turkey
(anis@gelisim.edu.tr)

‡ Corresponding Author, Anıl Niş, Department of Civil Engineering, Istanbul Gelisim University, Istanbul, Turkey
Tel: +90 212 422 7020, Fax: +90 212 422 7401, anis@gelisim.edu.tr

Received: 28.09.2017 Accepted: 12.01.2018

Abstract- In this study, steel fiber reinforced self - compacting concrete (SFR-SCC) specimens were examined by considering the effects of different parameters on the material performance and to promote the use of fiber materials in building industry. Use of steel fibers in SCC is still limited due to lack of required codes and standards in this field. More research is required to understand the effects of steel fibers on mechanical properties of the concrete. For this purpose, 5 mixes; control and reinforced with 2 different fiber volumes and two different fiber types; were produced. Compressive strength, splitting tensile strength and 3-point notched bending tests were carried out on these specimens for thoroughly evaluating mechanical performance of steel fiber reinforced self-compacting concretes.

Keywords Steel fiber reinforced self-compacting concrete, flexural toughness, ductility, three point notched bending, flexural strength.

1. Introduction

Self-compacting concrete (SCC) is widely used for construction of civil engineering structures, especially in pre-cast industries, high rise buildings and structures that need congested reinforcement. SCC technology achieved a significant breakthrough in construction industry with the three main advantages which are workability, flowability and passing ability. Thanks to these properties, concrete can be placed to complex shape moulds under its own weight without segregation and/or bleeding. During casting, energy consumption, labour works and construction time are reduced since external vibration is not required. SCC can flow between narrower openings easily; thus, reducing structural element sizes, formwork and material costs.

Plain concrete is a brittle heterogeneous material that is strong in compression conversely weak in tension and flexure. From the light of the structural steel reinforcement contribution to the tensile strength of concrete, steel fiber usage in concrete industry has also been developed recently. Steel fiber reinforced concrete has superior tensile and flexural performance with respect to plain concrete depending on the type and amount of the steel fibers. In addition to this, the role of crack bridging ability and crack

width control increases interest in using steel fibers in concrete, especially in the post-cracking phase. Most important contributions of the steel fibers into the concrete are increased toughness (area under the load-deflection curve) especially under flexural loading, increased tensile and shear strength capacity and modified crack formation mechanism. These important properties made fiber reinforced concrete popular in the research.

Steel fiber reinforced concrete (SFRC) has been used in both columns and beams where shear stresses are of critical and steel fibers have been partially used instead of stirrups as shear reinforcement. In high seismic zones, design codes impose the use of transverse reinforcements in order to obtain ductile behaviour and large amounts of transverse reinforcements are required especially in heavier structural elements. However, such congested reinforcements may cause concrete placement problem in narrower structural elements. The use of steel fiber can reduce the amount of transverse reinforcements and can be a solution for the concrete placement. In most situations, high amount of steel fiber reinforcement ($\geq 1\%$) is required to obtain better structural performance. However, such amount of steel fiber may also cause workability problem in concrete. A combination of steel fiber reinforced concrete with a self-

compacting concrete is used and defined as steel fiber reinforced self-compacting concrete (SFR-SCC) in order to obtain high flowability to solve workability and concrete placement problem [1].

SFR-SCC usage has many advantages in concrete industry. SFR-SCC has contributed to noise pollution, construction time and labour cost due to lack of external vibration. In nowadays, electric energy and labour costs become a significant part in the overall cost of the structure. However, SFR-SCC has not been used alone due to lack of structural design codes. It has been used with structural rebar (primary reinforcement) and steel fibers take place as secondary reinforcement in design phase. Structural applications of the SFR-SCC are; slabs and pavements, water tanks, channels, pipes, precast piles, precast walls, and blast resistance structures. SFR-SCC will be used more when steel fibers totally take place of the conventional steel reinforcement with further investigation [2]. In order to promote use of steel fiber, its effects on the mechanical properties of concrete should be further investigated.

1.1. Factors Influencing Mechanical Properties of SFR-SCC

Mechanical properties of SFR-SCC are influenced by concrete material components (cement, cementitious material and water amounts) and steel fiber characteristics (steel fiber type, amount and aspect ratio). The effects of the concrete material components to mechanical strength of SRF-SCC has already known in the concrete industry. However, the effect of steel fibers on the mechanical strength of concrete is required further investigation.

1.1.1. Influence of steel fiber type

There is a wide range of fiber types, steel fiber, synthetic fiber, glass fiber, natural organic and inorganic fibers; however, steel fibers are the most used fiber types in construction industry. Steel fiber performance is influenced by 3 different properties: (1) the aspect ratio (L/d) of the steel fiber; (2) steel fiber shape (straight, hook-end) and surface deformation; (3) surface treatment. Surface deformation is generally conducted in order to increase the anchorage between matrix and fiber. The used steel fibers have a circular cross section with a diameter changing from 0.2 mm to 1 mm, with a length varying from 10 mm to 60 mm and with an aspect ratio less than 100. For better bond between steel fiber and concrete matrix, steel fibers may be modified by surface and mechanical deformations [3].

For structural applications, straight and hooked-end type steel fibers have been widely used. Plain concrete goes into failure under tensile or flexural loading by formation of a single crack. However, steel fiber reinforced concrete resists additional crack openings and multiple cracks observed before the failure. This is due to two separate mechanisms: (1) when tensile stress on the concrete exceeds its tensile strength, micro-cracks start to emerge. The steel fiber has a capability of arrest the micro cracks and hence prevent the formation of macro-cracks (Micro-crack arrest mechanism); (2) for further stresses, micro-cracks widen and turn into macro cracks. After macro-crack formation, steel

fibers bridge the cracks and prevent further widening of the cracks (Crack bridging mechanism) [4].

1.1.2. Influence of steel fiber amount

SFR-SCC properties mainly depend on the steel fiber amount or fractions in the mixture. As the amount of steel fibers increases in the mix, flexural strength, shear strength and flexural toughness values are improved due to the enhancement in the ductility of the mix. In addition, tensile strength and crack opening displacement capacity of the concretes improve with an increasing steel fiber fractions (V_f). Inclusion of the high amount steel fibers especially improved the post crack residual tensile strength and ductility of the concretes [5].

Steel fiber content in a mixture generally ranges from 0.3 to 2%. For lower fiber amounts, impact of the fibers on the SCC concrete remains limited. For higher volume fractions than 2%, workability of the SCC reduces and passing ability problems emerge especially in the structures that high percentage structural reinforcement. In addition, steel fibers are expensive materials, usage of higher percentages may become costly. For economic considerations, optimum usage of the steel fibers is considered as 1% for the majority of structures [6].

1.1.3. Influence of steel fiber aspect ratio (l/d)

Fiber aspect ratio is the ratio of steel fiber length to diameter. In structural applications, l/d ranges from 50 to 100. Large fiber aspect ratio, representing a higher fiber matrix bond area that better bond is available between fiber and matrix and so high energy absorption capacity is obtained in the concretes. The fiber length is also another important factor for structural behavior of the SFR-SCC. Under same fiber aspect ratio, shorter fibers include larger number of fibers than longer fibers; which result in better crack bridging and stress transfer across the cracks [7].

From the light of the literature, two types of steel fibers (hook-end long and straight short), two different fiber volumes (0.5 % and 1 %) were selected considering economic aspects and different fibrous mixes were produced and mechanically tested to evaluate the mechanical performance of the SFR-SCC specimens.

2. Materials

2.1 SCC Materials and Mix Design

Ordinary Portland cement (CEM I 42.5R) and fly ash (F-Type) were used as binder materials with densities of 3.14 and 2.13 kg/dm³, respectively. A polycarboxylic ether based superplasticizer was used to obtain high flowability. As aggregates, natural sand, crushed sand and coarse aggregate with a maximum grain size (d_{max}) of 10 mm were used in the concrete mixture and aggregate densities were 2.60, 2.68 and 2.74 kg/dm³, respectively. Two types of steel fibers; hooked-end long fibers with fractions of 0.5% and 1%, straight short fibers with a fraction of 0.5% and hybrid fibers (combination of short and long fibers) with a fraction of 1% (0.5% short fiber + 0.5% long fiber) were used in the study. Straight short fibers have a length of 13 mm and

aspect ratio of 81 and hooked-end long fibers have a length of 35 mm and aspect ratio of 64. Preliminary experiments were conducted in order to obtain required flowability and stability. After reaching required control mix design with a water-to-cementitious ratio of 0.37, all other ingredients were kept constant while superplasticizer amount was changed with inclusions of different steel fiber types and fractions in

the other mixes. As a total, five different types of self-compacting concretes including steel hooked-end and straight fibers were produced as control mix, 0.5% long FRC mix, 1% long FRC mix, 0.5% short FRC mix and 1% hybrid (0.5% short + 0.5% long) FRC mix as can be seen in Table 1.

Table 1. Mix ingredients and SCC Mixes

Ingredients, (1m ³)	Batches for SCC (water to binder ratio: 0.37)				
	SCC 1 Control mix	SCC 2 0.5 % Long FRC Mix	SCC 3 1 % Long FRC Mix	SCC 4 0.5 % Short FRC Mix	SCC 5 1% Hybrid FRC Mix
Water (kg)	220	220	220	220	220
Cement (kg)	420	420	420	420	420
Fly Ash (kg)	180	180	180	180	180
Gravel<10 mm (kg)	636	636	636	636	636
Crush Sand (kg)	353	353	353	353	353
Sand (kg)	424	424	424	424	424
Steel Fiber (kg)	0	39	78	39	78
Superplasticizer (kg)	3.4	3.6	4.2	4.2	4.5

Mixing procedure was as follows; in the first stage, cementitious material (cement + fly ash) and aggregates added to the mixer and all dry ingredients without fibers were mixed for 2 minutes. After that water and superplasticizer added to the mixer in 1 minute duration and mixed for 1 more minute. Finally, steel fibers were added (for fiber-reinforced mixes) to the mixer in 1 minute and further mixed for 1 minute for homogeneity. For non-fibrous mixes, dry + wet ingredients were mixed for another 2 minute for equal mixing procedure with mixes including steel fibers. The overall mixing procedure was terminated in 6 minutes. After mixing, fresh state performances of the SCC mixes were evaluated and all of the mixes showed superior flowability characteristics, which was thoroughly investigated in the previous study [8].

2.2 Casting and Curing of Specimens

Prepared concrete mixes were cast to the moulds from one end of the specimen and left to flow to the other end. During casting, vibration and/or shaking was not applied to the specimens since concrete was flowing under its self-weight. Concrete surplus was taken by a trowel and

surface levelling was applied to all specimens. The specimens were demoulded after 24 hours and kept in a water tank at a temperature of 20 ± 2 °C for 28 day curing period time to obtain required strength for tests.

3. Experimental Program

3.1 Compressive Strength Tests

Force controlled compressive strength tests were carried out on 150x150x150 mm cube specimens according to TS EN 12390-3 [9] standard at the ages of 1, 7 and 28 days to measure material properties under compression. Specimens were axially loaded at a rate of 13.5 kN/s (0.6 MPa/s), Figure 1. The compressive strength of the cube specimen is calculated by dividing the maximum load reached during the compressive strength test by the cross-sectional area of the specimens. For all of the 5 different series, three cube specimens were tested for average values. Specimens were tested under force-controlled test.



Fig. 1. Compressive strength test

3.2 Splitting Tensile Strength Test

Splitting tensile strength tests were carried out on cylinder specimens with a diameter of 100 mm and a length of 200 mm at the 28-day in accordance with ASTM C496 /

C496 M-11 standard [10]. Specimens were transversely loaded at a rate of 0.5 kN/s (1 MPa / min) as is seen in Figure 2. Three cylinder specimens were cast for all of the 5 series of concretes for splitting tensile strength tests.



Fig. 2. Splitting tensile strength test

3.3 Three Point Bending Test on Notched Specimens

Three-point bending tests were employed on notched specimens to in order to evaluate bending behaviour of different SFR-SCC specimens. Two specimens were poured for each group, and as a total 10 specimens were produced in accordance with EN 14651 standard [11].

All specimens having widths and depths of 150 mm and lengths of 600 mm and notches were composed on the bottom of the specimens with a 4 mm width and 25 mm height as is seen in Figure 3. Specimens had a 125 mm effective height after notch and were tested under three point bending using MTS testing machine.

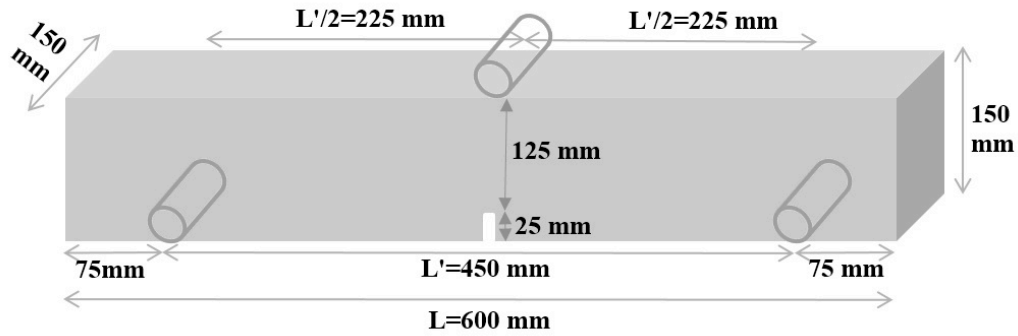


Fig. 3. Three point loading scheme

Based on the standard, three point flexural loading was applied in crack mouth opening displacement (CMOD) control at two different rates; CMOD rate was of 0.05 mm/min from zero to 0.1 mm CMOD, and was increased to 0.2 mm/min from 0.1 mm CMOD to 4 mm CMOD, Figure 4.

Experimental procedure was terminated when a CMOD value of 4 mm was reached. As a result of the tests, force versus CMOD curves of the SCC specimens was obtained and results were evaluated accordingly.

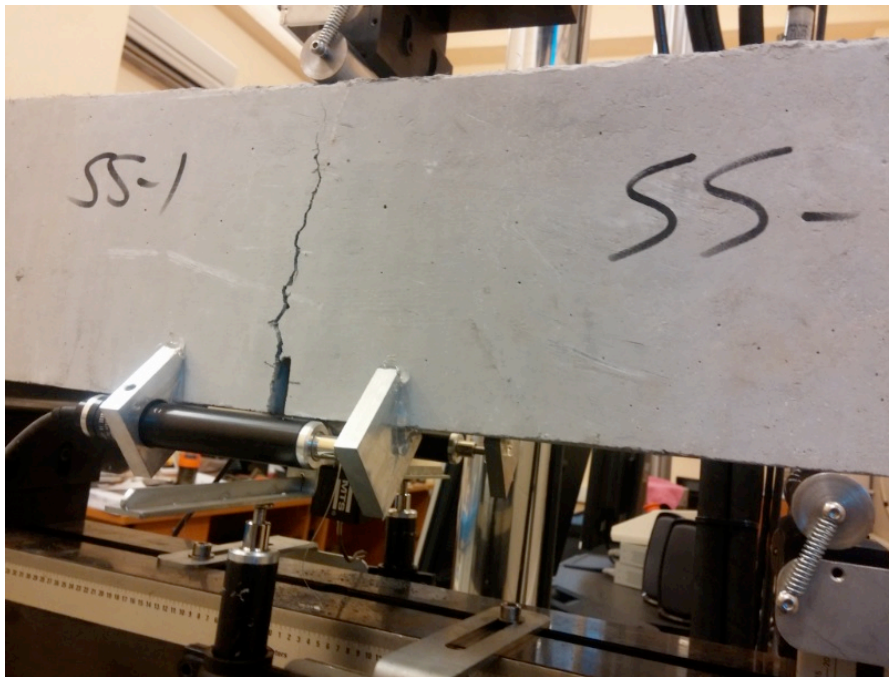


Fig. 4. CMOD controlled flexural loading

4. Results and Discussions

4.1 Compressive Strength Test Results

Compressive strength test results of the cube SCC specimens were determined at the ages of 1, 7 and 28 days as is given in Table 2. Results indicated the average of the three specimens for each mix. Compressive strength values ranged from 19 MPa to 24.5 MPa, 44.5 MPa to 50 MPa and 57.5 MPa to 62 MPa at the ages of 1,7, and 28 days, respectively. Increase in compressive strength values was found when fibers were added. The extent of increase was around 2-3 % when 0.5 % short and long fibers were added, while 6-7 %

increase was observed for 1.0 % long and hybrid fiber added specimens.

4.2 Splitting Tensile Strength Results

Splitting tensile strength results showed that steel fibers have a significant influence on splitting tensile strength of concrete especially for high steel fiber fractions ($\geq 1\%$). For 0.5 % long and short fiber reinforced SCC specimens, splitting tensile strengths increased up to 5 % and 13 %, respectively, whereas for 1 % long and hybrid fiber reinforced SCC specimens, splitting tensile strength increased up to 83 % and 55 %, respectively as is seen in Table 3.

Table 2. Compressive strength values of concretes

SCC specimens	Compressive Strength (MPa)		
	1 st day	7 th day	28 th day
Control (Non-Fibrous)	20.72	44.47	57.75
0,5 % Long FRC	19.01	48.06	59.23
0,5 % Short FRC	20.44	47.79	58.92
1 % Long FRC	23.46	47.53	61.98
1%Hybrid FRC (0,5%S+0,5%L)	24.53	50.05	61.18

4.3 Three Point Bending Test Results

Three-point bending tests results on notched specimens indicated that SFR-SCC specimens showed higher load bearing and displacement capacity when compared to plain concretes as can be seen in Figures 5 to 8. The reason

of the sharp decrease in the load was resulted from the CMOD controlled loading. In Figures 5 and 6, maximum flexural load was around 20 kN for control specimens; whereas maximum flexural load ranged from 23 kN to 32 kN, 26 kN to 33 kN for 0.5 % long and short FRC specimens, respectively. In Figures 7 and 8, maximum flexural load ranged from 44 kN to 48 kN, 45 kN to 47 kN for 1 % long and hybrid FRC specimens. Area under the load – CMOD curve (toughness) was highest for 1% fiber reinforced mixes and lowest for the control specimens.

Table 3. Splitting tensile strength results of concretes

Specimens	Splitting Tensile Strength (28 day) (MPa)
Control (Non-fibrous)	4.14
0.5 % Long FRC	4.35
0.5 % Short FRC	4.67
1 % Long FRC	7.57
1% Hybrid FRC (0.5%S+0.5%L)	6.39

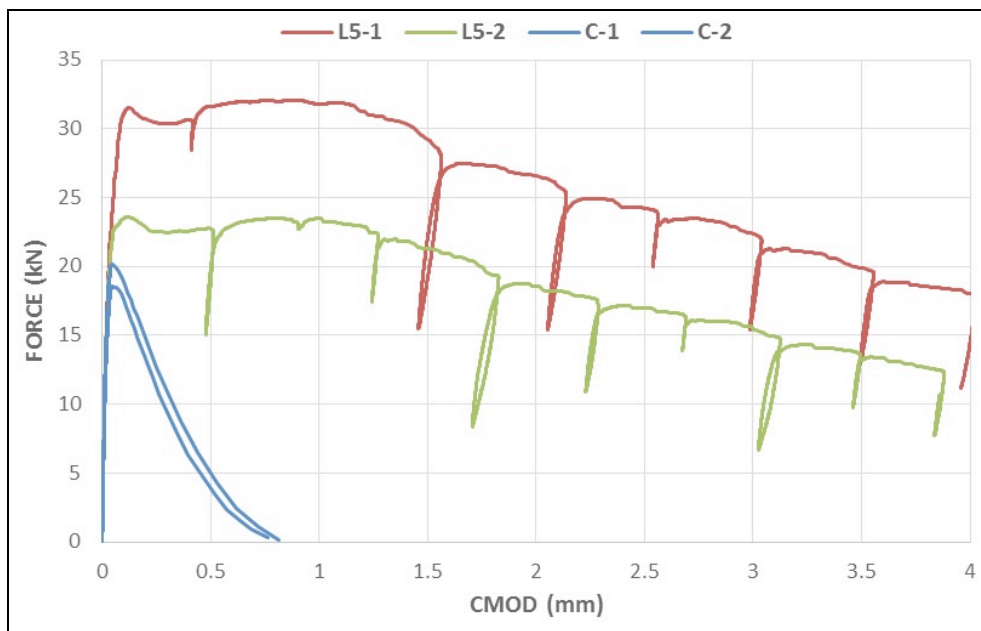


Fig. 5. Experimental results of 0.5% long FRC specimens (L5) and control (C) specimen

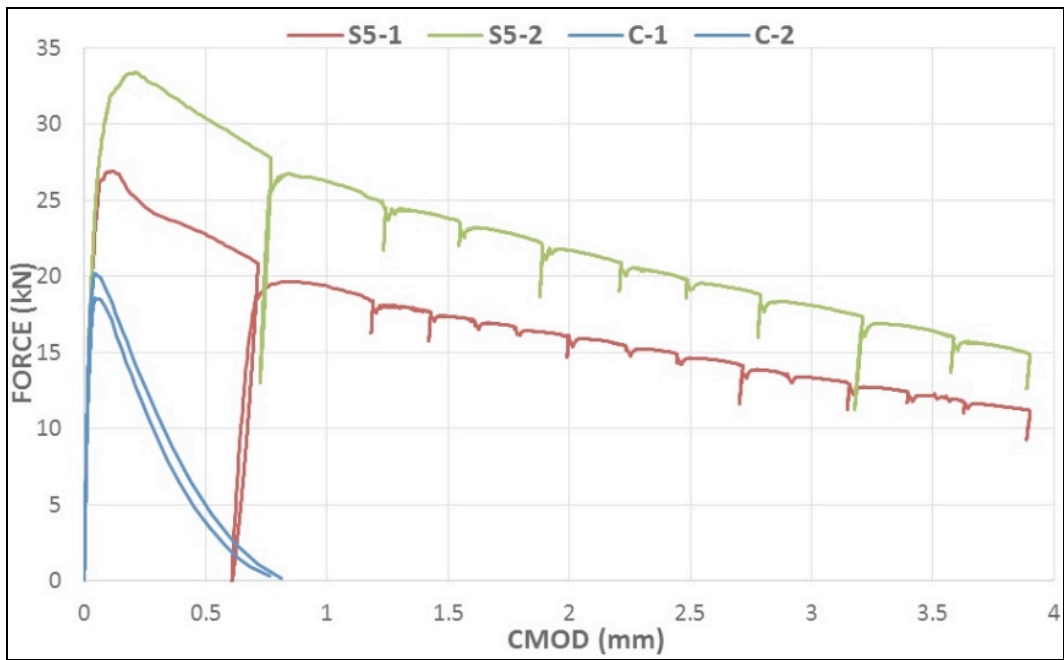


Fig. 6. Experimental results of 0.5% short FRC specimens (S5) and control (C) specimens

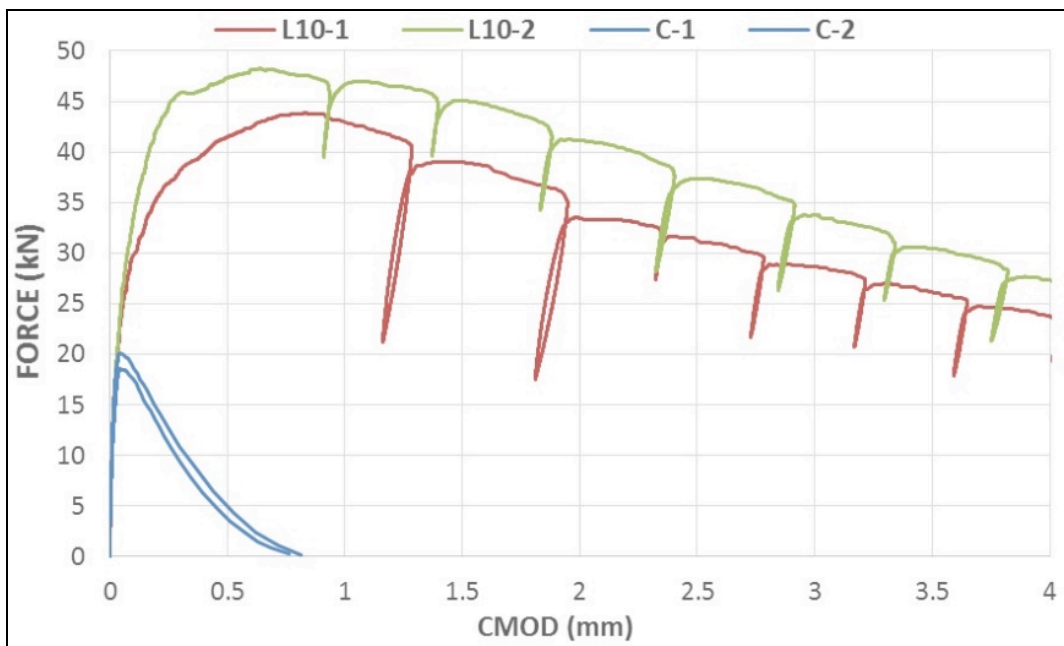


Fig. 7. Experimental results of 1% long FRC specimens (L10) and control (C) specimens

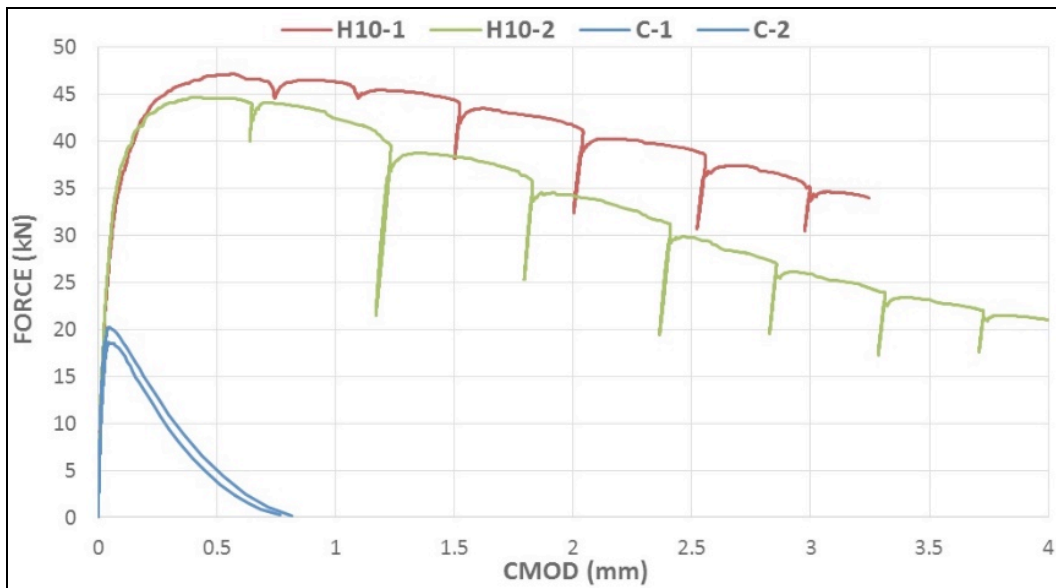


Fig. 8. Experimental results of 1% hybrid FRC specimens (H10) and control (C) specimens

5. Conclusion

Compressive strength, splitting tensile strength and 3-point notched bending tests were carried out on different SFR-SCC specimens and following conclusions were drawn:

Steel fiber addition to the SCC mixes slightly increased the compressive strength compared to plain mix. The extent of the increase was higher for 1% fiber – reinforced mixes.

Steel fibers were found to have a significant influence on splitting tensile strength of concrete, especially for high steel fiber fractions ($\geq 1\%$). Low amount of steel fibers (0.5%) had no or little contribution to splitting tensile strength results.

Maximum flexural load increased with an increase in steel fiber volumes of SCC specimens. Long and hybrid fibrous specimens with a fiber volume of 1% were found to show the best performance by means of flexural strength and toughness. However, lower amounts of steel fiber addition into SCC improved ductility of SCC specimens significantly as compared to plain SCC specimens. It can be also concluded that steel fiber volume improved flexural strength and toughness more than steel fiber type and aspect ratio.

References

[1] Aoude H., “Structural behaviour of steel fiber reinforced concrete beams”, PhD Thesis, McGill University, Montreal, Quebec, Canada, 2007.
[2] Cunha V. M. C. F., “Steel Fibre Reinforced Self-Compacting Concrete”, PhD Thesis, University of Minho, Braga, Portugal, 2010.
[3] Löfgren I., “Fibre Reinforced Concrete for Industrial Construction”, PhD Thesis, Chalmers University of Technology, Gothenburg, Sweden, 2005.

[4] Mpegetis S. O., “Behavior and Design of Steel Fiber Reinforced Concrete Slabs”, PhD Thesis, Imperial College London, London, United Kingdom, 2012.

[5] Kooiman A.G., “Modelling Steel Fibre Reinforced Concrete for Structural Design”, PhD Thesis, Delft University of Technology, Delft, Netherlands, 2000.

[6] Prisco M.D., Felicetti R., Iorio F. and Gettu R., “On the Identification of SFRC Tensile Constitutive Behaviour”, *Fracture Mechanics of Concrete Structures*, Vol.2, No.1, pp.541-548, 2001.

[7] Luo J.W., “Behavior and Analysis of Steel Fibre - Reinforced Concrete under Reversed Cyclic Loading”, PhD Thesis, University of Toronto, Toronto, Ontario, Canada, 2014.

[8] Niş A., Özyurt N., and Özturan T., “Fresh State Properties of Steel Fiber Reinforced Self-Compacting Concretes with Various Fiber Volumes”, ACE Conference, 2016.

[9] TS EN 12390-3, “Testing Hardened Concrete - Part 3: Compressive Strength of Test Specimens”, 2003.

[10] ASTM C496/C496 M-11, “Standard Test Method for Splitting Tensile Strength of Cylindrical Concrete Specimens”, 2011.

[11] EN 14651, “Test Method for Metallic Fibered Concrete – Measuring the Flexural Tensile Strength (Limit of Proportionality (LOP), Residual)”, European Standard, 2005.

Mechanical Properties of Aluminum–4043/Nickel-coated Silicon Carbide Composites Produced via Stir Casting

Peter Kayode Farayibi*, Basil Olufemi Akinnuli*, Sylvester Ogu**

*Department of Industrial and Production Engineering, Federal University of Technology, Akure, PMB 704, Ondo State, Nigeria

**Department of Mechanical Engineering, Federal University of Technology, Akure, PMB 704, Ondo State, Nigeria
(pkfarayibi@futa.edu.ng, boakinnuli@futa.edu.ng, onyekasyvester@yahoo.com)

‡ Corresponding Author. Department of Industrial and Production Engineering, Federal University of Technology, Akure, PMB 704, Ondo State, Nigeria, Tel: +234 906 659 0609,

pkfarayibi@futa.edu.ng

Received: 18.09.2017 Accepted: 02.07.2018

Abstract- In this study, Al-4043/Ni-coated SiC composite was developed via stir casting process and the mechanical properties of the composites investigated. The composites were produced with varying SiC reinforcement fraction between 5-25 wt%. The microstructure of the composites was characterized using optical microscope and tensile properties of the composite with the monolithic Al-4043 alloy were assessed using a universal testing machine. The composite hardness was assessed using a Brinell hardness testing machine, energy required to break the composite was assessed using Charpy impact testing machine and the wear rate of the composites were evaluated using a Rubin Disc machine. The composites were characterized to possess Al-SiC eutectic microstructure with SiC solid solution precipitates and SiC particles uniformly distributed in the Al matrix. The density of the composites was found to linearly increase with increasing SiC reinforcement fractions. The tensile strength, yield strength and elastic modulus were found to increase with increasing SiC reinforcement fraction and highest values obtained for composite with 25 wt% SiC were 350 MPa, 254 MPa and 13.4 GPa respectively. However, the elongation of the composite with the highest reinforcement was lowest at a value of 10%. The hardness, compressive strength and impact energy of the composites increased significantly as composite with 25 wt% SiC possessed 76 HB, 184 MPa and 48 J respectively. The wear resistance of the Al-4043/SiC composites with highest SiC reinforcement was found to be eleven times that of the monolithic Al-4043 alloy.

Keywords Metal Matrix Composite, Aluminum, Silicon carbide, Nickel coating, Mechanical properties, Wear, Hardness, Impact.

1. Introduction

Advances in technology has placed a demand on the development of novel engineering materials which would possess high strength to weight ratio, excellent toughness, high wear- and corrosion-resistant properties such that these materials can easily replace heavy ferrous alloys in automobile, aerospace, turbomachinery, nuclear, defence and other industrial applications. For example, in automobile industries, the reduction of fuel consumption as well as greenhouse gas emissions is of great concern and can be

achieved through the use of light metal alloys or composites for the development of some vehicle parts such as engine block, piston, connecting rod, brake disc, and car bodies amongst others. In light of this, Natarajan *et al.* [1] proposed the use of Aluminum metal matrix composites as brake disc material to replace the conventional grey cast iron. Metal-Matrix composites, especially the particulate reinforced ones, have been reported as a suitable material for various engineering applications where high stiffness-to-weight ratio, significant weight reduction, improved wear resistance and high thermal stability are desired when compared to

unreinforced monolithic alloy [2,3]. Aluminum-silicon carbide (Al-SiC) composites have been found promising as engineering structural materials owing to its excellent properties and are produced via either solid phase (powder metallurgy, hot isostatic pressing etc) or liquid phase (squeeze casting, stir casting etc) processing routes. These Al/SiC composites are being developed using different Al alloys as matrix and are subjected to both microstructural examination and mechanical tests.

In a recent study, Moses *et al.* [4] developed Al-6061/SiC composites with varied SiC content from 5-15 wt.% using stir casting approach and examined the microstructure and mechanical properties of the composites. It was reported that the presence of the SiC reinforcement in the composites improved the microhardness to 105 HV and tensile strength to 220 MPa as recorded for composite with 15 wt.% SiC. In another similar study, Balasubramanian and Maheswaran [5] investigated the mechanical resistance behavior of AA6063/SiC composites with reinforcement fraction ranging 5-15 wt.% SiC produced via stir casting, and observed an increased resistance against indentation with 860 N/mm² as highest hardness value and tensile load with 175 MPa as highest tensile strength for the highest reinforcement fraction. The examination of the composites under SEM revealed that the addition of SiC initiated cleavage facets and led to brittle fracture when subjected to tensile forces with minimal elongation, and low material removal under sliding load. Rahman and Rashed [6] investigated the microstructure, mechanical properties and wear characteristics of as-cast Al/SiC composites with varied SiC composition ranging 5-20 wt.%. It was reported that maximum hardness of 45 HV and tensile strength of 77.6 MPa were obtained from composite possessing 20 wt.% SiC reinforcement and also had the lowest cumulative mass loss during wear experiment. Selvam *et al.* [7] fabricated Al MMC reinforced with varying fractions of SiC and Fly ash with addition of magnesium during a modified stir casting technique and the wetting of the SiC and Fly ash particles was enhanced by the presence of the magnesium. The addition of the Fly ash was reported to have prevent the dissolution of the SiC_p and formation of Al₄C₃, and the hardness and tensile strength of the Al matrix were significantly improved with increase in reinforcement fraction employed. In another study, Anand and Gowda [8] disclosed, upon fabrication of Al MMCs with varying SiC reinforcement fractions, that the composite hardness, tensile strength and compressive strength improved with increasing SiC wt.% reinforcement fraction with highest values of tensile strength 136 MPa, compressive strength 656 MPa and hardness 68 HB reported for Al MMC with 8 wt.% SiC reinforcement. Hassan *et al.* [9] developed Al-6063/SiC MMCs via stir casting and evaluated their mechanical properties. It was reported that the tensile, compressive and impact strengths improved by 48%, 43% and 79% respectively when compared to that of the monolithic alloy.

Previous work on the development and characterization of Al/SiC composites have acknowledged that the mechanical properties of the composites are enhanced by the inclusion of reinforcement in the Al matrix. Moreover, the degree of enhancement of the mechanical and wear resistant

properties is dependent on the SiC reinforcement fraction employed for the production of the Al metal matrix composites. The formation of Al₄C₃ phase has been noted to be undesirable, as it limits the composite mechanical performance, and was found to be prevented by using Fly ash and particle wetting with the matrix enhanced with the addition of magnesium to the Al melt during casting. However, it has been noted that previous researches have concentrated on the use of Al-6000 series alloy and uncoated SiC particle as reinforcement, hence in this study, Al-4043 alloy was reinforced with nickel coated SiC particles to produce Al MMCs via stir casting technique and the mechanical and wear resistant properties characterized. Al-4043 alloy is majorly used as filler material and was considered as it contains high silicon content thus, a good wetting of the embedded SiC reinforcement particles is anticipated and better mechanical and tribological properties achieved.

2. Materials and Methods

2.1. Materials

The materials used for the fabrication of the Al-SiC composites were aluminum (Al-4043) alloy ingots, as shown in Figure 1, obtained from System Metal Industries Ltd. Aba, Nigeria and silicon carbide powder with angular morphology, typical of water atomization and having a particle size range of 10 – 60 μm, was supplied by Logitech Materials Company, UK.



Fig. 1. Aluminum Al-4043 alloy ingots used in the study.

2.2. Nickel-Coating of Silicon Carbide Particles

In order to prevent interfacial reaction which could result in the formation of Al₄C₃ phase, the SiC powder particles were coated with nickel using a model-12A4D vacuum coating machine, made by Hind High Vacuum Company Limited, Bangalore. The SiC particles were cleansed using acetone and a 10g/l H₂SO₄ acidic solution for 10mins and 7mins respectively. Thereafter, the SiC particles were immersed in a solution of 0.5g/l PdCl₂ and 3ml/l HCl for 15 mins to activate their surfaces. The cleansed and dried SiC

particles were gently dispersed in the vacuum chamber of the machine. The nickel coating was carried out in the vacuum at temperature range of 80-86°C. The coating took place for 75mins to achieve an approximately 15 µm Ni-coating thickness on SiC particles in the vacuum chamber which is anticipated to be sufficient to prevent rapid dissolution and formation of the deleterious Al₄C₃ phase around the particles in the Al matrix.

2.3. Stir casting of Al- Ni-Coated SiC Composites

Aluminum alloy (Al-4043) was used as matrix reinforced with Ni-coated SiC particles. The MMCs were fabricated by melting the aluminum (Al-4043) alloy in an improvised furnace (black smith hearth furnace) then the reinforced Nickel coated SiC particles were added and stirred slowly. Thermocouple was utilized during the melting process to measure temperature. Aluminum (Al-4043) alloy was first preheated to 450°C for 45 mins before melting and Ni-coated SiC powder were preheated to 900°C for 30 mins to remove moisture in the powder for better wettability. The furnace temperature was first raised above the melting point of aluminum to 720°C in order to melt the matrix completely and then it was allowed to decrease to temperature below the melting temperature (540°C) to keep the slurry in a semi-solid state. At this stage, the preheated SiC particles were added into the aluminum slurry and mechanically agitated. The composite slurry was then reheated to a fully liquid state and stirred for 8 mins to ensure the formation of a homogenous mixture. The furnace temperature was controlled within 720±10°C. After melting, slurry mix was poured into a prepared mould, as shown in Figure 2, with pouring temperature maintained at 680°C.



Fig. 2. Cast preparation by pouring the Al/SiC slurry from the crucible into the mould.

Cast composites with varying SiC reinforcement fractions were produced ranging from 5 – 25 wt.% SiC and a cast sample of Al-4043 alloy only was also produced as a control sample during the casting process.

2.4. Mechanical characterisation

The cast samples were characterised using a Model 0524011 Maker Optical microscope to examine the composite microstructure and to be able to establish a microstructure-composition-property relationship for the Al-

4043/Ni-coated SiC composites. Prior to microstructural examination, samples of the composites were mounted in a conductive resin and polished to a 1 µm Ra finish. The samples were prepared from the cast composite for mechanical characterisation. Tensile test specimens were prepared according to BS:EN 10002 and the tensile properties of the composite specimens were investigated using a M-500 25 kN Gunt, Tensiometer (Hamburg) equipped with a Model 3542 Epsilon Technology Extensometer for elongation measurement. The density of the composites was assessed using eureka can and water. The composite hardness was established using a model LM 2481T Wilson hardness tester (USA) with an applied load of 981 N (100 kgf) over a spherical indenter with a diameter of 1.59 mm. Circular wear specimens with a height of 30 mm and 40 mm diameter were prepared and a model K93500 Rubin Disc machine was employed for the wear test. Each specimen was subjected to sliding abrasion wear test for 10mins at 200 rpm using a coarse SiC paper with grit size P-220 and weight differentials after the test were used to establish the wear rate of each sample. The compressive strength of the composites was established using a compression testing machine and the Charpy impact strength and toughness of the composites was assessed using a Model 9050 Avery Impact testing machine with maximum impact energy of 300 J and a hammer velocity of 5.24 ms⁻¹. Three repetitions of each test conducted were made for each sample with same reinforcement composition to assess standard error that may be associated with the experimentation.

3. Results and Discussion

3.1. Composite microstructure

Figure 3 shows the optical micrograph of the cast Al-4043/15 wt.% SiC composite and the SiC particles were observed to be uniformly distributed in the composite. The microstructure of the composite matrix is characterized by Al-SiC eutectics. The SiC solid solution precipitates were seen as the filament-like or whisker structures which are randomly oriented to reinforce the Al solid solution matrix. The formation of Al₄C₃ phase was not observed and this suggested that the Ni coating prepared on the SiC particles before casting had prevented the formation of this deleterious phase. However, it has been presumed that if SiC particle dissolution had occurred during casting, the presence of Ni in the Al melt would have promoted the formation of the Al-SiC eutectic microstructure while the carbon could act as interstitial solid solutions in the Al matrix and the SiC precipitates [10]. It was also observed that the area density of the whiskers and the particle reinforcements increases with increasing wt.% SiC employed to produce the cast Al-4043/SiC composites. Few pores were also observed which is presumably due to gas entrapment during casting and few agglomerations of SiC particles was observed which may be absolutely inevitable but can be ameliorated by optimising the stirring operation during casting.

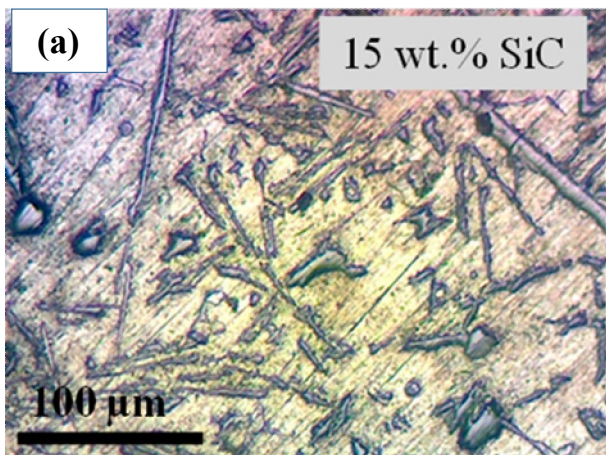


Fig. 3. Optical micrograph of cast Al-4043/15 wt% SiC composite.

3.2. Tensile properties

Having assessed the microstructure of the Al-4043/SiC composites formed, the mechanical properties of the composites can be discussed. Figure 4 shows the stress-strain curves for the Al-4043/SiC composites with varying SiC reinforcement fraction and Al-4043 alloy. The tensile strength of the cast Al-4043 alloy was obtained as 100 MPa which is lower than that of wrought Al-4043 alloy (145 MPa) [11] and strength of 140 MPa obtained for AlSi7 alloy produced via squeeze casting [12]. This may be directly attributed to the presence of pores in the cast which led to partial densification of the cast. Upon the subjection of the cast to tensile forces, the pores act as stress concentrators in the cast to accelerate the failure of the alloy. Moreover, the tensile strength of the cast Al-4043 alloy was found to improve with increasing SiC reinforcement fraction with the tensile strength ranging between 110 – 130 MPa for composite with reinforcement fraction ranging between 5 – 15 wt.% SiC. However, the tensile strengths of Al-4043/SiC composites with reinforcement fraction of 20 wt.% and 25 wt.% were significantly higher with tensile strength of 220 MPa and 350 MPa respectively. It is worthy to note that the composites with higher SiC reinforcement fraction such as 25 wt.% could not withstand high level of strain before breaking when compared to composite with 5 wt.% SiC reinforcement. The yield strength and elastic modulus of the composites were found to increase with increasing SiC reinforcement fraction as shown in Figure 5. The yield strength and elastic modulus of the cast Al-4043 alloy was found to be 74 MPa and 5596 MPa respectively and these were found to increase quadratically to yield strength 254 MPa and elastic modulus 13,399 MPa for Al-4043/25 wt.% SiC composite.

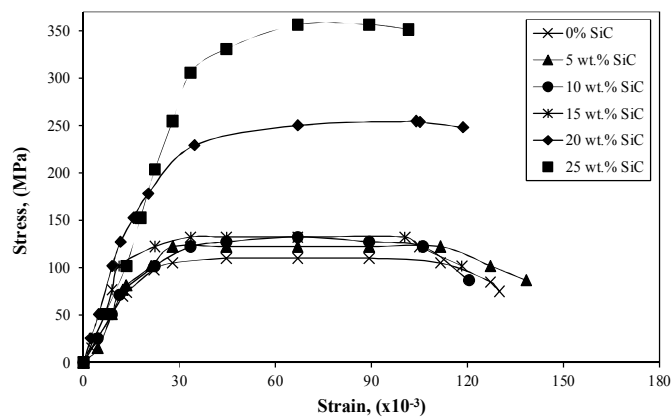


Fig. 4. The stress-strain curves for the Al-4043/SiC composites with variation in wt.% reinforcement.

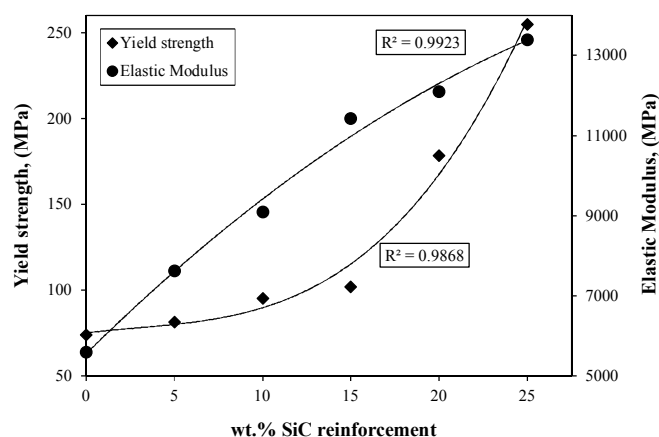


Fig. 5. Increase in yield strength and elastic modulus with increasing wt.% SiC reinforcement.

The elastic modulus result which is a measure of material stiffness was corroborated by the stress-strain curves in Figure 5, as the SiC reinforcement fraction increases, the strength of the composite increases too due to increasing SiC solid solution precipitates and uniformly distributed SiC particles which are responsible for effective load bearing capability. Figure 6 shows the elongation recorded for the tensile samples and the corresponding densities of their Al-4043/SiC composites. Whilst, density of composite increases linearly, the elongation was found to decrease exponentially with increasing SiC reinforcement fraction employed during casting. The cast Al-4043 alloy was found to possess 29.5% elongation when subjected to tensile load, however, the composite with the highest SiC fraction in this study (25 wt.% SiC) possessed 10% elongation due to the resistance provided by the reinforcing elements (SiC whiskers and SiC particles in the matrix) against deformation. The elongation values obtained in this study were greater than those recorded for Al-6061/SiC MMCs [13], this was attributed to the different elongation values of the matrices used with monolithic Al-4043 alloy having 22% [11] and Al-6061, 17% [14].

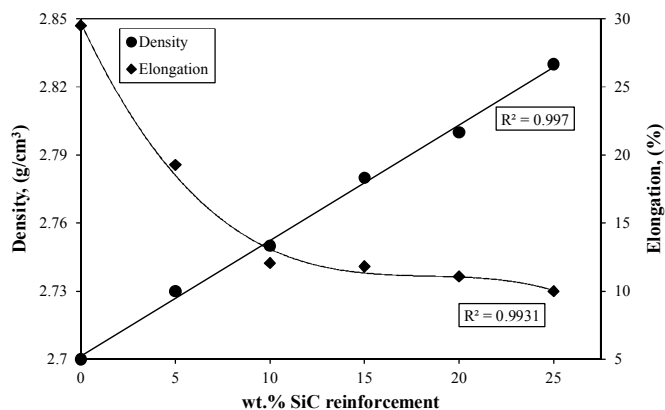


Fig. 6. An increase in density and decrease in elongation of the composites with increasing wt.% SiC reinforcement.

3.3. Composite hardness and wear rate

Figure 7 shows the variation in the Brinell hardness and wear rate of the Al-4043/SiC composites with increasing SiC reinforcement fraction. Whilst the composite hardness was found to increase with increasing reinforcement fraction, the wear rate was found to decrease exponentially. The hardness of the cast Al-4043 alloy was 30 HB which is less than that of the wrought alloy (39 HB) [11] and was raised to 76 HB when 25 wt.% SiC was added to the Al matrix which is more than 100% hardness improvement. However, the hardness value of squeeze-cast Al-MMC with 15 wt.% SiC was reported as 97 HB [12], which is higher than those observed in this study. This is due to near improved densification of cast Al-MMC produced via squeeze casting than stir casting employed in this study. The wear rate of the cast Al-4043 alloy was measured to be $33 \times 10^{-11} \text{ m}^3/\text{s}$ which was drastically reduced to $3 \times 10^{-11} \text{ m}^3/\text{s}$ with a 25 wt.% SiC reinforcement fraction in Al matrix. This indicated that the composite with 25 wt.% SiC reinforcement fraction is eleven (11) times wear resistant when compared to the monolithic Al-4043 alloy.

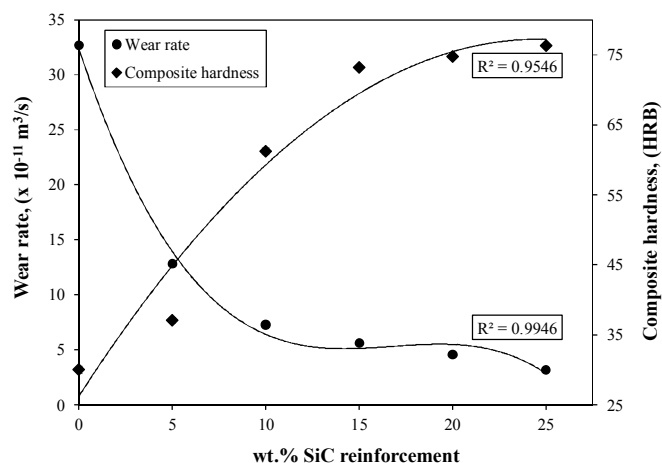


Fig. 7. A decrease in wear rate and an increase in hardness of Al-4043/SiC composites with increasing wt.% SiC reinforcement.

The improvement in wear resistance can be anchored on the increase in composite hardness and elastic modulus as the

SiC reinforcement fraction employed increases. Increased resistance to indentation and improved material stiffness are central to abrasion resistance of the Al-4043/SiC composites.

3.4. Compressive and impact properties

Figure 8 shows the compressive strength and the impact energy requirement of the Al-4043/SiC composites. In both cases, the compressive strength and the impact energy vary linearly with the SiC reinforcement fraction in the composites. The amount of energy absorbed by the cast Al-4043 alloy to yield was 40 J and was raised to 48 J for composite with a 25 wt.% SiC reinforcement fraction. This is indicative of increased toughness of the composites with increasing reinforcement fraction as the composites absorb more energy to deform plastically without fracture. The compressive strength of the Al-4043 alloy was found to be 144 MPa, which increased to 184 MPa with a 25 wt.% SiC reinforcement fraction. This indicated that the composites have improved resistance to deformation under compressive load when compared to the unreinforced monolithic Al-4043 alloy.

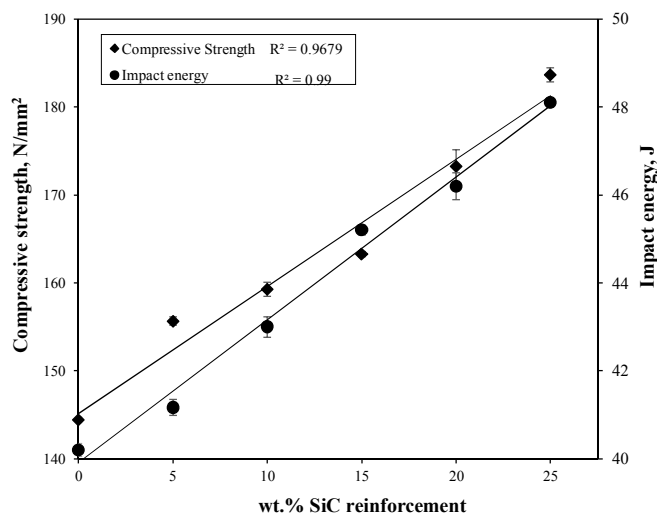


Fig. 8. An increase in compressive strength and impact energy of composite with increasing wt.% SiC reinforcement.

4. Conclusion

In this study, the mechanical properties of Al-4043/SiC composites with varying Ni-coated SiC reinforcement fraction have been successfully investigated. The composites were characterized to possess Al-SiC eutectic microstructure with SiC solid solution precipitates and SiC particles uniformly distributed in the Al matrix. The density of the composites was found to linearly increase with increasing SiC reinforcement fractions. The tensile strength, yield strength and elastic modulus were found to increase with increasing SiC reinforcement fraction and highest values obtained for composite with 25 wt.% SiC were 350 MPa, 254 MPa and 13.4 GPa respectively. However, the elongation of the composite with the highest reinforcement was lowest at a value of 10%. The hardness, compressive strength and impact energy of the composites increase

significantly as composite with 25 wt.% SiC possessed 76 HB, 184 MPa and 48 J respectively. The wear resistance of the Al-4043/SiC composites with highest SiC reinforcement was found to be eleven times that of the monolithic Al-4043 alloy.

References

- [1] S. S. Natarajan, S. P. Kumaresh, and B. Anoop, "Analysis of factors influencing dry sliding wear behavior of Al/SiC_p-Brake pad tribo-system", *Journal of Materials and Design*, Vol. 30, pp. 3831-3838, 2009.
- [2] V. K. Varna, S. V. Kamat, M. K. Jain, V. V. Prasad, and Y. R. Mahajan, "Effect of homogenization treatment on fatigue behavior of 2124Al/20 vol% SiC_p composite", *Journal of Material Science*, Vol. 28(2), pp. 477-481, 1993.
- [3] H. M. Zakaria, "Microstructural and corrosion behavior of Al/SiC metal matrix composites", *Ain Shams Engineering Journal*, Vol. 5(3), pp. 831-838, 2014
- [4] J. J. Moses, I. Dinaharan, and S. J. Sekhar, "Characterisation of Silicon Carbide Particulate Reinforced AA6061 Aluminum Alloy Composites Produced via Stir Casting", *Procedia Materials Science*, Vol. 5, pp. 106-112, 2014.
- [5] I. Balasubramanian, and R. Maheswaran, "Effect of inclusion of SiC particulates on the mechanical resistance behavior of stir-cast AA6063/SiC composites", *Materials and Design*, Vol. 65, pp. 511-520, 2015.
- [6] M. H. Rahman, and H. M. M. Al-Rashed, "Characterization of Silicon Carbide Reinforced Aluminum Matrix Composites", *Procedia Engineering*, Vol. 90, pp. 103-109, 2014.
- [7] J. D. R. Selvam, D. S. R. Smart, and I. Dinaharan, "Synthesis and Characterisation of Al6061-Fly Ash_p-SiC_p Composites by Stir Casting and Compocasting Methods", *Energy Procedia*, Vol. 34, pp. 637-646, 2013.
- [8] A. Anand, and S. S. C. Gowda, "Characterisation of Aluminum-Silicon Carbide Composite using Stir Casting Technique". *International Journal for Scientific Research and Development*, Vol. 3(8), pp. 232-1-0613, 2015.
- [9] M. A. Hassan, T. C. Ofor, A. M. Usman, and N. Y. Godi, "Development of Aluminum Metal Matrix Composite Using Stir Casting Method", *The International Journal of Engineering and Science*, Vol. 3(8), pp. 36-39, 2014.
- [10] G. K. Sigworth, "Fundamentals of Solidification in Aluminum Castings", *International Journal of Metalcasting*, Vol. 8 (1), pp. 7-20, 2014.
- [11] "Aluminum 4043 alloy (UNS A94043)", *Azo Materials*, available at <https://www.azom.com/article.aspx?ArticleID=8685>, retrieved on 16th October, 2017.
- [12] T. Ozben, E. Kilickap, and O. Cakir, "Investigation of Mechanical and machinability properties of SiC particle reinforced Al-MMC", *Journal of Materials Processing Technology*, Vol. 198, pp. 220-225, 2008.
- [13] D. C. Neelima, V. Mahesh, and N. Selvaraj, "Mechanical characterization of Aluminum silicon carbide composite", *International Journal of Applied Engineering Research*, Vol. 1(4), pp. 793-799, 2011.
- [14] "Aluminum 6061-T6", *MatWeb Material Property Data*, available at http://www.matweb.com/search/datasheet_print.aspx?matguid=1b8c06d0ca7c456694c7777d9e10be5b, retrieved on 17th October, 2017.

Determination of Basic Saturation Flow Rate in Istanbul

Süleyman Dündar*, Kemal Selçuk Ögüt**‡

* Istanbul Technical University, Graduate School of Science, Engineering and Technology, 34469, Istanbul/Turkey,
dundar23@yahoo.com.

** Istanbul Technical University, Department of Civil Engineering 34469, Istanbul/Turkey,
oguts@itu.edu.tr.

‡ Kemal Selçuk ÖGÜT, oguts@itu.edu.tr, Tel: +90 212 285 3663, ** ITU, Department of Civil Eng. 34469, Istanbul

Received: 20.10.2017 Accepted: 09.02.2018

Abstract- In traffic signal operations, the saturation flow rate is one of the key parameter for the calculation of signal timing. The saturation flow rate for different type of roads is simply calculated by multiplying the basic saturation flow rate, which is determined for predefined road and flow conditions with site factors. The aim of this study is to calculate the basic saturation flow rate in Istanbul with the help of field data. This calculation is based on the evaluation of vehicles' headways at signalized intersection.

The field study is conducted at 23 signalized intersections having basic conditions and 18,311 vehicle headways are analyzed. The initial calculations in this study are the determination of the saturation flow regions, in other word from which vehicle in the queue does the saturation flow start. It is found that the saturated headway starts from 2nd to 8th vehicle while the saturated headway is determined as 1.9 seconds, which is equivalent to 1,894 passenger cars unit per hour per lane as basic saturation flow rate.

Keywords Signalized intersection, Saturated headway, Saturation flow rate, Basic saturation flow rate.

1. Introduction

The increase of population and car ownership causes dramatic traffic jam especially in the cities of developing countries due to the lack of sufficient transportation infrastructure. The intersections, where traffic flows from different directions join, are the most affected areas from this traffic jam. These areas are not only the bottlenecks of the road network, but also critical road sections with high risk of traffic accident.

As the intersections are crucial areas in the road network, many studies have been focused on those areas since the mid-20th Century [1-10].

When the traffic volumes of intersected roads reach to a threshold value, the design of the signalization system offers more efficient and safer solution. The green and red intervals at a signalized intersection depend on traffic volume, saturation flow rate (SFR), lost time and delay. SFR is defined as the max number of vehicles per hour per lane that

could pass through a signalized intersection if the green signal was displayed for the full hour continuously. Several researchers [2, 11-15] studied the SFR, which is mainly affected by the characteristics of drivers and environment conditions. SFR can be calculated by multiplying all the factors of variables that affect it by basic saturation flow rate (BSFR). BSFR is determined for default road and operation conditions.

The aim of this study is to determine the basic saturation flow rate (BSFR) in Istanbul, which has 15 million residents and more than 2,000 signalized intersections, making it, one of the mega cities of developing countries.

2. Saturation Flow Rate and Saturated Headway

SFR, which is a fundamental parameter to determine signalized intersection capacity, can be calculated by the average saturated headway (SH), which can directly be measured with field study. The mathematical relation between SFR (S) and SH (h_s) is as follows:

$$S = 3600/h_s \tag{1}$$

When a vehicle in the queue starts crossing the stop line (or any other reference line) at a signalized intersection after the signal turns green, the departure headway (discharge headway) is the time that elapses between consecutive vehicles. The departure headways quickly decrease for the first few vehicles, and then a constant average departure headway is reached. This constant average departure headway is defined as SH.

First vehicle departure headway in the queue is the time until the first vehicle's rear wheels cross the stop line. The second vehicle departure headway is the elapsed time between the crossings of the first vehicle's rear wheels and the second vehicle's rear wheels over the stop line. The driver of the vehicle needs to react to the signal change and accelerate. The second vehicle moves faster than the first one by crossing the stop line, because of the greater distance to accelerate. The third and fourth vehicles perform a similar procedure, each achieving a slightly lower departure headway than the preceding vehicle. The decrease of departure headway terminates after few vehicles and the departure headway spreads around a constant value which is named as SH.

SFR, which can be calculated with the help of SH, has attracted attention of several researchers all over the world since 1947 [16], as given in Table 1.

From Table 1, it is seen that the range of SFR for through movement changes between 2,222 vehicles per hour per lane (vehphpl) [27] and 1,232 vehphpl [22]. Moreover, the effects of driver behaviours are modelled in Turkey, by determining the SFR between 1,110 and 1,829 vehphpl [32].

As the SFR is affected by geometrical and operating conditions, its base value, BSFR, is determined for default conditions such as:

- Lane width of 3.60 m.
- A flat grade (between $\pm 2\%$).
- No heavy vehicles, only passenger cars.
- No parking on the approach within 75 m upstream from the stop lane.
- No bus stop on the approach within 75 m upstream and downstream from the stop lane.
- No pedestrians and bicycles crossing during vehicle green.
- Located outside of central business district.

One of the initial studies conducted on BSFR was published in 1950 [1] that suggested 1,500 passenger cars unit per hour per lane (pcuphpl) for BSFR which was later revised as 1,800 pcuphpl in 1965 [33] and as 1,900 pcuphpl in 1997 which is not changed until today [10, 34]. Several researches determined that local conditions can change BSFR, which is calculated as 2246 pcuphpl in South Africa [15], 1773 and 1535 pcuphpl in China [35,36].

Table 1. Overview of SFR studies.

Study	Country	Published year	SH (sec)	SFR (vehphpl)
Greenshields et al [16]	USA	1947	2.10	1,714
Webster and Cobbe [2]	England	1966	2.05	1,756
Gerlough and Wagner [17]	USA	1967	2.30	1,565
Miller [18]	Australia	1968	2.11	1,710
Branston and Van Zilen [3]	England	1978	2.06	1,750
Branston [19]	England	1979	2.05	1,757
Akova [20]	Turkey	1979	2.50	1,440
Kimber and Semmens [21]	England	1982	1.86	1,935
Bhattacharya et al. [22]	India	1982	2.92	1,232
Lee and Chen [11]	USA	1986	1.90	1,895
Shoukry and Huzayyin [23]	Egypt	1986	2.23	1,617
Coeymans and Meely [24]	Chile	1988	2.25	1,603
De Andrade [25]	Brazil	1988	2.17	1,660
Hussain [5]	Malaysia	1990	1.85	1,945
Stanić [26]	Serbia	1991	1.98	1,818
Al-Ghamdi [27]	Saudi Arabia	1999	1.62	2,222
German Highway Capacity Manual [28]	Germany	2001	1.80	2,000
Lee and Do [14]	South Korea	2002	1.82	1,978
Čelar [29]	Serbia	2007	1.86	1,935
Çalışkanelli [30]	Turkey	2010	2.43	1,480
Polat et al. [31]	Turkey	2015	2.13	1,687

3. Field Study

As the aim of this study is to determine the BSFR, the intersections approaches with default conditions, as given in the previous section, are selected for data collection. However, the default values of the lane width is determined as 3.5 m instead of 3.6 m due to its common usage in Istanbul.

3.1. Determination of Intersections and Data Collections

Twenty-seven different signalized approaches across Istanbul were selected for our study by taking into account the presence of long queues, which are needed for the calculation of the SH. Sixteen of these approaches have two lanes, seven have three lanes and four have four lanes. From forty-nine lanes located on these intersections, the departure headway data were collected during weekday peak periods (07:00 to 09:00 and 17:00 to 19:00) where there were no jam conditions on the downstream flow direction. The traffic data were collected manually with the help of a stopwatch in all these approaches. The twenty-three different signalized intersections with default conditions are determined in all of the selected intersections.

The lane positions at each approach are defined according to the total number of lanes in the lane groups as shown in Table 2.

Table 2. Lane positions and symbols of analyzed lanes.

Number of lanes in the approaches	Lane position (LP)	Lane symbol (LS)
2 lanes	Left	L _{II}
	Right	R _{II}
3 lanes	Left	L _{III}
	Middle	M _{III}
	Right	R _{III}
4 lanes	Left	L _{IV}
	Left Middle	LM _{IV}
	Right Middle	RM _{IV}
	Right	R _{IV}

The intersection numbers (given by İstanbul Metropolitan Municipality), types of studied signalized intersection, selected approach directions, number of lanes and LS of observed lanes are given in Table 3. The headway analysis includes 20,250 vehicles, and 18,311 quality headway data. For each vehicle position in the queue, if the headway is observed more than 20 times, it is named as quality headway and included to the study. All quality data were collected during 1,579 cycles. Data were collected from all through lanes excluding shared lane (lanes having “through and right turns” and “through and left turns”) at the movement groups for each approach.

3.2. Determination of the Saturated Headway

In order to calculate the SH, the first step is to determine the rank of queued vehicles from which the SH started. The ANOVA test is applied to determine this rank at 5% level of significance. The data groups are determined according to vehicle ranks in the queue. The headways of first vehicles in the queue formed first group, the headway of second vehicles in the queue formed second group and so on. ANOVA test is performed initially with all groups. If F_{sta} is found greater than F_{cri} , the first groups is excluded from data set and the ANOVA test is performed for a second time, this elimination of groups is performed from first to last queued vehicles and stopped when F_{sta} is smaller than F_{cri} . The statistical basis for the ANOVA test is the hypothesis H_0 that the vehicle rank does not have any statistical impact on the departure headways.

Previous studies commonly indicated that the departure headway would converge to SH from 3rd to 6th queued vehicle [10, 16]. Initially, the SH region was individually determined to be based on lanes in our study. The queue headway rank of the first vehicle at SH area is determined for all approaches separately. The percentage of the rank of first SH are shown in Table 4 for two lanes, three lanes and four lanes.

The SH region varies from 2nd to 7th vehicle for 2-lane, from 2nd to 8th for 3-lane and from 2nd to 5th vehicle for 4-lane approaches as given in Table 4. It can be said that the starting position of the SH varied from approach to approach and even by the position of the lane.

In order to calculate the BSFR for an approach, it is necessary to determine if the SHs of each lane on this approach are statically similar. ANOVA test is applied to determine the statistical similarity of SH of each lane on an approach as seen in Table 5. If the SHs of each lane are statistically the same for an approach, the null hypothesis will be accepted, while p-value will be greater than 5%.

As shown in Table 5, the SHs are statistically same when the number of lanes of an approach is two. However, for the approaches with three lanes, the SHs of three lanes are statistically equal to each other on the 67% of the approaches.

For the approaches with four lanes, the SH of the right lane is always higher than the three others due to the frequently stops of taxi and minibuses to pick-up and drop-off passengers. On the other hand, when three lanes of these approaches are analysed, the SHs of these three lanes are equal to each other on the 67% of the approaches.

The average SHs for the lane position at two, three and four lanes approaches are given in Table 6, where it is seen that all the lanes average SHs are extremely close to each other and the lane position does not affect the SHs

Table 3. Data collection at signalized intersections for basic saturation flow rate.

Intersection number (IN)	Type of intersection	Observed approach		Observed lanes
		Direction	# of lanes	
1119	3-leg	Northwest	2	L _{II}
1119	3-leg	Southeast	2	L _{II} and R _{II}
1121	3-leg	Northwest	2	L _{II}
1155	Only pedestrian	Northwest	4	L _{IV} , ML _{IV} and MR _{IV}
1157	Only pedestrian	Northwest	4	L _{IV} , ML _{IV} and MR _{IV}
1192	3-leg	Southeast	4	L _{IV} and ML _{IV}
1211	3-leg	South	2	L _{II} and R _{II}
1320	3-leg	South	2	L _{II} and R _{II}
1380	3-leg	Southeast	4	L _{IV} , ML _{IV} and MR _{IV}
1832	3-leg	Southeast	2	L _{II} and R _{II}
1837	Only pedestrian	North	2	L _{II}
1850	3-leg	Southeast	3	L _{III}
1951	3-leg	North	2	L _{II} and R _{II}
2204	3-leg	Southwest	3	L _{III} and M _{III}
2242	3-leg	East	3	L _{III} , M _{III} and R _{III}
2262	3-leg	North	3	L _{III} , M _{III} and R _{III}
2271	3-leg	Northeast	2	L _{II}
2278	3-leg	Northeast	3	L _{III} and M _{III}
2278	3-leg	Southwest	3	L _{III} , M _{III} and R _{III}
2280	3-leg	Northeast	2	L _{II}
2280	3-leg	Southwest	2	L _{II} and R _{II}
3589	Only pedestrian	Southwest	3	L _{III} and R _{III}
3662	4-leg	Southwest	2	L _{II}
3662	4-leg	Northeast	2	L _{II}
3671	3-leg	South	2	L _{II}
3673	Only pedestrian	Northeast	2	L _{II}
3974	4-leg	Southwest	2	L _{II}

Table 4. Lane positions and symbols of analyzed lanes.

Number of lanes	1 st saturated veh.	%
2 lanes	2 nd	9
	3 rd	50
	4 th	36
	5 th	0
	5 th +	5
	Total	100
3 lanes	2 nd	19
	3 rd	50
	4 th	13
	5 th	13
	5 th +	5
	Total	100
4 lanes	2 nd	18
	3 rd	46
	4 th	18
	5 th	18
	5 th +	0
	Total	100

Table 5. ANOVA tests results for the similarity of the SHs of lanes.

Number of lanes	IN	Direction	SH	P-value
2 lanes	1119	SE	1.93	0.16
	1211	S	1.97	0.27
	1320	S	1.89	0.09
	1832	SE	1.86	0.07
	1951	N	1.77	0.22
	2280	SW	1.92	0.53
3 lanes	2242	E	1.95	0.94
	2262	N	1.88	0.16
	2278	SW	1.86	0.01
4 lanes*	1155	NW	1.96	0.37
	1157	NW	1.85	0.04
	1380	SE	1.88	0.80

* 4th lane (R_{IV}) data is not available, due to the frequently stops of taxis and minibuses.

Table 6. Results of average headways.

Number of lanes	Position of all lanes	Number of observed lanes	Average SH per lane	Average SH per approach
2 lanes	L _{II}	16	1.87	1.88
	R _{II}	6	1.92	
3 lanes	L _{III}	7	1.90	1.91
	M _{III}	6	1.91	
	R _{III}	3	1.95	
4 lanes	L _{IV}	4	1.88	1.89
	LM _{IV}	4	1.91	
	RM _{IV}	3	1.90	

3.3. Determination of BSFR

The BSFR is the reciprocal of average of the SH vehicles. The BSFRs for through lanes are calculated between 1,800 pcuphpl and 2,045 pcuphpl, with the average is 1,894 pcuphpl, which is exceptionally close to the estimation of Highway Capacity Manual [10]. The frequency histogram of BSFRs is given in Figure 1.

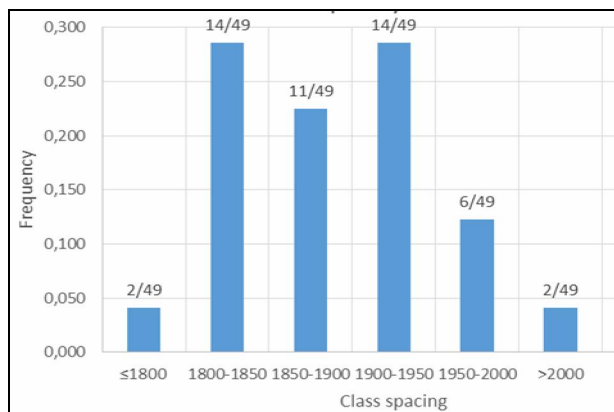


Figure 1. Histogram of BSFRs of observed lanes.

4. Conclusion

Using the survey of forty-nine lanes of signalized intersections in Istanbul, this study focuses on the determination of the basic saturation flow rate for through movements. The basic saturation flow rates are calculated with the help of SHs, which are obtained by field study.

The initial study for the calculation of SH is the identification of its interval. ANOVA test is performed to determine from which vehicle of the queue, the SH is started. It is calculated that the rank of queued vehicle from which the SH started, changes from 2 to 8 for different lanes.

When the SHs for each lane are calculated, their changes with respect to the number of lanes of an approach are studied. It is determined that when the number of lanes of an

approach increases, the similarity of SH of each lane decreases.

Finally, the average basic saturation flow rate is calculated as 1,894 pcuphpl, which is extremely similar to the assumption of Highway Capacity Manual [10] 1900 pcuphpl. Moreover, the standard deviation of basic saturation flow rate is found extremely small among lanes. (61 pcuphpl).

References

- [1] Transportation Research Board, Highway Capacity Manual, HRB and the Bureau of Public Roads, Washington, DC, USA, 1950.
- [2] Webster, F. V. and Cobbe, B. M., “Traffic Signals”, Technical Paper 56, HMSO, London, England, 1966.
- [3] Branston, D. and Van Zuylen, H., “The Estimation of Saturation Flow, Effective Green Time and Passenger Car Equivalents at Traffic Signals by Multiple Linear Regression”, Transportation Research, Vol. 12 (1), 47–53, 1978
- [4] Akçelik, R., “Traffic Signals: Capacity and Timing Analysis Research Report ARR 123”, Australian Road Research Board, Vermont, South Victoria, 1981.
- [5] Hussain, A. M., “Determination of Saturation Flows at Signalized Intersection in Malaysian Urban Areas”, Proceedings of the Sixth Conference, Road Engineering Association of Asia and Australasia, [CD-ROM] Kuala Lumpur, Malaysia, 1990.
- [6] Turner J. and Harahap, G., “Simplified Saturation Flow Data Collection Methods”, Transportation Research Laboratory, England, 1993.
- [7] Bonneson, P.E., Nevers, B. and J. Zegeer, J., “Guidelines for Quantifying the Influence of Area Type and Other Factors on Saturation Flow Rate”, Texas Transportation Institute, College Station, Texas, USA, 2005.
- [8] Rahman, M., Nur-ud-deen, S. A. and Hassan, T., “Comparison of Saturation Flow Rate at Signalized Intersections in Yokohama and Dhaka”, Proceedings of the Eastern Asia Society for Transportation Studies, Vol. 5, 959–966, 2005.
- [9] CCG, Canadian Capacity Guide for Signalized Intersections, Institute of Transportation Engineers, Canada, 2008.
- [10] Transportation Research Board, Highway Capacity Manual, National Research Council, Washington, DC, USA, 2010.
- [11] Branston, D. and Gipps, P., “Some Experiences with a Multiple Regression Method of Estimating Parameters at the Traffic Departure Process”, Transportation Research, Vol. 6A, 445–458, 1981.
- [12] Kimber, R.M., McDonald, H. and Hounsell, N.B., “Passenger Car Units in Saturation Flows: Concept, Definition, Derivation”, Transportation Research, Vol. 1B, 39–61, 1985.

- [13] Lee, J. and Chen R. L., "Entering Headway at Signalized Intersections in a Small Metropolitan Area", *Transportation Research Record* 1091, 117-126, Washington, DC, USA, 1986.
- [14] Lee, H.S. and Do, T.W., "Saturation Headway of Through Movement at Signalized Intersections in Urban Area", *Journal of Transportation Research Society of Korea*, Vol. 20, No. 5, 23-31, 2002.
- [15] Bester, C. J., Meyers W.L., "Saturation Flow Rates", *Proceedings of the 26th South African Transport Conference (SATC)*, 560-568, Johannesburg, 2007.
- [16] Stanić, B., Tubić Vladan and Čelar, N., "Straight Lane Saturation Flow and Its Rate in Serbian Cities", *Transport*, Vol. 26, No. 3, 329-334, 2011.
- [17] Gerlough, D.L., Wagner, F.A., "Improved Criteria for Traffic Signals at Individual Intersections", *Highway Research Board NCHRP No.32*, Washington, DC, 1967.
- [18] Miller, A. J., "Australian Road Capacity Guide-Provisional Introduction and Signalized Intersections", *ARR 79*. Australian Road Research Board, 1968.
- [19] Branston, D., "Some Factors Affecting the Capacity of Signalized Intersections", *Traffic Engineering and Control* 20 (8/9), 390-396, 1979.
- [20] Akova, M., "Investigation of Effect of Posture, Departure and Discharge Conditions in Calculation Methods and Appropriate to the Reality of Our Country at Signalized Intersection", PhD Thesis, Istanbul Technical University, Turkey, 1979.
- [21] Kimber, R. M. and Semmens, M.C., "An Experiment to Investigate Saturation Flows at Traffic Signal Junctions", *Traffic Engineering and Control* 23, 110-117, 1982.
- [22] Bhattacharya, P. G. and Bhattacharya, A. K., "Observation and Analysis of Saturation Flow through Signalized Intersections in Calcutta", *Indian Highways*, 10, 11-33, 1982.
- [23] Hussayin, A. S. and Shoukry, W.S., "Saturation Flow and Effective Approach Width at Signalized Intersections in Greater Cairo", *6th African Highway IRF Conference*, 1986.
- [24] Coeymas, J. E. and Meely, C. B., "Basic Traffic Parameters in the Case of Santiago", 1988 (Unpublished).
- [25] De Andrade, J. P., "The Performance of Urban Intersections in Brazil", PhD Thesis, University of Southampton, 1988 (Unpublished).
- [26] Stanić, B., "Research on Signal Timing Plan Effects at Saturation Flow", PhD Thesis, University of Belgrade, Serbian, 1991.
- [27] Al-Ghamdi, A. S., "Entering Headway for Through Movements at Urban Signalized Intersections", *Transportation Research Record* 1678, 42-47, Washington, DC, USA, 1999.
- [28] HBS, *German Highway Capacity Manual*, Germany, 2015.
- [29] Čelar, N., "Contribution to the Survey of Design Values of Saturated Flow at Signalized Intersections", MSc Thesis, University of Belgrade, Serbian, 2007.
- [30] Çalışkanelli, S.P., "Investigation of Headway Distribution of the Vehicles Departing From Signalized System at 9 Signalized Intersections in Izmir", PhD Thesis, Dokuz Eylül University, Turkey, 2010.
- [31] Polat, A., Sarısoy, G. and Ögüt, K.S., "Determining of Start-up Lost Time and Saturation Flow Rate at Signalized Intersections in Small Cities", *11th Transportation Congress*, 129-138, Istanbul, Turkey, 2015.
- [32] Cetin, M. Murat and Y. S., "A Mathematical Model for Determining Saturation Flows", *Technical Journal of Turkish Chamber of Civil Engineers*, Volume 24, Number 2, April 2013, p 4759-4777, 2013.
- [33] *Transportation Research Board, Highway Capacity Manual*, National Research Council, Washington, DC, USA, 1965.
- [34] *Transportation Research Board, Highway Capacity Manual*, National Research Council, Washington, DC, USA, 1998.
- [35] Shao, C., Rong, J. and Liu, X., "Study on the Saturation Flow Rate and Its Influence Factors at Signalized Intersections in China", *6th International Symposium on Highway Capacity and Quality of Service*, Sweden, 2011.
- [36] Shang, H., Zhang, Y. and Fan, L., "Heterogeneous Lanes' Saturation Flow Rates at Signalized Intersections", *9th International Conference on Traffic & Transportation Studies (ICTTS'2014)*, Vol. 138, 3-10, 2014.

Gear Shift Efforts Analysis and User Interface Software Development

Emrah Arslan*[‡], Ahmet Sagirli**

* Yildiz Technical University, Department of Mechanical Engineering, Besiktas 34220, Istanbul, Turkey, Ford Otomotiv Sanayi A.S. Sancaktepe Engineering, 34885 Sancaktepe, Istanbul, Turkey

** Yildiz Technical University, Department of Mechanical Engineering, Besiktas 34220, Istanbul, Turkey

(earslan9@ford.com, sagirli@yildiz.edu.tr)

[‡]Corresponding Author; Emrah Arslan, Department of Mechanical Engineering, Faculty of Machine, Yildiz Technical University, 34220, Istanbul, Turkey, Tel: +90 216 664 9451, earslan9@ford.com

Received: 06.12.2017 Accepted: 05.03.2018

Abstract- Nowadays, with the increasing demand of comfort on passenger cars, many car manufacturer companies focus on manual transmission and external control system. There are many gearshift control mechanisms available such as rod mechanism, hydraulics mechanism and cable mechanism in the current technics that need to be designed resplendently. In the meantime, base manual transmission has a lot of components such as synchronizer, gear cones, friction plates, poppet balls, hubs and rods which affect gear shift comfort. All these main components should be designed and optimized for customer satisfaction. In order to measure gear shift efforts and comfort, Gear Shift Quality Analysis (GSQA) device is developed by Ricardo Company. Using this GSQA device, gear shift force, gear shift integral, free plays, cross gate positions, fore-aft positions, shifter angles are able to be measured objectively. To collect all these attributes data, engineers should spend minimum one day on a selected vehicle. This means loss of work and money for the car manufacturers. The gear shift effort software (GSEA) for a manual transmission and external control mechanism are developed to evaluate/calculate shift and select mechanical ratio, cable strokes, length lever and shift force to provide desirable shifting quality. In addition to software calculation, the vehicle is tested using gear shift quality device. At the end of this study input parameters are discussed in terms of outputs of vehicle shift quality attributes. The results of simulation software are plotted to present easy understanding for the last user.

Keywords Synchronizer, shift quality, shift effort, external control.

1. Introduction

Vehicle manual transmission systems are main parts of the automotive powertrain pack. To reach the aim to achieve gear shift, synchronizers should move through the target gears. External control components allow fore-aft and cross gate movement to the driver thanks to the fact that shifter knob is one of the main components that interface with customers. Its key properties are to change the work of gear at certain vehicle speeds. Many car manufacturer companies use cable shift system for their manual transmission system because of smooth installation, transformable routing and flexibility.

The efforts of gear shift force can be typified by using different calculation methods. There are three main systems to understand the whole shifting process:

External Control System

- Handball Mechanism (Shifter)
- Shifter Cables
- Shift Turret Mass

Internal Control System

- Selector Springs and Poppet Balls
- Push Rods and Levers
- Gear Shift Sleeve Forks

Synchronizer System

- Clutch gear with cone
- Gear Wheel
- Synchronizer Ring
- Synchronizer Rotational Hub
- Sliding Sleeve
- Strut Detent
- Output Shaft

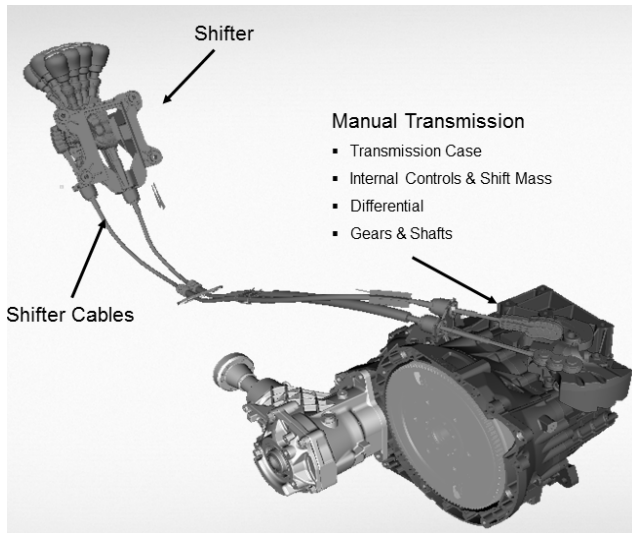


Fig. 1. Complete manual transmission system.

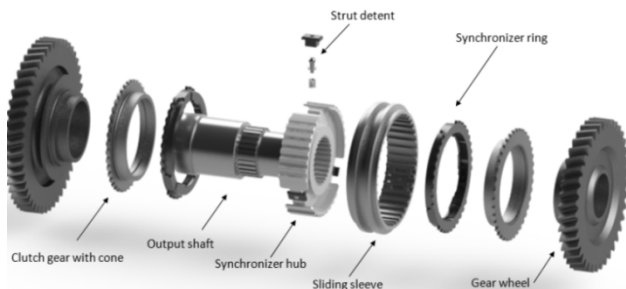


Fig. 2. Synchronizer detail view [4].

The gear shift comfort for a manual transmission is directly connected to operator’s feeling of the gear force transferred. Reduced shifting force and increased uniformity should be considered for developing manual transmission [2]. Within this scope, driver effects on gear shift force are broken down using different trained operator. Thus, the results were correlated and transferred to theoretical function [3].

The Synchronizer sleeve is manually triggered using fork and internal shift control system connected to the external control in the vehicle system. Although synchronizer system is the most critical component for shift quality, there are other systems that stimulate customer complaints. In order to simulate other attributes effects such as gear knob, forks, levers and poppet ball, a dynamic shift quality model was created using Matlab Simulink Software [5].

As it is a mere function of synchronizer a manual transmission’s dynamic gearshift quality is a very vital parameter. The behavior of dynamic gearshift parameter during gearshift is eminently nonlinear and random, therefore

it is challenging to obtain acceptable gearshift. The most complex circumstance in manual transmission is to design the synchronizer and its dynamic behavior. The prediction of the behavior of most dynamic and static parameters such as pull out force, synchronization force, detent force and end stop force is managed via calculation and they are dependent on the design of the synchronizer and gearbox layout [10].

Ana Pastor Bedmar [4] simplified linear synchronizer model and presented that if synchronizer parameters are selected correspondingly, that may help reduce the gearbox shift effort. Synchro parameters are very key elements to reduce handball effort issue.

In order to establish optimum cone parameter, a mathematical optimization model can be developed. Between the cone angle and sleeve chamfers angle, synchronizer size, coefficient of friction, cone torque and index torque, a model of relationship can be set up. To find a global minimum value of cone angle to satisfy a pack of assigned and known constraints, a model was framed in the Matlab optimization toolbox pattern-search solver. The mentioned model can be applied for selecting the first cut synchro parameter within moderate accuracy. These values can be finer tuned afterwards with the help of customized and specialized software systems [6].

In this paper, a mathematical calculation was utilized based on perfect conditions by using parameters of compression shift and select mechanical ratio, cone angle, friction coefficient, shifting time in order to understand the driver’s felling of a manual transmission. Theoretical calculations in this study are compared to real vehicle measurements. Simulation results are presented with guide interface to the engineers. Gear Shift Calculation Tool is developed using Microsoft .NET Framework 4.5 backend platform.

2. Mathematical model of gear shift calculation

A detailed knowledge of the process of gear-change is required to study the synchronizer behavior. Successive phases are able to be distinguishable with the help of both different relative positions of the synchronizer parts and the characteristic points of synchronized angular velocity and the axial force variation [8].

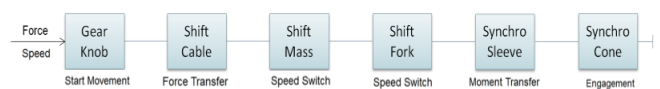


Fig. 3. Shift control system force and velocity transfer.

Figure 3 shows handball forces and velocity transformation between key elements. All these sub components create concurrent execution together. The gear knob transfers force transmission via shifter cable and shift mass. In this system, there are two speed cycles between components.

- Shift mass converts linear movement to angular movement
- Shift fork converts angular movement to linear movement.

Synchro sleeve pushes the gear cones to target gear with the movement of the fork.

There are 4 main sections of gear shifting process. The following Fig. 5 shows the generic simulation process that affects the driver hand lever ball.

Neutral: Neutral position is the center of gear knob, fore-aft and gross gate movements start from this position.

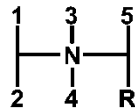


Fig. 4. 5 Speed gear hand ball pattern.

Start of Synchronization: The gear shift sleeve moves to fore-aft direction from the N position. Driver passes this phase without remarkable force effect, only with internal frictions.

Synchronization: At this phase synchronization hub moves axial to target gear and gear cones work in parallel with synchro sleeve. The cones complete physical connection.

Blocking Release: The dog teeth fully engage into each other and synchronizer sleeve completes shape connection.

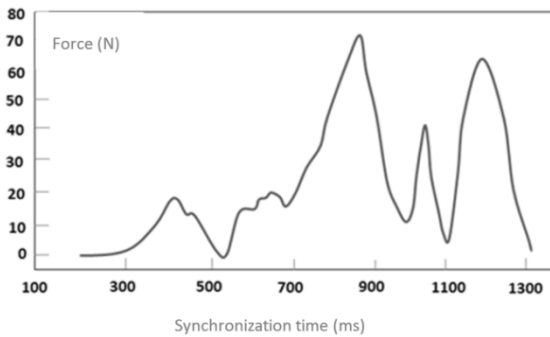


Fig. 5. Synchronization handball force-time chart.

The synchronization integral (I_s) can be defined as hand ball gear shift force that depends on the time period of shifting.

$$I_s = \int_{t_0}^{t_1} F_{handball}(t) \cdot dt \quad (1)$$

Where I_s is the synchronization integral force, t_0 is the time of synchronization start, t_1 is the time of synchronization finish, $F_{handball}$ is the force which applied on shifter gear knob. If we consider non-variable values in $F_{handball}$, we can convert it to Eq. (2).

$$F_{handball} = \frac{K \cdot F_{cone}}{\gamma_h \cdot \gamma_m \cdot \gamma_i} \quad (2)$$

Where K is the shift mechanical ratio which is proportional with shifter lengths, γ_h is gear shift/select cable efficiency which is provided by cable suppliers, γ_m is shifter

efficiency, γ_i is internal control system efficiency, F_{cone} is cone force at the mean point.

$$I_s = \int_{t_0}^{t_1} \frac{K \cdot F_{cone}}{\gamma_h \cdot \gamma_m \cdot \gamma_i} \cdot dt \quad (3)$$

The following equations are derived from Eq. (3).

$$I_s = \frac{K}{\gamma_h \cdot \gamma_m \cdot \gamma_i} \cdot \int_{t_0}^{t_1} F_{cone} \cdot dt \quad (4)$$

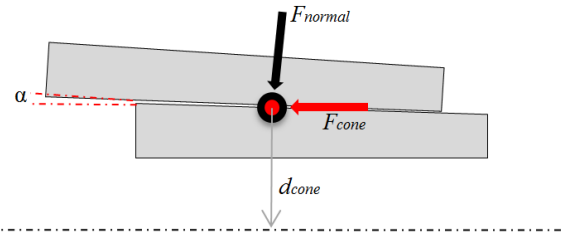


Fig. 6. Forces on gear cones.

Applied friction force on synchronizer sleeve at cone diameter creates cone torque. The equation of forces in the following form .

$$F_{cone} = F_{normal} \cdot \sin \alpha \quad (5)$$

$$T_{friction} = F_{normal} \cdot r_m \cdot \mu \cdot n_k \quad (6)$$

$$r_m = d_{cone} / 2 \quad (7)$$

$$T_{friction} = \frac{F_{cone} \cdot d_{cone} \cdot \mu \cdot n_k}{2 \cdot \sin \alpha} \quad (8)$$

This friction torque corresponds to the angular speed of the synchronizer.

$$T_{friction} = J \cdot \frac{\Delta \omega}{t} \quad (9)$$

$$F_{cone} = \frac{J \cdot \Delta \omega \cdot 2 \cdot \sin \alpha}{d_{cone} \cdot \mu \cdot n_k \cdot t} \quad (10)$$

Where J is total inertia of the system which can be divided as drag and rotational inertia, $\Delta \omega$ is speed difference of the target gear and current gear, α is cone angle of synchronizer, d_{cone} is cone diameter, r_m is cone radius, μ is friction coefficient of cone, n is friction coefficient of cone, n_k is the number of cone and t is the synchronization period of gear shift process. The handball force is the driver's feeling of force which is defined as following

$$F_{handball} = \frac{K}{\gamma_h \cdot \gamma_m \cdot \gamma_i} \cdot \frac{J \cdot \Delta \omega \cdot 2 \cdot \sin \alpha}{d_{cone} \cdot \mu \cdot n_k \cdot t} \quad (11)$$

Manual transmission synchronizers use friction cones to equalize current gear and target gear speed. Working principle of manual transmission cones is similar to the dry clutch mechanism [9]. In Table 1, synchronizer cone angles are given corresponding to cone number.

Table 1. Cone numbers and angles [9]

Single Cone	Multi Cone
$n=1$	$n>1$
$\alpha=6.5-8^\circ$	$\alpha=7-12^\circ$

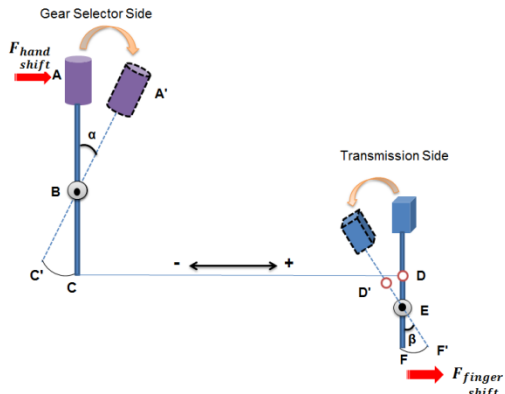


Fig. 7. Shift movement mechanical dimensions.

According to Fig.7 shift mechanical ratio is as follows,

$$K (\text{Shift Mechanical Ratio}) = \frac{|AB|}{|BC|} \times \frac{|DE|}{|EF|} \quad (11)$$

Where |AB| is hand lever length of shift knob, |BC| is shift radius on shifter, |DE| is shift radius on transmission and |EF| is finger radius on transmission shift shaft. To protect synchronizers, shift mechanical ratio is limited by the car manufacturer companies. According to research and experimental results, mechanical ratio proposals are defined as follows

- Heavy Commercial Transmissions ($\leq 7,5$)
- Passenger Car Transmissions (≤ 6)

Here, the force on shift forks can be defined below,

$$F_{hand\ shift} = \frac{F_{fingershift}}{K} \quad (12)$$

Where $F_{fingershift}$ is a force that is activated by shifter and lever mass.

3. Guide interface development studies

Gear shift effort analyzer (GSEA) software is developed using Devexpress Winforms tool. As programing language, .Net platform was selected.

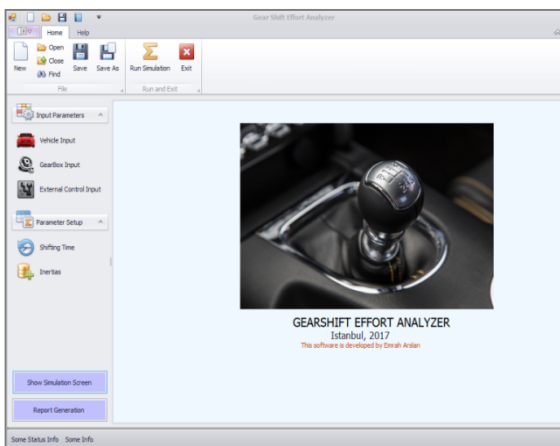


Fig. 8. Opening page of the GSEA.

To classify calculation, vehicle input parameter page is created, the user can select project id, vehicle segment, model year, engine type and transmission information in this section. When the user selects transmission and drive configuration, software brings external control inputs, synchronizer inputs and inertia values from the database. The database is created using Microsoft Access 2012. After all inputs selected, we need to save these configurations.

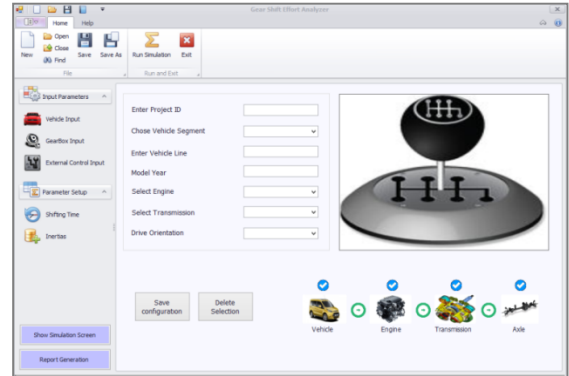


Fig. 9. New project page.

External control parameters can be determined and selected in Fig.10. There are two main sections as select and shift calculation in this page. In addition to main calculation like mechanical ratio and travels, cable adjustment comparison is added in the select tab. Shift cable and select cable efficiencies were also added in tool and the user can arrange these values easily.

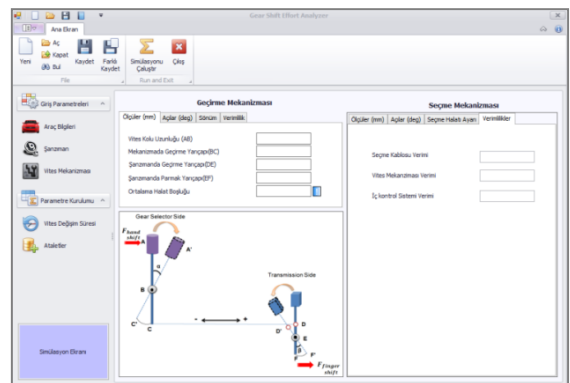


Fig. 10. External control input page.

Figure 11 shows synchronizer input parameters screen, the user needs to enter cone angle (degree), cone number, cone friction and mean cone radius in this tab.

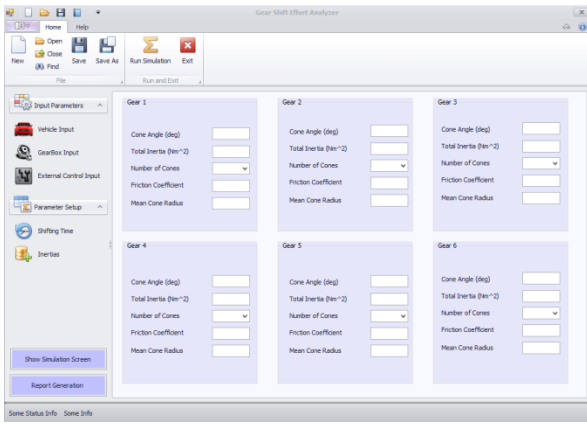


Fig. 11. Synchronizers input page.

In parameter setup section, the user sets clutch inertia, drag inertia and speed difference in both upshift and downshift gear change. The speed differences between gears come from the gear ratios. Gear shift speed was selected as nominal 3000 rpm.

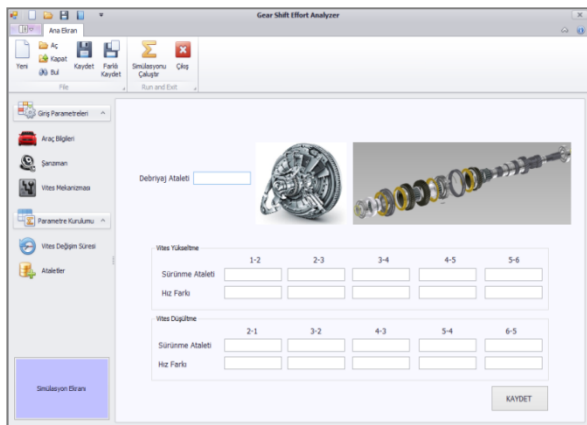


Fig. 12. Inertia and speed input page.

After above parameters set-up, the user needs to run simulation. During simulation process, solver prepares charts and summary pages. There are three tabs in the result page as external control summary, external control chart and shift force tabs.

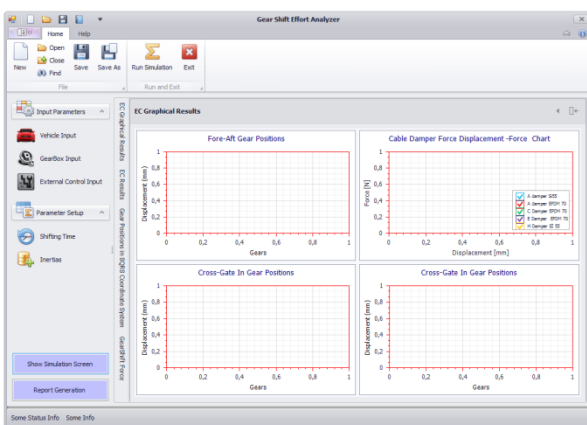


Fig. 13. Results Page.

Using GSEA software, we can evaluate and calculate as follows,

- Upshift Force (N)
- Downshift Force (N)
- Fore-Aft Positions (mm)
- Cross-Gate Positions (mm)
- Shifter Mechanical Ratio
- Gear Positions in Coordinate System (mm)

4. Gear shift quality device (GSQA) and test setup

Transmission gear shift quality can be evaluated using Ricardo's GSQA device. The advantages of the device to show us objective results, also this device can be used in back to back comparison between vehicle lines and transmissions.



Fig. 14. Ricardo GSQA device.

The GSQA measures shift and select travels, free plays, shift and select forces on the system using many sensor setups and acquisition devices. The acquisition device collects all measured data and analyses, after processing the data, test driver is shown the results on the main screen. For the setup process, light commercial vehicle 6 speed transmission was selected.

Table 2. Gear Ratios

1st	2nd	3rd	4th	5th	6th
3,62	2,05	1,19	0,810	0,902	0,71

Table 3. Synchronizers Parameters

Gears	Cone Angele	Cone Numbers	Cone Friction	Cone Radius
1st	7,3°	3	0,1	73
2nd	7,3°	3	0,1	73
3rd	7,1°	3	0,1	65
4th	7,1°	3	0,1	65
5th	6,8°	2	0,1	68
6th	6,8°	2	0,1	68

In this study, dry clutch disk inertia is selected as 0,0091 kgm².

5. Simulation and Experimental Test Results

Figure 15 shows simulation results for cross-gate positions. Travel response of the forks and levers are plotted. There are two motion cables for manual transmission system which are shift and select cable. The select cable works for cross-gate positions such as 1-2, 5-6 and reverse lines. At the same time manual transmission system has adjustment system on the select cable. The adjustment part assures handball positions for 1-2 and 5-6 lines.

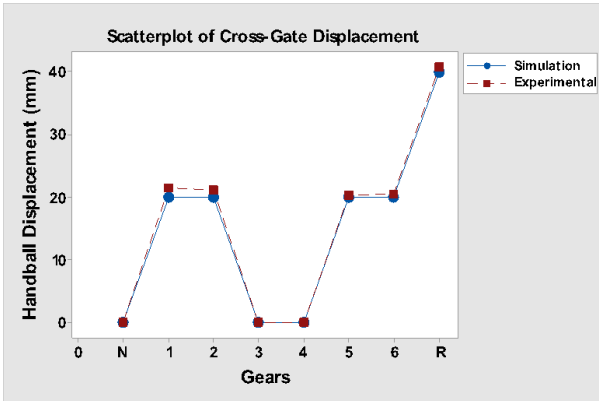


Fig. 15. Simulation & experimental cross-gate positions.

Car manufacturer companies check select cable adjustment for each car with a camera system. The camera measures gear knob positions and informs the operator whether it is a pass or fail. This is because it is important to know select cable adjustment effects on shift quality before production phase. Another point to evaluate is the symmetry of the gear knob lever in the vehicle console. If the symmetry of the knob is not achieved, we can say that cable adjustment is not correct.

Figure 16 shows simulation and experimental results for fore-aft positions. Travel response of the sleeve is plotted. The simulation results give 50 mm for fore-aft simulation and this is the same for all gears due to the same shifter angle.

Due to end stop stiffness of the shifter cable, we see a minor wave on fore-aft positions for the experimental test results. Shifter cable that has low end stop stiffness creates high free play on gear lever knob. Transmission transmits powertrain vibrations to gear knob via shifter cable, for this reason stiffness value should be within the defined range.

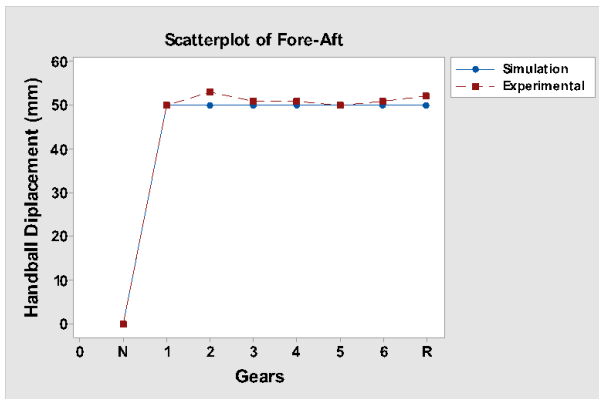


Fig. 16. Simulation & experimental fore-aft positions.

The most important attribute of shift quality is hand ball efforts. We can divide efforts into two sections as downshift and upshift. In Fig. 18, experimental and simulation results for upshift forces are shown. In here, number of cones plays a major role in shiftability. Using more than one synchro cone marks up the transmission price.



Fig. 17. Ricardo GSQA device [7].

Figure 17 shows GSQA test system in vehicle compartment. Expert driver collects shift quality data to give sign off to customer vehicles.

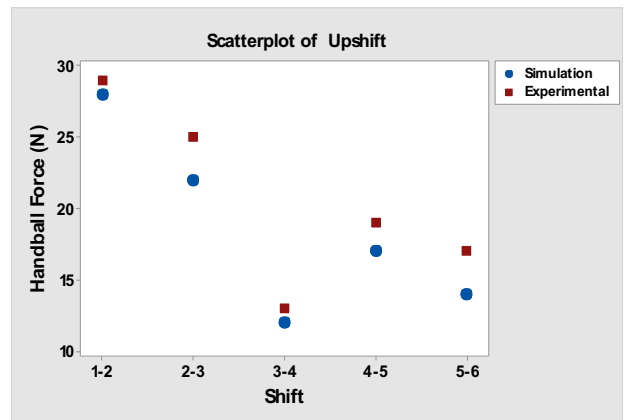


Fig.18. Simulation & experimental upshift force.

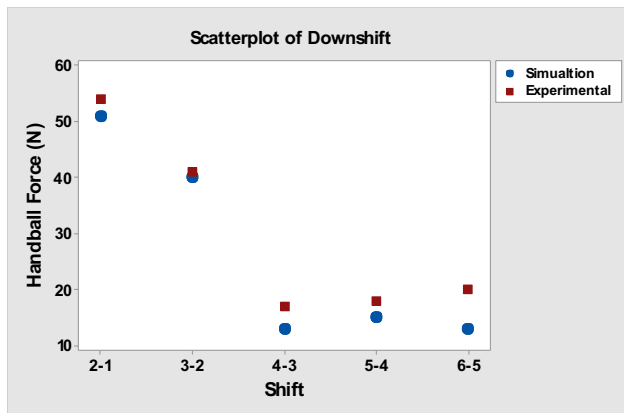


Fig.19. Simulation & experimental downshift force.

Figure 19 explains that lower shifts especially the 1st and 2nd gears have high efforts. The reason is that these gears have bigger cones and gear change inertias. The drag inertia

can be measured in transmission rig test. Oil viscosity is an important factor for drag inertia. Using oil that has high viscosity increases shift force. Transmission suppliers share catalogue inertia values with OEM's. In addition to inertia and cone size, there is another important factor which is cone number. Especially lower gear changes like 1st to 2nd and 2nd to 1st need high energy to engage gears to each other. In such case, transmission manufacturers use more than one friction cone to reduce sleeve force. We have tested two and three cones system for the selected case. For passenger cars, all transmission manufactures use one cone systems for high shifts such as 4/5 and 5/6 due to lower torque indexing.

The shift quality can be affected by components with elastic properties within the system. In general, these components are poppet ball springs, cable end eyes and abutments. With arranging the parameters in themselves, we can change shift efforts accordingly. As a sequence of this, companies focus on optimization methods to constitute the best system for their customers.

Above Fig. 18 and 19 show us experimental and simulation results converge approximately %85 which is an acceptable value if we consider test prices and time loss.

Table 4. Comparison of upshift efforts [N]

Gear Shift →	1/2	2/3	3/4	4/5	5/6
GSQA	28	22	12	17	14
GSEA	31	24	15	19	17

Table 5. Comparison of downshift efforts [N]

Gear Shift →	2/1	3/2	4/3	5/4	6/5
GSQA	49	41	13	14	12
GSEA	53	46	16	16	20

6. Conclusion

This paper has shown how a guide user interface modelling software has been used for a comparison between gear shift quality device test systems. The synchronizer sleeve and cones are patterned as four stages close to real time conditions. The GSEA tool calculates the gear knob travels, positions, shift force and select force. Modelling offers transparent pictures of design parameters such as cone number, frictions, cone radius and drag inertias that has effect on dynamic shiftability. The simulation results correlate with the GSQA data collected from the target

vehicle. Thus, the developed GSEA software can be used for new model vehicle transmission systems development in terms of gear shift quality.

Acknowledgements

The authors would like to thank Dr. Onur Ozansoy, Mehtap Kartal Sayar and Ford Otosan Product Development staffs for their support.

References

- [1] S.Krishnan, Gear Shift Quality Benchmarking for Manual Transmissions, SAE Paper, India.
- [2] K.Park, S.Hongsuk and S. Bonggyu, "Design Optimization of a Control System with a Variable Inertia Mechanism to Improve Shift Feeling in a Manual Transmission", SAE-15AP-0020, October 2015.
- [3] E. Luciano Duque and P.Thomaz Aquino Jr, "Human Factors analysis of manual gear shifting performance in passenger vehicles", Science Direct, 6th International Conference on Applied Human Factors and Ergonomics (AHFE 2015) and the Affiliated Conferences, AHFE 2015.
- [4] A.Pastor Bedmar, "Synchronization processes and synchronizer mechanisms in manual transmissions", Department of Applied Mechanics, Chalmers University of Technology, 2013.
- [5] D.Kelly and C.Kent "Gear Shift Quality Improvement in Manual Transmissions Using Dynamic Modelling", FISITA World Automotive Congress, June, 2000.
- [6] Kholam.S.C, Mhaske M S, Belkar S B "A Method to Optimize Brass Type Single Synchronizer Ring for Manual Gearbox" International Journal of Engineering and Advanced Technology (IJEAT) ISSN: 2249 – 8958, Volume-3, Issue-3, February, 2014.
- [7] <https://automotive.ricardo.com/driveline-transmissions/benchmarking>.
- [8] L.Lovas, D.Play1, J.Marialigeti, and J.F Rigal "Mechanical behaviour simulation for synchro mechanism improvements" Proc. IMechE Vol. 220 Part D: J. Automobile Engineering, 2006.
- [9] H.Naunheimer, B.Bertsche, J.Ryborz, W.Novak "Automotive Transmissions, Fundamentals, Selection, Design and Application" Second Edition 2010.
- [10] Nilesh A. Phalke, Dr. V. Singh "Improvement in Gear Shift Performance of Manual Transmission System" International Journal of Science and Research (IJSR) ISSN (Online): 2319-7064, 2015.

INTERNATIONAL JOURNAL OF ENGINEERING TECHNOLOGIES-IJET

Guide for Authors

The **International Journal of Engineering Technologies (IJET)** seeks to promote and disseminate knowledge of the various topics of engineering technologies. The journal aims to present to the international community important results of work in the fields of engineering such as imagining, researching, planning, creating, testing, improving, implementing, using and asking. The journal also aims to help researchers, scientists, manufacturers, institutions, world agencies, societies, etc. to keep up with new developments in theory and applications and to provide alternative engineering solutions to current.

The *International Journal of Engineering Technologies* is a quarterly published journal and operates an online submission and peer review system allowing authors to submit articles online and track their progress via its web interface. The journal aims for a publication speed of **60 days** from submission until final publication.

The coverage of IJET includes the following engineering areas, but not limited to:

All filed of engineering such as;

Chemical engineering

- Biomolecular engineering
- Materials engineering
- Molecular engineering
- Process engineering

Civil engineering

- Environmental engineering
- Geotechnical engineering
- Structural engineering
- Transport engineering
- Water resources engineering

Electrical engineering

- Computer engineering
- Electronic engineering
- Optical engineering
- Power engineering

Mechanical engineering

- Acoustical engineering
- Manufacturing engineering
- Thermal engineering
- Vehicle engineering

Systems (interdisciplinary) engineering

- Aerospace engineering
- Agricultural engineering
- Applied engineering
- Biological engineering
- Building services engineering
- Energy engineering
- Railway engineering
- Industrial engineering
- Mechatronics
- Military engineering
- Nano engineering
- Nuclear engineering
- Petroleum engineering

Types of Articles submitted should be original research papers, not previously published, in one of the following categories,

- Applicational and design studies.
- Technology development,
- Comparative case studies.
- Reviews of special topics.
- Reviews of work in progress and facilities development.
- Survey articles.
- Guest editorials for special issues.

Editor-in-Chief and Associate Editors

Editor-in-Chief:

Prof. Dr. Mustafa BAYRAM

Associate Editors:

Assoc. Prof. Dr. Baris SEVIM

Asst. Prof. Dr. Ahmet AKTAS

Asst. Prof. Dr. Yalcin CEKIC

Asst. Prof. Dr. Ali ETEMADI

Ethic Responsibilities

The publication of an article in peer-reviewed “*International Journal of Engineering Technologies*” is an essential building block in the development of a coherent and respected network of knowledge. It is a direct reflection of the quality of the work. Peer-reviewed articles support and embody the scientific method. It is therefore important to agree upon standards of expected ethical behavior for all parties involved in the act of publishing: the author, the journal editor, the peer reviewer, the publisher and the society of society-owned or sponsored journals.

All authors are requested to disclose any actual or potential conflict of interest including any financial, personal or other relationships with other people or organizations within three years of beginning the submitted work that could inappropriately influence, or be perceived to influence, their work.

Submission of an article implies that the work described has not been published previously that it is not under consideration for publication elsewhere. The submission should be approved by all authors and tacitly or explicitly by the responsible authorities where the work was carried out, and that, if accepted, it will not be published elsewhere in the same form, in English or in any other language, including electronically without the written consent of the copyright-holder.

Upon acceptance of an article, authors will be asked to complete a “Copyright Form”. Acceptance of the agreement will ensure the widest possible dissemination of information. An e-mail will be sent to the corresponding author confirming receipt of the manuscript together with a “Copyright Form” form or a link to the online version of this agreement.

Author Rights

As a journal author, you retain rights for a large number of author uses, including use by your employing institute or company. These rights are retained and permitted without the need to obtain specific permission from *IJET*. These include:

- ❖ The right to make copies (print or electronic) of the journal article for your own personal use, including for your own classroom teaching use;

- ❖ The right to make copies and distribute copies (including via e-mail) of the journal article to research colleagues, for personal use by such colleagues for scholarly purposes;
- ❖ The right to post a pre-print version of the journal article on internet web sites including electronic pre-print servers, and to retain indefinitely such version on such servers or sites for scholarly purposes
- ❖ the right to post a revised personal version of the text of the final journal article on your personal or institutional web site or server for scholarly purposes
- ❖ The right to use the journal article or any part thereof in a printed compilation of your works, such as collected writings or lecture notes.

Article Style

Authors must strictly follow the guide for authors, or their articles may be rejected without review. Editors reserve the right to adjust the style to certain standards of uniformity. Follow Title, Authors, Affiliations, Abstract, Keywords, Introduction, Materials and Methods, Theory/Calculation, Conclusions, Acknowledgements, References order when typing articles. The corresponding author should be identified with an asterisk and footnote. Collate acknowledgements in a separate section at the end of the article and do not include them on the title page, as a footnote to the title or otherwise.

Abstract and Keywords:

Enter an abstract of up to 250 words for all articles. This is a concise summary of the whole paper, not just the conclusions, and is understandable without reference to the rest of the paper. It should contain no citation to other published work. Include up to six keywords that describe your paper for indexing purposes.

Abbreviations and Acronyms:

Define abbreviations and acronyms the first time they are used in the text, even if they have been defined in the abstract. Abbreviations such as IEEE, SI, MKS, CGS, sc, dc, and rms do not have to be defined. Do not use abbreviations in the title unless they are unavoidable.

Text Layout for Peer Review:

Use single column layout, double spacing and wide (3 cm) margins on white paper at the peer review stage. Ensure that each new paragraph is clearly indicated. Present tables and figure legends in the text where they are related and cited. Number all pages consecutively; use 12 pt font size and standard fonts; Times New Roman, Helvetica, or Courier is preferred.

Research Papers should not exceed 12 printed pages in two-column publishing format, including figures and tables.

Technical Notes and Letters should not exceed 2,000 words.

Reviews should not exceed 20 printed pages in two-column publishing format, including figures and tables.

Equations:

Number equations consecutively with equation numbers in parentheses flush with the right margin, as in (1). To make equations more compact, you may use the solidus (/), the exp function, or appropriate exponents. Italicize Roman symbols for quantities and variables, but not Greek symbols. Use an dash (–) rather than a hyphen for a

minus sign. Use parentheses to avoid ambiguities in denominators. Punctuate equations with commas or periods when they are part of a sentence, as in

$$C = a + b \tag{1}$$

Symbols in your equation should be defined before the equation appears or immediately following. Use “Eq. (1)” or “equation (1),” while citing.

Figures and Tables:

All illustrations must be supplied at the correct resolution:

- * Black and white and colour photos - 300 dpi
- * Graphs, drawings, etc - 800 dpi preferred; 600 dpi minimum
- * Combinations of photos and drawings (black and white and color) - 500 dpi

In addition to using figures in the text, upload each figure as a separate file in either .tiff or .eps format during submission, with the figure number.

Table captions should be written in the same format as figure captions; for example, “Table 1. Appearance styles.”. Tables should be referenced in the text unabbreviated as “Table 1.”

References:

Please ensure that every reference cited in the text is also present in the reference list (and viceversa). Any references cited in the abstract must be given in full. Unpublished results and personal communications are not recommended in the reference list, but may be mentioned in the text. Citation of a reference as “in press” implies that the item has been accepted for publication. Number citations consecutively in square brackets [1]. Punctuation follows the bracket [2]. Refer simply to the reference number, as in [3]. Use “Ref. [3]” or Reference [3]” at the beginning of a sentence: “Reference [3] was ...”. Give all authors’ names; use “et al.” if there are six authors or more. For papers published in translated journals, first give the English citation, then the original foreign-language citation.

Books

- [1] J. Clerk Maxwell, *A Treatise on Electricity and Magnetism*, 3rd ed., vol. 2. Oxford:Clarendon Press, 1892, pp.68-73.

Journals

- [2] Y. Yorozu, M. Hirano, K. Oka, and Y. Tagawa, “Electron spectroscopy studies on magneto-optical media and plastic substrate interface”, *IEEE Transl. J. Magn. Japan*, vol. 2, pp. 740-741, August 1987.

Conferences

- [3] Çolak I., Kabalci E., Bayindir R., and Sagiroglu S, “The design and analysis of a 5-level cascaded voltage source inverter with low THD”, *2nd PowerEng Conference*, Lisbon, pp. 575-580, 18-20 March 2009.

Reports

- [4] IEEE Standard 519-1992, Recommended practices and requirements for harmonic control in electrical power systems, *The Institute of Electrical and Electronics Engineers*, 1993.

Text Layout for Accepted Papers:

A4 page margins should be margins: top = 24 mm, bottom = 24 mm, side = 15 mm. Main text should be given in two column. The column width is 87mm (3.425 in). The space between the two columns is 6 mm (0.236 in). Paragraph indentation is 3.5 mm (0.137 in). Follow the type sizes specified in Table. Position figures and tables at the tops and bottoms of columns. Avoid placing them in the middle of columns. Large figures and tables may span across both columns. Figure captions should be centred below the figures; table captions should be centred above. Avoid placing figures and tables before their first mention in the text. Use the abbreviation “Fig. 1,” even at the beginning of a sentence.

Type size (pts.)	Appearance		
	Regular	Bold	<i>Italic</i>
10	Authors' affiliations, Section titles, references, tables, table names, first letters in table captions, figure captions, footnotes, text subscripts, and superscripts	Abstract	
12	Main text, equations, Authors' names, ^a		<i>Subheading (1.1.)</i>
24	Paper title		

Submission checklist:

It is hoped that this list will be useful during the final checking of an article prior to sending it to the journal's Editor for review. Please consult this Guide for Authors for further details of any item. Ensure that the following items are present:

- ❖ One Author designated as corresponding Author:
 - E-mail address
 - Full postal address
 - Telephone and fax numbers
- ❖ All necessary files have been uploaded
- Keywords: a minimum of 4
- All figure captions (supplied in a separate document)

- All tables (including title, description, footnotes, supplied in a separate document)
 - ❖ Further considerations
- Manuscript has been "spellchecked" and "grammar-checked"
- References are in the correct format for this journal
- All references mentioned in the Reference list are cited in the text, and vice versa
- Permission has been obtained for use of copyrighted material from other sources (including the Web)
- Color figures are clearly marked as being intended for color reproduction on the Web (free of charge) and in print or to be reproduced in color on the Web (free of charge) and in black-and-white in print.

Article Template Containing Author Guidelines for Peer-Review

First Author*, Second Author**‡, Third Author***

*Department of First Author, Faculty of First Author, Affiliation of First Author, Postal address

**Department of Second Author, Faculty of First Author, Affiliation of First Author, Postal address

***Department of Third Author, Faculty of First Author, Affiliation of First Author, Postal address

(First Author Mail Address, Second Author Mail Address, Third Author Mail Address)

‡Corresponding Author; Second Author, Postal address, Tel: +90 312 123 4567, Fax: +90 312 123 4567,corresponding@affl.edu

Received: xx.xx.xxxx Accepted:xx.xx.xxxx

Abstract- Enter an abstract of up to 250 words for all articles. This is a concise summary of the whole paper, not just the conclusions, and is understandable without reference to the rest of the paper. It should contain no citation to other published work. Include up to six keywords that describe your paper for indexing purposes. Define abbreviations and acronyms the first time they are used in the text, even if they have been defined in the abstract. Abbreviations such as IEEE, SI, MKS, CGS, sc, dc, and rms do not have to be defined. Do not use abbreviations in the title unless they are unavoidable.

Keywords- Keyword1; keyword2; keyword3; keyword4; keyword5.

2. Introduction

Authors should any word processing software that is capable to make corrections on misspelled words and grammar structure according to American or Native English. Authors may get help by from word

processor by making appeared the paragraph marks and other hidden formatting symbols. This sample article is prepared to assist authors preparing their articles to IJET.

Indent level of paragraphs should be 0.63 cm (0.24 in) in the text of article. Use single column layout, double-spacing and wide (3 cm) margins on white paper at the peer review stage. Ensure that each new paragraph is clearly indicated. Present tables and figure legends in the text where they are related and cited. Number all pages consecutively; use 12 pt font size and standard fonts; Times New Roman, Helvetica, or Courier is preferred. Indicate references by number(s) in square brackets in line with the text. The actual authors can be referred to, but the reference number(s) must always be given. Example: "..... as demonstrated [3, 6]. Barnaby and Jones [8] obtained a different result"

IJET accepts submissions in three styles that are defined as Research Papers, Technical Notes and Letter, and Review paper. The requirements of paper are as listed below:

- Research Papers should not exceed 12 printed pages in two-column publishing format, including figures and tables.
- Technical Notes and Letters should not exceed 2,000 words.
- Reviews should not exceed 20 printed pages in two-column publishing format, including figures and tables.

Authors are requested write equations using either any mathematical equation object inserted to word processor or using independent equation software. Symbols in your equation should be defined before the equation appears or immediately following. Use "Eq. (1)" or "equation (1)," while citing. Number equations consecutively with equation numbers in parentheses flush with the right margin, as in Eq. (1). To make equations more compact, you may use the solidus (/), the exp function, or appropriate exponents. Italicize Roman symbols for quantities and variables, but not Greek symbols. Use an dash (–) rather than a hyphen for a minus sign. Use parentheses to avoid ambiguities in denominators. Punctuate equations with commas or periods when they are part of a sentence, as in

$$C = a + b \tag{1}$$

Section titles should be written in bold style while sub section titles are italic.

3. Figures and Tables

3.1. Figure Properties

All illustrations must be supplied at the correct resolution:

- Black and white and colour photos - 300 dpi
- Graphs, drawings, etc - 800 dpi preferred; 600 dpi minimum
- Combinations of photos and drawings (black and white and colour) - 500 dpi

In addition to using figures in the text, Authors are requested to upload each figure as a separate file in either .tiff or .eps format during submission, with the figure number as Fig.1., Fig.2a and so on. Figures are cited as “Fig.1” in sentences or as “Figure 1” at the beginning of sentence and paragraphs. Explanations related to figures should be given before figure. Figures and tables should be located at the top or bottom side of paper as done in accepted article format.



Figure 1. Engineering technologies.

Table captions should be written in the same format as figure captions; for example, “Table 1. Appearance styles.”. Tables should be referenced in the text unabbreviated as “Table 1.”

Table 1. Appearance properties of accepted manuscripts

Type size (pts.)	Appearance		
	Regular	Bold	<i>Italic</i>
10	Authors’ affiliations, Abstract, keywords, references, tables, table names, figure captions, footnotes, text subscripts, and superscripts	Abstract	
12	Main text, equations, Authors’ names, Section titles		<i>Subheading (1.1.)</i>
24	Paper title		

4. Submission Process

The *International Journal of Engineering Technologies* operates an online submission and peer review system that allows authors to submit articles online and track their progress via a web interface. Articles that are prepared referring to this template should be controlled according to submission checklist given in “Guide f Authors”. Editor handles submitted articles to IJET primarily in order to control in terms of compatibility to aims and scope of Journal.

Articles passed this control are checked for grammatical and template structures. If article passes this control too, then reviewers are assigned to article and Editor gives a reference number to paper. Authors registered to online submission system can track all these phases.

Editor also informs authors about processes of submitted article by e-mail. Each author may also apply to Editor via online submission system to review papers related to their study areas. Peer review is a critical element of publication, and one of the major cornerstones of the scientific process. Peer Review serves two key functions:

- Acts as a filter: Ensures research is properly verified before being published
- Improves the quality of the research

5. Conclusion

The conclusion section should emphasize the main contribution of the article to literature. Authors may also explain why the work is important, what are the novelties or possible applications and extensions. Do not replicate the abstract or sentences given in main text as the conclusion.

Acknowledgements

Authors may acknowledge to any person, institution or department that supported to any part of study.

References

- [1] J. Clerk Maxwell, *A Treatise on Electricity and Magnetism*, 3rd ed., vol. 2. Oxford:Clarendon Press, 1892, pp.68-73.
(Book)
- [2] H. Poor, *An Introduction to Signal Detection and Estimation*, New York: Springer-Verlag, 1985, ch. 4. (Book Chapter)
- [3] Y. Yorozu, M. Hirano, K. Oka, and Y. Tagawa, "Electron spectroscopy studies on magneto-optical media and plastic substrate interface", *IEEE Transl. J. Magn. Japan*, vol. 2, pp. 740-741, August 1987. (Article)
- [4] E. Kabalcı, E. Irmak, I. Çolak, "Design of an AC-DC-AC converter for wind turbines", *International Journal of Energy Research*, Wiley Interscience, DOI: 10.1002/er.1770, Vol. 36, No. 2, pp. 169-175. (Article)
- [5] I. Çolak, E. Kabalci, R. Bayindir R., and S. Sagiroglu, "The design and analysis of a 5-level cascaded voltage source inverter with low THD", *2nd PowerEng Conference*, Lisbon, pp. 575-580, 18-20 March 2009. (Conference Paper)
- [6] IEEE Standard 519-1992, Recommended practices and requirements for harmonic control in electrical power systems, *The Institute of Electrical and Electronics Engineers*, 1993. (Standards and Reports)

Article Template Containing Author Guidelines for Accepted Papers

First Author*, Second Author**‡, Third Author***

*Department of First Author, Faculty of First Author, Affiliation of First Author, Postal address

**Department of Second Author, Faculty of First Author, Affiliation of First Author, Postal address

***Department of Third Author, Faculty of First Author, Affiliation of First Author, Postal address

(First Author Mail Address, Second Author Mail Address, Third Author Mail Address)

‡Corresponding Author; Second Author, Postal address, Tel: +90 312 123 4567,

Fax: +90 312 123 4567,corresponding@affl.edu

Received: xx.xx.xxxx Accepted:xx.xx.xxxx

Abstract- Enter an abstract of up to 250 words for all articles. This is a concise summary of the whole paper, not just the conclusions, and is understandable without reference to the rest of the paper. It should contain no citation to other published work. Include up to six keywords that describe your paper for indexing purposes. Define abbreviations and acronyms the first time they are used in the text, even if they have been defined in the abstract. Abbreviations such as IEEE, SI, MKS, CGS, sc, dc, and rms do not have to be defined. Do not use abbreviations in the title unless they are unavoidable.

Keywords Keyword1, keyword2, keyword3, keyword4, keyword5.

1. Introduction

Authors should use any word processing software that is capable of making corrections on misspelled words and grammar structure according to American or British English. Authors may get help from word processor by making visible the paragraph marks and other hidden formatting symbols. This sample article is prepared to assist authors preparing their articles to IJET.

Indent level of paragraphs should be 0.63 cm (0.24 in) in the text of article. Use single column layout, double-spacing and wide (3 cm) margins on white paper at the peer review stage. Ensure that each new paragraph is clearly indicated. Present tables and figure legends in the text where they are related and cited. Number all pages consecutively; use 12 pt font size and standard fonts; Times New Roman, Helvetica, or Courier is preferred. Indicate references by number(s) in square brackets in line with the text. The actual authors can be referred to, but the reference number(s) must always be

given. Example: "... as demonstrated [3,6]. Barnaby and Jones [8] obtained a different result"

IJET accepts submissions in three styles that are defined as Research Papers, Technical Notes and Letter, and Review paper. The requirements of paper are as listed below:

➤ Research Papers should not exceed 12 printed pages in two-column publishing format, including figures and tables.

➤ Technical Notes and Letters should not exceed 2,000 words.

➤ Reviews should not exceed 20 printed pages in two-column publishing format, including figures and tables.

Authors are requested to write equations using either any mathematical equation object inserted to word processor or using independent equation software. Symbols in your equation should be defined before the equation appears or immediately following. Use "Eq. (1)" or "equation (1),"

while citing. Number equations consecutively with equation numbers in parentheses flush with the right margin, as in Eq. (1). To make equations more compact, you may use the solidus (/), the exp function, or appropriate exponents. Italicize Roman symbols for quantities and variables, but not Greek symbols. Use an dash (-) rather than a hyphen for a minus sign. Use parentheses to avoid ambiguities in denominators. Punctuate equations with commas or periods when they are part of a sentence, as in

$$C = a + b \quad (1)$$

Section titles should be written in bold style while sub section titles are italic.

6. Figures and Tables

6.1. Figure Properties

All illustrations must be supplied at the correct resolution:

- Black and white and colour photos - 300 dpi
- Graphs, drawings, etc - 800 dpi preferred; 600 dpi minimum
- Combinations of photos and drawings (black and white and colour) - 500 dpi

In addition to using figures in the text, Authors are requested to upload each figure as a separate file in either

Table 1. Appearance properties of accepted manuscripts

Type size (pts.)	Appearance		
	Regular	Bold	<i>Italic</i>
10	Main text, section titles, authors' affiliations, abstract, keywords, references, tables, table names, figure captions, equations, footnotes, text subscripts, and superscripts	Abstract-	<i>Subheading (1.1.)</i>
12	Authors' names,		
24	Paper title		

6.2. Text Layout for Accepted Papers

A4 page margins should be margins: top = 24 mm, bottom = 24 mm, side = 15 mm. The column width is 87mm (3.425 in). The space between the two columns is 6 mm (0.236 in). Paragraph indentation is 3.5 mm (0.137 in). Follow the type sizes specified in Table. Position figures and tables at the tops and bottoms of columns. Avoid placing them in the middle of columns. Large figures and tables may span across both columns. Figure captions should be centred below the figures; table captions should be centred above. Avoid placing figures and tables before their first mention in

.tiff or .eps format during submission, with the figure number as Fig.1., Fig.2a and so on. Figures are cited as "Fig.1" in sentences or as "Figure 1" at the beginning of sentence and paragraphs. Explanations related to figures should be given before figure.



Fig. 1. Engineering technologies.

Figures and tables should be located at the top or bottom side of paper as done in accepted article format. Table captions should be written in the same format as figure captions; for example, "Table 1. Appearance styles.". Tables should be referenced in the text unabbreviated as "Table 1."

the text. Use the abbreviation "Fig. 1," even at the beginning of a sentence.

7. Submission Process

The International Journal of Engineering Technologies operates an online submission and peer review system that allows authors to submit articles online and track their progress via a web interface. Articles that are prepared referring to this template should be controlled according to submission checklist given in "Guide f Authors". Editor handles submitted articles to IJET primarily in order to control in terms of compatibility to aims and scope of Journal. Articles passed this control are checked for

grammatical and template structures. If article passes this control too, then reviewers are assigned to article and Editor gives a reference number to paper. Authors registered to online submission system can track all these phases. Editor also informs authors about processes of submitted article by e-mail. Each author may also apply to Editor via online submission system to review papers related to their study areas. Peer review is a critical element of publication, and one of the major cornerstones of the scientific process. Peer Review serves two key functions:

- Acts as a filter: Ensures research is properly verified before being published
- Improves the quality of the research

8. Conclusion

The conclusion section should emphasize the main contribution of the article to literature. Authors may also explain why the work is important, what are the novelties or possible applications and extensions. Do not replicate the abstract or sentences given in main text as the conclusion.

Acknowledgements

Authors may acknowledge to any person, institution or department that supported to any part of study.

References

- [7] J. Clerk Maxwell, A Treatise on Electricity and Magnetism, 3rd ed., vol. 2. Oxford:Clarendon Press, 1892, pp.68-73. (Book)
- [8] H. Poor, An Introduction to Signal Detection and Estimation, New York: Springer-Verlag, 1985, ch. 4. (Book Chapter)
- [9] Y. Yorozu, M. Hirano, K. Oka, and Y. Tagawa, "Electron spectroscopy studies on magneto-optical media and plastic substrate interface", IEEE Transl. J. Magn. Japan, vol. 2, pp. 740-741, August 1987. (Article)
- [10] E. Kabalcı, E. Irmak, I. Çolak, "Design of an AC-DC-AC converter for wind turbines", International Journal of Energy Research, Wiley Interscience, DOI: 10.1002/er.1770, Vol. 36, No. 2, pp. 169-175. (Article)
- [11] I. Çolak, E. Kabalcı, R. Bayindir R., and S. Sagiroglu, "The design and analysis of a 5-level cascaded voltage source inverter with low THD", 2nd PowerEng Conference, Lisbon, pp. 575-580, 18-20 March 2009. (Conference Paper)
- [12] IEEE Standard 519-1992, Recommended practices and requirements for harmonic control in electrical power systems, The Institute of Electrical and Electronics Engineers, 1993. (Standards and Reports)

**INTERNATIONAL JOURNAL OF ENGINEERING TECHNOLOGIES (IJET)
COPYRIGHT AND CONSENT FORM**

This form is used for article accepted to be published by the IJET. Please read the form carefully and keep a copy for your files.

TITLE OF ARTICLE (hereinafter, "The Article"):

.....
.....
.....

LIST OF AUTHORS:

.....
.....
.....

CORRESPONDING AUTHOR'S ("The Author") NAME, ADDRESS, INSTITUTE AND EMAIL:

.....
.....
.....

COPYRIGHT TRANSFER

The undersigned hereby transfers the copyright of the submitted article to International Journal of Engineering Technologies (the "IJET"). The Author declares that the contribution and work is original, and he/she is authorized by all authors and/or grant-funding agency to sign the copyright form. Author hereby assigns all including but not limited to the rights to publish, distribute, reprints, translates, electronic and published derivatives in various arrangements or any other versions in full or abridged forms to IJET. IJET holds the copyright of Article in its own name.

Author(s) retain all rights to use author copy in his/her educational activities, own websites, institutional and/or funder's web sites by providing full citation to final version published in IJET. The full citation is provided including Authors list, title of the article, volume and issue number, and page number or using a link to the article in IJET web site. Author(s) have the right to transmit, print and share the first submitted copies with colleagues. Author(s) can use the final published article for his/her own professional positions, career or qualifications by citing to the IJET publication.

Once the copyright form is signed, any changes about the author names or order of the authors listed above are not accepted by IJET.

Authorized/Corresponding Author

Date/ Signature